Alma Mater Studiorum · University of Bologna

School of Science
Department of Physics and Astronomy
Master Degree in Physics

ALP leptogenesis

Supervisor:
Dr. Filippo Sala

Submitted by:
Martina Cataldi

Co-supervisors:
Prof. Alberto Mariotti
Prof. Silvia Pascoli

Academic Year 2022/2023

ABSTRACT

This master thesis project explores cosmological aspects of beyond the Standard Model physics, and aims at addressing the baryon asymmetry of the Universe (BAU) and how it could be affected by axion-like particles (ALPs). It intends to provide an alternative path to the standard thermal leptogenesis mainly studied in the literature, focusing on the possibility to source non-thermal leptogenesis via decays of ALPs.

ALPs are weakly-interacting pseudo Nambu-Goldstone bosons of spontaneously broken global symmetries, predicted by many high-energy extensions of the Standard Model and they are natural targets to discover new physics. We study the evolution of ALPs in the Early Universe, probing their thermal production and decay, considering their couplings with gluons, top quarks and, in addition, Majorana right-handed neutrinos, Ns. In particular, we investigate the decay $a \to NN$ and its implications, notably the non-thermal production of Ns.
In this thesis, the contribution of this non-thermal ALP leptogenesis is estimated and computed by solving the associated Boltzmann Equations. Moreover, we explore the region of viable parameter space for ALP leptogenesis where the ALP induces a matter-dominated phase, diluting significantly the pre-existing relics.

Results favour values for the ALP decay constant f_a such that $f_a > 10^{11}$ GeV and for the Majorana neutrino mass M_N such that $M_N > 1$ TeV. The advantages of this alternative approach are that, while standard leptogenesis would undergo strong washout regime, the non-thermal leptogenesis via ALP decays avoids this, and the secondary non-thermal population of Ns, produced via ALP decays, fuels leptogenesis and enhances the resulting baryon asymmetry.

Contents

Contents III

1 Introduction 1
- 1.1 Baryon Asymmetry of the Universe . . . 2
- 1.2 What is an ALP? . . . 6
- 1.3 Reading this thesis . . . 9

2 Thermal leptogenesis 10
- 2.1 Basic set-up . . . 10
  - 2.1.1 Heavy Majorana neutrino mass models: see-saw type I . . . 10
  - 2.1.2 CP-violation . . . 12
  - 2.1.3 Anomalous $B + L$ violation: sphaleron processes . . . 14
- 2.2 Hierarchical heavy neutrino masses . . . 16
- 2.3 Integrated Boltzmann Equations . . . 19
- 2.4 Resonant leptogenesis . . . 25

3 ALP in the Early Universe 28
- 3.1 ALP production in the Early Universe . . . 28
  - 3.1.1 Thermal ALP production . . . 29
  - 3.1.2 ALP production via coupling to Majorana neutrinos . . . 32
  - 3.1.3 Cosmological ALP Yield . . . 34
- 3.2 ALP's decay . . . 36

4 Non-thermal leptogenesis via ALP 38
- 4.1 Parameter space for ALP leptogenesis . . . 38
  - 4.1.1 Dilution factor . . . 41
- 4.2 Boltzmann Equations . . . 44
  - 4.2.1 Kinetic equilibrium . . . 45
  - 4.2.2 Extra washout due to boosted Ns . . . 45
  - 4.2.3 Numerical solution of Boltzmann Equations and computation of baryon asymmetry . . . 46

4.3 Leptogenesis from a matter-dominating ALP . . . 53
4.3.1 Temperature scaling . . . 55
4.3.2 Dilution in ALP leptogenesis . . . 58

5 Conclusion **62**
5.1 Outlook . . . 64

Acknowledgements **66**

Appendices **68**

A Cosmology **68**
A.1 Thermal history of the Universe . . . 69

B Boltzmann Equations **73**
B.1 Standard thermal leptogenesis . . . 74
B.2 ALP leptogenesis . . . 78

C ALP production via Majorana neutrino coupling **81**

List of Figures **84**

Bibliography **88**

Chapter 1

Introduction

The current theory of particle physics, the Standard Model (SM), is consistent and extremely successful: it describes the properties of known matter and forces with remarkable accuracy, predicting experimental measurements with an outstanding precision. For instance, we enumerate among the SM triumphs the theoretical predictions of: the Higgs boson, detected in 2012 [1, 2], the anomalous magnetic dipole moment of the electron, $g-2$, that matches the experimentally measured value to twelve digit precision [3, 4], the masses of W and Z bosons, which agree with experimental data [4].
Nevertheless, the SM cannot be considered as a complete and fundamental theory, because it suffers from both theoretical and phenomenological striking shortcomings. On top of the theoretical ones (notably the lack of a theory of quantum gravity), the most relevant phenomenological evidence that cannot be explained within the SM framework are the following: the observed neutrino flavour oscillations [5, 6], which imply that neutrinos are massive (see Sect. 2.1.1), while the SM predicts them to be massless, the nature of dark matter, which constitutes approximately the 25% of the total energy content of the Universe [7], the generating mechanism of the Baryon Asymmetry of the Universe (BAU), i.e. the observed ratio of matter to radiation (see [8, 9] for reviews).

This master thesis aims at exploring the cosmological aspects of beyond the Standard Model physics, focusing on the BAU. Indeed, even though the SM contains all the necessary ingredients to produce it, this is not enough to generate the observed amount of BAU, as we will review in the next section. Among the various solutions proposed in the literature (see Sect. 1.1), leptogenesis [10] plays a relevant role: it creates a lepton asymmetry, which is partially converted into a baryon asymmetry through sphaleron processes, which are only active before the Electroweak Phase Transition, i.e. for the temperature range $10^2\,\mathrm{GeV} \lesssim T \lesssim 10^{12}\,\mathrm{GeV}$ (see Chapt. 2). Leptogenesis actually addresses two shortcomings of the SM: it uses neutrino mass models (see Sect. 2.1.1) to generate the BAU. The core of leptogenesis relies on the out-of-equilibrium decays of Majorana right-handed neutrinos Ns into leptons and Higgs bosons, namely $N \to \ell\,\phi$.

These decays are both lepton-number violating, because Majorana particles do not carry lepton number, and CP-violating, because of the complex phases in the Yukawa matrix. This thesis intends to provide an alternative path to the standard thermal leptogenesis mainly studied in the literature [9–12], in which the right-handed neutrinos (RHNs) are thermally produced in the primordial plasma through scatterings and inverse decays involving SM particles. Instead, we focus on the possibility to source leptogenesis non-thermally via decays of axion-like particles (ALPs): $a \to NN$, where the ALP, a, is coupled to N via the interaction term $\frac{M_N}{f_a} a \overline{N}_R N_R$, with f_a the ALP decay constant and M_N the Majorana mass of the RHNs. We rely on ALPs (see e.g. axion/ALP reviews [13, 14]), which are light, weakly-interacting pseudo Nambu-Goldstone bosons, because their existence is motivated in any ultraviolet extension of the Standard Model which includes the spontaneous breaking of an approximated global symmetry [13].
Thus, the main body of this thesis explores first the thermal production of ALPs in the Early Universe due to its couplings with top quarks and gluons, then the decay $a \to NN$ and the resulting non-thermal ALP leptogenesis, estimating its contribution to the BAU and, finally, numerically computing it by solving the associated Boltzmann Equations (BEs) [11, 12, 15]. We first study the case of hierarchical Majorana neutrino masses and then we address the resonant case. In addition, in part of the viable parameter space the ALP induces a matter-dominated epoch, diluting significantly any pre-existing relics, and we study its effect on the ALP leptogenesis mechanism.

Therefore, we investigate the new mechanism of ALP leptogenesis, which evaluates how the BAU could be affected by ALPs. The advantages of this alternative approach are that the strong washout regime can be evaded, while standard leptogenesis would go through it [9, 11], and that the secondary non-thermal population of Ns, produced via ALP decays, fuels leptogenesis and enhances the resulting baryon asymmetry. Then, we discuss the possible gain in the final baryon asymmetry generated through this ALP leptogenesis. Our results favour $f_a > 10^{11}$ GeV and $M_N > 1$ TeV for successful ALP leptogenesis.

In the remainder of this Chapter, the problem regarding the BAU is reviewed as well as the theoretical motivations for the ALPs.

1.1 Baryon Asymmetry of the Universe

Observational evidence, such as measurements of the Cosmic Microwave Background (CMB) radiation [7, 16], of the baryon density during the Big Bang Nucleosynthesis (BBN) [17, 18] and of the Alpha Magnetic Spectrometer (AMS) [19, 20], indicate that there is more matter than antimatter in the Universe: the number of baryons is not equal to the number of antibaryons. Structures like stars, galaxies, clusters, consist pre-

dominantly of matter, while antimatter is present in negligible quantities [21–23]. The direct determinations of the fraction of antiprotons and positrons in cosmic ray observations [24], which can be explained by pair production in astrophysical processes [25], is consistent with the milky way made up of only matter. Moreover, evidence from other galaxies shows that the existence of antimatter in the Universe is excluded by the diffuse γ-ray background [26]. Indeed, considering the Universe as a patchwork consisting of distinct regions of matter and antimatter, annihilations near regional boundaries must occur, providing a contribution to the cosmic diffuse γ-ray background. The signal would exceed observational limits unless the matter domain is virtually the entire visible Universe.

The BAU can be defined through the parameters [8, 9]

$$\eta_B \equiv \left.\frac{n_B - n_{\overline{B}}}{n_\gamma}\right|_0 , \tag{1.1}$$

$$Y_{\Delta B} \equiv \left.\frac{n_B - n_{\overline{B}}}{s}\right|_0 , \tag{1.2}$$

where n_B, $n_{\overline{B}}$, n_γ and s are, respectively, the number densities of baryons, antibaryons, photons and entropy density at present time (see App. A for definitions of these quantities). η_B and Y_B are expected to be constant from the production of the BAU onwards [8]. Indeed, the photon number density today, $n_\gamma|_0$, is fixed by the CMB's temperature $T_0 \approx 2.7\text{K}$ at present time [7, 16] and $s|_0$ does not get modified during an adiabatic evolution of the Universe. Then η_B is constant in absence of baryon number changing processes as well as $Y_{\Delta B}$. Moreover, the definitions (1.1) and (1.2) can be related via the calculable relation between the entropy density and the photon number density, $s|_0 \approx 7.04 n_\gamma|_0$ (for details see App. A), as

$$Y_{\Delta B} = \frac{\eta_B}{7.04} . \tag{1.3}$$

There are two main independent measurements of the primordial baryon asymmetry which rely on BBN and CMB, respectively. The former allows to measure the relic abundance of light elements and therefore to determine $Y_{\Delta B}$, which is the only free parameter in that computation [27]. The latter detects the baryon density of the Universe, because it affects the relative size of the peaks in the CMB power spectrum. Thus, the experimental values

$$\eta_B = (6.12 \pm 0.04) \cdot 10^{-10} , \tag{1.4}$$

$$Y_{\Delta B} = (8.69 \pm 0.22) \cdot 10^{-11} , \tag{1.5}$$

have been obtained by the latest CMB measurements [7], and they are consistent with the most recent analysis of primordial nucleosynthesis [28].

The measured value of $Y_{\Delta B}$ significantly differs from the baryon number density determined by freeze-out mechanism in a symmetric Universe, which corresponds to $\frac{n_B}{s} = \frac{n_{\overline{B}}}{s} \approx 7 \cdot 10^{-20}$ [21]. These observations lead us to conclude that a matter-antimatter symmetric Universe is empirically excluded and some mechanism explaining the Baryon Asymmetry of the Universe is needed.

The BAU cannot be an initial condition of any Universe including an inflationary phase [8]: indeed any primordial baryon asymmetry would have been exponentially diluted away by inflaton's decay, leading to the consequence that today we would have $\eta_B = 0$ due to the entropy injection at reheating. Therefore, the baryon asymmetry must have been dynamically generated between the inflationary phase and the BBN: a scenario which is known as *baryogenesis*.
The necessary conditions required to achieve a successful baryogenesis in any CPT conserving theory were formulated by Sakharov in Ref. [29] in 1967: the matter/antimatter asymmetry is related to the baryon-number violation in the fundamental theory and to CP-violation, the product of charge conjugation (C) and parity (P), and the processes leading to the production of the BAU have to occur out-of-equilibrium. Thus, the three Sakharov's conditions are the following [9, 11, 29]:

1. *Baryon-number violation*
   Associating the number of baryons with the quantum number B, e.g. $B = +1$ for one baryon, and the number of antibaryons with $\overline{B}$, e.g. $\overline{B} = -1$ for one antibaryon, the number densities n_B and $n_{\overline{B}}$ are defined as usual in cosmology (see App. A). As we know, B cannot be different from zero after an inflationary phase. Then, baryon number cannot be conserved if the Universe has to evolve from an initial state with $Y_{\Delta B} = 0$ to a state with $Y_{\Delta B} \neq 0$;

2. *C- and CP- violation*
   If the fundamental interactions were invariant under C and CP transformations, then
   $$\Gamma(X \to Y + B) = \Gamma(X^c \to Y^c + B^c)\,, \tag{1.6}$$
   i.e. the reaction rate for the two processes, where one involves baryons and the other one their antiparticles, i.e. the antibaryons, would be precisely the same. Therefore, even in presence of baryon number violation, these two processes would produce the same asymmetry with opposite sign and the overall effect would be that no net baryon asymmetry would be generated. Hence, the Universe can be neither C- nor CP-symmetric in order to get a non zero net baryon asymmetry [25];

3. *Departure from thermal equilibrium*
   Thermal equilibrium means that the system is time translationally invariant, i.e., a reaction proceeds at precisely the same rate as the inverse reaction:
   $$\Gamma(X \to Y + B) = \Gamma(Y + B \to X) \tag{1.7}$$

Then, an initially vanishing baryon number would always be zero.

Even though the three Sakharov's conditions can be considered excellent guidelines while attempting to generate the BAU, they are not sufficient conditions and finding models that accomodate them in a way that produces a non-zero BAU compatible with the observed one (1.4) is by far non trivial. In principle, all the three Sakharov's conditions are qualitatively satisfied in the SM [11]:

1. Baryon number is an accidental symmetry in the SM [30–32]: it is conserved by the Lagrangian but it is violated at quantum level by the triangle anomaly. These baryon number violating processes are non-perturbative interactions called sphalerons [33–35]: they preserve $B - L$ number, where L is the lepton number, while they violate $B + L$ number [9, 11, 36]. Sphaleron effects are treated more in detail in Sect. 2.1.3;

2. The weak interactions of the SM violate CP: the CP-violating source can be found in the non-vanishing complex phase in the CKM matrix (see Ref. [37] and textbooks [31, 32]). However, this amount of CP-violation turns out to be too small [11, 38, 39] and, consequently, baryogenesis implies that there must exist new sources of CP violation beyond the CKM phase of the SM;

3. The expansion of the Universe drives processes out-of-equilibrium. Within the SM, one departure from equilibrium occurs at the Electroweak Phase Transition (EWPT) [11, 36, 40]. However, a successful baryogenesis requires a strongly first order phase transition [9] and the EWPT is second order [41, 42]. Thus, a different kind of mechanism of departure from thermal equilibrium needs to be taken into account. For instance, it may arise from new physics that modifies the EWPT.

As seen, the BAU poses a puzzle in particle physics, requiring new physics to extend the SM theory. During the past decades, many possible new physics mechanisms for baryogenesis have been proposed. They include:

- **GUT baryogenesis**
  Grand Unified Theories (GUTs) have played an important role in the development of realistic models of baryogenesis (see Refs. [8, 9, 43, 44]). GUT baryogenesis generates the baryon asymmetry via the out-of-equilibrium decays of heavy bosonic leptoquarks, that violate both baryon and lepton number. However, in the simplest GUT models based on $SU(5)$, these decays can only produce a $B + L$ asymmetry with a vanishing asymmetry for $B - L$, because $B - L$ number is conserved. Consequently, the $B + L$ violating SM sphalerons would destroy this asymmetry [9, 45];

- **Electroweak baryogenesis**
  It is a process far from thermal equilibrium where the departure is provided by

a strongly first order phase transition (see Refs. [12, 45] and Refs. [8, 9, 21] for reviews). Viable models of electroweak baryogenesis (EWB) need a modification of the scalar potential and new sources of CP-violation [11], imposing constraints on masses and couplings of Higgs bosons. EWB involves nucleation and propagation of bubbles, CP-violating interactions on the wall separating the broken and unbroken phases and a crucial change of sphaleron rate across the wall [9];

- **Leptogenesis**
  It was proposed by Fukugida and Yanagida in Ref. [10] as an attractive mechanism which is able to generate a lepton asymmetry through lepton-number violating processes (see reviews [9, 11] and, for calculational methods, Refs [12, 15, 46]). It extends the SM by adding right-handed neutrinos, which also explain neutrino oscillations via the see-saw mechanism [11, 47, 48]. Then, their Yukawa couplings provide the necessary new source of CP-violation. The rate of these Yukawa interactions can be slow enough that the departure from thermal equilibrium occurs. Lepton number violation comes from the Majorana masses of these new particles. Finally, the SM sphaleron processes partially convert the generated lepton asymmetry into a baryon asymmetry [9, 49].

This thesis explores the problem regarding the BAU, focusing on leptogenesis as tool to achieve a successful baryogenesis.

1.2 What is an ALP?

Generally, new light, pseudo-scalar particles with derivative couplings to the SM appear in any theory with a spontaneously broken global symmetry: the so-called axion-like particles (ALPs) (see Refs. [13] and reviews [14, 50, 51]).
ALPs are pseudo Nambu-Goldstone bosons, a, arising at energies below their symmetry breaking scale v, as massless excitations of the angular part of the SM singlet complex scalar field ϕ [13, 14]:

$$\phi(x) = \frac{(v + \sigma(x))}{\sqrt{2}} e^{ia/v}\,, \tag{1.8}$$

with $< \phi >= \frac{v}{\sqrt{2}}$ the vacuum expectation value (vev) of ϕ and σ its propagating 'radial mode'. Since ALPs are massless excitations of the angular part of ϕ, they features a shift symmetry $a \to a + \theta$, indeed the vacuum is degenerate. In general, small explicit breakings of global symmetries are expected such that the ALP acquires a small mass, i.e. $m_a \ll v$. The name ALP is inspired by the QCD axion, which is the pseudo Nambu-Goldstone boson associated with the breaking of the $U(1)_{PQ}$ Peccei-Quinn symmetry, proposed to address the strong CP problem [52–54].
Possible ALP masses and couplings to SM particles range over many orders of magnitude. In general, ALPs are weakly-interacting. Indeed, their interactions with SM particles,

e.g., with gluons (described by the gluonic field strength $G_{\mu\nu}$), photons (described by the electromagnetic field strength $F_{\mu\nu}$) and fermions (described by the Dirac spinor f), are suppressed by inverse powers of the supposedly large symmetry breaking scales, $f_a = v \gg v_{EW}$, where $v_{EW} = 246$ GeV is the electroweak Higgs vev and f_a the so-called axion decay constant. Then, the low-energy effective Lagrangian including the leading operators in the $1/f_a$ expansion that couple the ALP to SM particles reads [55, 56]

$$\mathcal{L} = \frac{1}{2}\partial_\mu a \partial^\mu a - \frac{1}{2}m_a^2 a^2 - \frac{\alpha_s}{8\pi} C_g \frac{a}{f_a} G^b_{\mu\nu}\tilde{G}^{b,\mu\nu} - \frac{\alpha}{8\pi} C_\gamma \frac{a}{f_a} F_{\mu\nu}\tilde{F}^{\mu\nu} + \sum_f \frac{1}{2} C_{ff} \frac{\partial_\mu a}{f_a} \overline{f}\gamma^\mu\gamma^5 f \quad (1.9)$$

where the couplings constants C_g and C_γ arise from integrating out fermions with chirally anomalous $U(1)$ charge assignments, and the couplings to fermions C_{ff} we consider in this thesis will be the ones with the top and with the RHN. The ALP Lagrangian respects the shift symmetry mentioned above, which is only softly broken by a mass term. Its leading interactions with the SM particles are described by dimension-5 operators.

Now, we briefly review two particularly well-motivated examples for ALPs:

- **Axion**
  Peccei and Quinn introduced a $U(1)_{PQ}$ symmetry in order to solve the strong CP problem [52–54]. Indeed, in the QCD Lagrangian a term such as

  $$\theta \frac{g_s^2}{32\pi^2} G^b_{\mu\nu}\tilde{G}^{b,\mu\nu} \quad (1.10)$$

  is allowed. This θ-term is the theoretical source of CP-violation in QCD. Thus, the CP-symmetry is known to be broken in the weak sector of the SM and it is expected to be broken through strong interactions, which instead has not been observed in the experiments [51, 57]. Hence, the axion coming from the spontaneous breaking of symmetry $U(1)_{PQ}$ can replace this θ-parameter by a dynamical quantity, $\theta(x) = a(x)/f_a$, which spontaneously relaxes to $< \theta >= 0$. Finally, introducing this axion a, which experiences a shift symmetry, explains the non-observation of strong CP-violation, solving the CP problem in QCD [14, 51].
  In this case, the topologically induced potential gives the axion a small mass, rendering the axion a pseudo Nambu-Goldstone boson, in particular [58, 59]

  $$m_a \propto \frac{m_\pi f_\pi}{f_a} \quad (1.11)$$

  where m_π and f_π are the mass and the decay constant of the pion.

- **R-axion**
  Most of the generic, calculable models of dynamical supersymmetry breaking have

a spontaneously broken $U(1)_R$ R-symmetry [60–62], implying the existence of a Nambu-Goldstone boson, the so-called R-axion.
Supersymmetry (SUSY) (see reviews [63–65] and textbooks [66, 67]) has to be dynamically broken in order to solve the hierarchy problem, i.e. to have SUSY breaking scale much lower than the Planck scale. [68, 69]. It was proved that for a class of known models, where dynamical SUSY breaking is realized in a calculable way, a spontaneously broken R-symmetry is necessary and sufficient for dynamical SUSY breaking (the so-called Nelson-Seiberg theorem) [60, 61, 70]. The generators of this R-symmetry are the only ones that do not commute with the spinorial generators of SUSY, namely Q_α and $\overline{Q}^{\dot{\alpha}}$, i.e.,

$$[Q_\alpha, R] = Q_\alpha\,, \qquad\qquad [\overline{Q}_{\dot{\alpha}}, R] = -\overline{Q}_{\dot{\alpha}} \tag{1.12}$$

where R is the generator $U(1)_R$ transformations

$$\begin{cases} Q_\alpha \to e^{i\lambda} Q_\alpha \\ \overline{Q}_{\dot{\alpha}} \to e^{-i\lambda} \overline{Q}_{\dot{\alpha}} \end{cases} . \tag{1.13}$$

In spontaneous R-symmetry breaking models, the SUSY-breaking field with a finite R-charge acquires nonvanishing vacuum expectation value. The phase of the SUSY-breaking field is almost massless and identified as the pseudo Nambu-Goldstone boson, the R-axion. It acquires a small mass from gravitational coupling with explicit R-symmetry breaking constant W_0 term in the superpotential

$$W_{eff} = \Lambda_{eff}^2 X + W_0 \tag{1.14}$$

where Λ_{eff} gives the nonvanishing F-term for the R-charged SUSY-breaking field X [71]. Other sources of small explicit R-symmetry breaking may well exist (see e.g. [72]), making the R-axion mass effectively a free parameter.
Hence the existence of an R-axion is a generic prediction of SUSY ultraviolet completion of the SM. Even if a precise embedding of the studied scenario in SUSY is beyond the scope of this work, the ALP in this thesis could be for instance the R-axion.

Finally, ALPs are fascinating new particles and natural targets of new physics, because they occur in many theoretically appealing UV completions of the SM, most notably in string theory [13, 14]. Indeed, many theories that aim at extending the SM feature one or several broken global symmetries. Moreover, in certain regions of parameter space where ALPs are long-lived, they can be non-thermal candidates for cold Dark Matter [73]. Instead, in other regions where they decay, they can play the role of mediators to a dark sector [14, 50, 51]. For large symmetry breaking scales, the ALP can be a

harbinger of a new physics sector at a scale f_a which would otherwise be experimentally inaccessible. These features make the ALP a prime target for future experiments aiming at discovering new physics which addresses some of the open questions of the SM: the discovery of such ALPs at colliders, laboratories or from astrophysical sources [4] could be the first sign of a whole sector of new physics.
Of course, these ALPs would also affect the cosmological history of the Universe (for a review see Ref. [50]). In this thesis, we study in particular the cosmological effects of the ALPs, addressing their influence on the leptogenesis mechanism.

1.3 Reading this thesis

This thesis is organized as follows. In Chapter 2, we present a review of the standard thermal leptogenesis mechanism, providing in Section 2.1 a basic introduction to the neutrino mass models, CP-violation in the right-handed Majorana neutrino decays and sphaleron processes. In particular, we focus on the hierarchical Majorana masses case in Sect. 2.2 and in Sect. 2.3 the set of coupled Boltzmann Equations for thermal leptogenesis is solved. Finally, we address the case of resonant leptogenesis, focusing on its main outlines and providing numerical estimates in Sect. 2.4.
In Chapt. 3, we study the evolution of an ALP in the Early Universe, starting from its production mechanism in Sect. 3.1 to the decay channels in Sect. 3.2. The innovative contribution consists in taking into account its coupling with Majorana neutrinos Ns.
Chapt. 4 contains only original material worked out for this thesis, indeed our alternative leptogenesis is presented: a non-thermal leptogenesis in which Ns are also produced through the ALP's decays. First of all, a suitable parameter space for this ALP leptogenesis is identified in Sect. 4.1 and then, a modified set of Boltzmann Equations is derived and implemented, obtaining the produced baryon asymmetry in Sect. 4.2. In Sect. 4.3, the region of the viable parameter space in which the ALP dominates the energy content of the Universe for a certain period of time is taken into account and its effects on the BAU are probed.
The Chapt. 5 shows the conclusion of this thesis and possible future directions.
Eventually, in Appendix A some useful conventions and definitions of cosmological parameters can be found, in App. B a detailed derivation of the Boltzmann Equations is shown and in App. C the ALP production due to its coupling to Majorana neutrinos is computed.

Chapter 2

Thermal leptogenesis

In this Chapter, the mechanism of leptogenesis is reviewed [9, 11, 12, 15, 74]. In particular, thermal leptogenesis is presented as possible explanation for the BAU. In Sect. 2.2 the case of hierarchical heavy neutrino masses is discussed. The integrated Boltzmann Equations for the Yields of the involved species are solved and the solutions are shown in Sect. 2.3. Finally, resonant leptogenesis is addressed, providing a numerical example in Sect. 2.4.

2.1 Basic set-up

Leptogenesis was proposed by Fukugida and Yanagida [10] as an elegant mechanism able to generate a lepton asymmetry through lepton-number violating processes. It consists of few simple ingredients and it addresses two of the most puzzling open questions in the Standard Model: the nature of neutrino masses and the present matter-antimatter asymmetry.
It is based on the out-of-equilibrium and CP-violating decay of a heavy Majorana neutrino N into a lepton ℓ and a Higgs boson ϕ, which produces a lepton asymmetry that is then converted in a baryon asymmetry through sphaleron processes [33–35, 49]. Therefore, leptogenesis can satisfy all the three Sakharov's conditions for baryogenesis stated in Sect. 1.1 and thus, it can be understood as a tool to achieve successful baryogenesis.

2.1.1 Heavy Majorana neutrino mass models: see-saw type I

Neutrino oscillations [5, 6] show evidence for nonzero neutrino masses, challenging the SM theoretical predictions. Measurements of fluxes of solar, atmospheric, reactor and accelerator neutrinos provide the following two neutrino mass-squared differences [6]

$$\Delta m^2_{21} = (7.39 \pm 0.20) \cdot 10^{-5}\text{eV}^2\,, \qquad \Delta m^2_{31} = (2.523 \pm 0.030) \cdot 10^{-3}\text{eV}^2 \tag{2.1}$$

Then new particles, right-handed sterile neutrinos Ns, can be added to the SM in order to account for neutrino masses via a see-saw mechanism [11, 47, 48]. See-saw models are high energy models [75] that induce an effective model-independent 5-dimensional operator, named Weinberg operator [76]

$$\mathcal{L}_5 = -\frac{c_5}{2}\frac{(\overline{\ell}^c \cdot \tilde{\phi}^*)(\tilde{\phi}^\dagger \cdot \ell)}{\Lambda} + h.c.\,, \tag{2.2}$$

where c_5 is its Wilson coefficient, Λ is the scale at which the new exchanged particle becomes dynamical degrees of freedom, $\ell^T = (\nu_L, l_L)$ is the left-handed lepton SU(2)-doublet, $\phi^T = (\phi^+, \phi^0)$ is the SU(2) Higgs doublet, with $\phi^0 = h/\sqrt{2}$ such that the vev $v_{EW} = \sqrt{2} < \phi^0 >=< h >\approx 246$ GeV [77] generates the quantity [75]

$$m_\nu = \frac{c_5 v_{EW}^2}{2\Lambda}\,, \tag{2.3}$$

$\tilde{\phi} = i\sigma_2\phi^*$, with Pauli matrix σ_2, $\ell^c = C\overline{\ell}^T$, with C the charge conjugation matrix. The operator (2.2) is both Lorentz and $SU(2)$ invariant. There are three types of see-saw models, which differ by the properties of the exchanged heavy particle: the neutrino mass model considered in this thesis is the see-saw type I [47, 48, 75], which is very well motivated by various extensions of the SM [11]. This see-saw is characterized by $SU(3) \times SU(2) \times U(1)$- singlet fermion Ns.
See-saw models are fascinating because they explain naturally the smallness of the observed neutrino masses [47]. Indeed, in the see-saw type I, a right-handed neutrino N is introduced and coupled to the Higgs and the left-handed neutrino via the complex Yukawa coupling y_ν (for just one generation, y_ν is a coupling, while, considering all the three generations, it is a 3×3 matrix with complex couplings [10]). Then, the UV Lagrangian reads [9, 48]

$$\mathcal{L}_{\text{see-saw}} = -y_\nu \overline{\ell} \cdot \tilde{\phi} N - \frac{1}{2} M_N \overline{N}^c N + h.c. \tag{2.4}$$

where M_N is the Majorana heavy mass of the right-handed neutrino. Dirac mass terms for the charged leptons and, in particular, for the neutrinos are generated through the electroweak symmetry breaking: $m_D = \frac{y_\nu}{\sqrt{2}} v_{EW}$. Taking into account all the generations, Eq. (2.4) can be written as

$$\mathcal{L}_{\text{see-saw}} = -\frac{1}{2}\overline{\psi}_L^c \mathrm{M} \psi_L + h.c.\,, \tag{2.5}$$

with Dirac spinor and full mass matrix respectively [48]

$$\psi_L \equiv \begin{pmatrix} \nu_L \\ N^c \end{pmatrix} \quad , \quad \mathrm{M} = \begin{pmatrix} 0 & m_D^T \\ m_D & M_N \end{pmatrix}. \tag{2.6}$$

Diagonalizing the matrix in (2.6) through a unitary transformation, the massive states turn out to be Majorana states [9, 48]: one remains very heavy, i.e., with M_N mass, while the light neutrino masses acquire a tiny mass, i.e., $m_\nu = -m_D M_N^{-1} m_D^T$. Thus, using the relation that links the Dirac mass term to the coupling y_ν and the vev v_{EW}, we have

$$m_\nu = \frac{y_\nu^2 v_{EW}^2}{2M_N}\,, \tag{2.7}$$

where for simplicity we have just considered one generation for neutrinos. Hence, the see-saw type I is an UV completion of the effective Weinberg operator (see Eq. (2.3)). Moreover, we find that Ns are usually very heavy, e.g. $M_N \simeq 10^{10}$ GeV, and their coupling y_ν is e.g. $y_\nu \simeq 10^{-2}$. Indeed, those values of coupling and mass for the N reproduce the experimental bound for the light neutrino mass [6]

$$m_\nu \simeq 0.1\,\text{eV}\,. \tag{2.8}$$

These heavy Majorana neutrinos Ns are the source of leptogenesis. Indeed, the first term of see-saw Lagrangian (2.4) introduces the coupling of N with ℓ and ϕ. Then, the Majorana neutrino's decay

$$N \to \ell\,\phi \tag{2.9}$$

and its complex conjugate

$$N \to \overline{\ell}\,\overline{\phi} \tag{2.10}$$

feed the leptogenesis mechanism [10]. Let us highlight that Ns are Majorana particles, i.e., $N = \overline{N}$, and their mass term

$$\mathcal{L}_{mM} = -\frac{1}{2} M_N \overline{N}^c N + h.c. = \frac{1}{2} M_N N^T C^{-1} N + h.c. \tag{2.11}$$

break the lepton-number L [48], indeed under a $U(1)_{Lepton}$ transformation such as $N \to e^{i\alpha} N$,

$$\mathcal{L}_{mM} \to e^{i2\alpha}\ \mathcal{L}_{mM}\,. \tag{2.12}$$

Then these processes, (2.9) and (2.10), violate L conservation, fulfilling the first Sakharov's condition [10, 29] thanks to sphalerons (see Sect. 2.1.3).

2.1.2 CP-violation

In order to perform a successful baryogenesis, leptogenesis mechanism has also to meet the second Sakharov's condition [29]: the N's decays need to be CP-violating to generate a lepton asymmetry, i.e.,

$$\Gamma(N \to \ell\ \phi) \neq \Gamma(N \to \overline{\ell}\,\overline{\phi})\,. \tag{2.13}$$

Let us consider the basic thermal leptogenesis scenario [10] that extends the SM by adding three right-handed neutrinos N_1, N_2, N_3, with hierarchical masses such that only

the decay of N_1 contributes significantly to the production of lepton asymmetry (see Sect. 2.2). Then, we can define the parameter $\epsilon_{\alpha\alpha}$ as the CP-asymmetry in the lepton flavour α [10]:

$$\epsilon_{\alpha\alpha} = \frac{\Gamma(N_1 \to \ell_\alpha\, \phi) - \Gamma(N_1 \to \overline{\ell}_\alpha\, \overline{\phi})}{\Gamma(N_1 \to \ell\, \phi) + \Gamma(N_1 \to \overline{\ell}\, \overline{\phi})}\,. \tag{2.14}$$

If just the tree-level decay is considered (see Fig. 2.1), no CP-asymmetry would be created, indeed the tree-level amplitude squared of the scattering matrix $|\mathcal{M}_0|^2$ for the decay (2.9) is equal to $|\overline{\mathcal{M}}_0|^2$ for the complex conjugate decay (2.10): [11]

$$|\mathcal{M}_0|^2 = |y_{\alpha 1} A_0|^2 = |\overline{\mathcal{M}}_0|^2 = |y^*_{\alpha 1} \overline{A}_0|^2\,, \tag{2.15}$$

with $A_0(N \to \ell\, \phi) = \overline{u}_\ell \frac{(1+\gamma_5)}{2} u_N$ and $|A_0|^2 = |\overline{A}_0|^2$. The Yukawa matrix is indicated by y. Then, a CP-asymmetry $\epsilon_{\alpha\alpha}$ arises from the interference of the tree-level and one-loop amplitudes. As noted in Ref. [78], all the one-loop diagrams, including wavefunction corrections, have to be included.

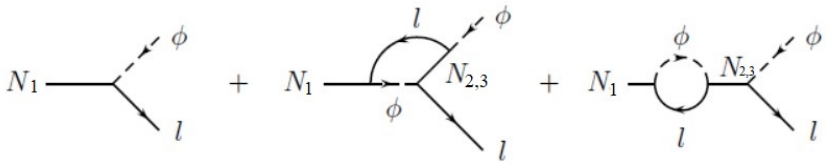

Figure 2.1: Tree-level, one-loop vertex and one-loop self-energy Feynman diagrams contributing to heavy neutrino decays [9].

The tree-level decay width of the heavy Majorana neutrino N_1 reads [10, 74]

$$\Gamma_D = \sum_\alpha \Gamma^0(N_1 \to \ell_\alpha\, \phi) + \Gamma^0(N_1 \to \overline{\ell}_\alpha\, \overline{\phi}) = \frac{(y^\dagger y)_{11}}{8\pi} M_1\,. \tag{2.16}$$

Computing the contributions coming from the tree-level, the vertex and the self-energy Feynman diagrams (Fig. 2.1), the CP-asymmetry parameter (2.14) becomes [11]

$$\epsilon_{\alpha\alpha} = \frac{1}{8\pi} \frac{1}{(y^\dagger y)_{11}} \sum_{j\neq 1} \left[Im\big\{(y^*_{\alpha 1})(y^\dagger y)_{1j} y_{\alpha j}\big\} F\left(\frac{M_j^2}{M_1^2}\right) + Im\big\{(y^*_{\alpha 1})(y^\dagger y)_{j1} y_{\alpha j}\big\} \frac{1}{1 - \frac{M_j^2}{M_1^2}} \right], \tag{2.17}$$

where $j = 2, 3$ and

$$F(x) = \sqrt{x}\left[\frac{1}{1-x} + 1 - (1+x) \log\left(\frac{1+x}{x}\right) \right] \xrightarrow{x \gg 1} -\frac{3}{2\sqrt{x}} - \frac{5}{6x^{3/2}} + \ldots \tag{2.18}$$

Summing over the lepton flavours α, the second term of Eq. (2.17) vanishes because it violates the single lepton flavours but it conserves the total lepton number [11, 79, 80].

Therefore, we have [11, 74]

$$\epsilon = \sum_{\alpha} \epsilon_{\alpha\alpha} = \frac{1}{8\pi} \frac{1}{(y^\dagger y)_{11}} \sum_{j\neq 1} \left[Im\{(y^\dagger y)^2_{1j}\} F\left(\frac{M_j^2}{M_1^2}\right)\right] . \tag{2.19}$$

2.1.3 Anomalous $B + L$ violation: sphaleron processes

Before studying the details of leptogenesis, let us focus on how the lepton asymmetry is converted into a baryon asymmetry via non-perturbative interactions, i.e., sphalerons (see Refs. [33–36, 49, 81, 82]). In the context of leptogenesis, we are looking for an anomaly in the $B + L$ current, which, within the four-dimensional SM, arises due to $SU(2)$ gauge interactions, which are chiral and non-Abelian [11].

In the SM, both baryon and lepton number are accidental symmetries: they are conserved according to classical equations of motions, but they are not preserved at quantum level due to the chiral anomaly (see for instance Ref. [83]), giving rise to the current [30]

$$\partial_\mu J^\mu_B = \frac{n_f}{32\pi^2} g_w^2 F^a_{\mu\nu} \tilde{F}^{a,\mu\nu} . \tag{2.20}$$

where $F^a_{\mu\nu}$ is the weak $SU(2)$ field strength, its dual $\tilde{F}^{a,\mu\nu} \equiv \frac{1}{2}\epsilon^{\mu\nu\rho\sigma} F^a_{\rho\sigma}$, g_w is the weak coupling constant and $n_f = 3$ is the number of families. An equation identical to (2.20) for the lepton-number current J^μ_L can also be obtained. Therefore, $B - L$ is conserved in the SM.
Then, the change of baryon number B is linked to the following dynamics of gauge fields [9]:

$$B(t) - B(0) = n_f Q(t) , \tag{2.21}$$

with

$$Q(t) \equiv \int_0^t dt' \int d^3x \frac{g_w^2}{32\pi^2} F^a_{\mu\nu} \tilde{F}^{a,\mu\nu} . \tag{2.22}$$

In four dimensions, the spacetime integral of Eq. (2.22) vanishes for an Abelian gauge field, but can be non-zero for non-Abelian fields, e.g. $SU(2)$ fields [11]. When $Q(t)$ is a non-zero integral, baryons will be created, even though there is no perturbative interaction in the Lagrangian that generates them. Thus, these baryon number changing processes are intrinsecally non-perturbative. Moreover, the right-hand side of (2.20) can be written as a total derivative involving gauge fields, $\partial_\mu K^\mu$, where [9]

$$K^\mu = \frac{\epsilon^{\mu\nu\rho\sigma} g_w^2}{32\pi^2} \left(F^a_{\nu\rho} A^a_\sigma - \frac{1}{3} g_w \epsilon^{abc} A^a_\nu A^b_\rho A^c_\sigma\right) . \tag{2.23}$$

with 4-potential A_ν. Hence, we can define the "winding number", or Chern-Simons number N_{CS}, of the field configuration such that [84]

$$N_{CS} = \int d^3x K^0 . \tag{2.24}$$

Then, we can write

$$Q(t) = N_{CS}(t) - N_{CS}(0)\,. \tag{2.25}$$

In order to change N_{CS} (which is an integer) by ± 1 one has to overcome an energy barrier [82]. In Fig. 2.2, the minimal static energy of the gauge fields is sketched as a function of N_{CS}. All the minima of the energy describe the vacuum state and differ by large gauge transformations [9]. The barrier is given by a static solution to the equations of motion, the so-called sphaleron [33], which has half integer N_{CS}. At zero temperature, gauge field configurations that give non-zero $Q(t)$ correspond to tunneling configurations, but the amplitude of such a process is negligible and has no observable consequences [9, 11, 85]. However, at finite temperature, there can be thermal fluctuations of the field that climb over the energy barrier. These are the sphaleron processes and they correspond to a vacuum-to-vacuum transition which changes the baryon number by multiples of n_f [33]. This means that sphalerons are source for three leptons (all generations) and nine quarks (all colours and generations), because they induce $\Delta B = \Delta L = \pm 3$ for a change of the Chern-Simons number of $N_{CS}(t) - N_{CS}(0) = \pm 1$ [11](see Eq. (2.21)).

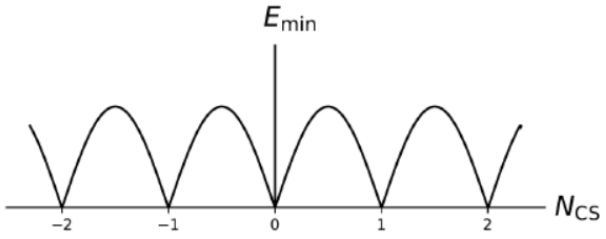

Figure 2.2: A sketch of the minimal field energy for a given value of the Chern-Simons number N_{CS} [82].

Now, returning to our discussion, leptogenesis is able to provide

$$B - L \neq 0\,, \tag{2.26}$$

which means that a lepton asymmetry has been created, as we shall see in the next sections. Then, knowing that the $B - L$ number is conserved in the SM and that those sphaleron processes are $(B + L)$-violating, we conclude that any non-zero $(B + L)$-asymmetry is washed out [9]: thus leptons are converted into baryons through these non-perturbative effects, obtaining a baryon asymmetry from an initial asymmetry of leptons only. Introducing the parameter c_{sph}, which corresponds to the fraction of $B - L$ asymmetry turned into B asymmetry, the baryon asymmetry today reads as a function of the $B - L$ asymmetry at time t_f when the leptogenesis process is completed [9, 49]

$$B(t_0) = c_{sph}(B - L)(t_f)\,. \tag{2.27}$$

In the SM, c_{sph} can be computed by considering the constraints among various chemical potentials induced by the spectator processes [11]

$$c_{sph} = \frac{8n_f + 4}{22n_f + 13} = \frac{28}{79}\,. \tag{2.28}$$

Furthermore, another element has to be considered: the temperature range at which the sphalerons are in thermal equilibrium with the primordial plasma, i.e. they are efficient (see App. A for a discussion about thermal equilibrium in the Early Universe). Indeed, the number of transitions per unit time and unit volume, Γ_{sph}, can be defined as the sphaleron rate. It is Boltzmann suppressed:

$$\Gamma_{sph} \propto e^{-E_{sph}/T}\,, \tag{2.29}$$

where E_{sph} is the height of the barrier at $T = 0$ [11]. Comparing Γ_{sph} with the Hubble parameter, H, the sphaleron processes turn out to be in thermal equilibrium for [11, 36, 86, 87]

$$10^2\,\text{GeV} \lesssim T \lesssim 10^{12}\,\text{GeV}\,. \tag{2.30}$$

This means that the generated lepton asymmetry can be converted into the baryon asymmetry only for this range of temperature.

2.2 Hierarchical heavy neutrino masses

In this Section, we proceed describing the key points of thermal leptogenesis and we study the scenario of hierarchical heavy neutrino masses. A precise numerical computation of the $B - L$ asymmetry produced is presented in Section 2.3, where the Boltzmann Equations in their integrated form are solved.
Here, the following simplifying assumptions hold:

- three right-handed neutrinos, namely N_1, N_2 and N_3, are considered in the basic scenario of hierarchical Majorana masses, i. e. $M_1 \ll M_{2,3}$;
- heavy Majorana neutrino population is produced thermally thanks to inverse decays and scatterings occurring in the thermal plasma. In particular, let the thermal production of N_2, N_3 be negligible with respect to the thermal production of N_1;
- we assume the one-flavour approximation: all lepton flavours are treated on the same footing in the interactions where they are involved.

The case in which the first assumption does not hold, i.e. no hierarchical masses for RHNs, is addressed in Sect. 2.4.

The aforementioned assumptions imply an effective theory of a propagating N_1 and effective 5-dimensional operators induced by N_2 and N_3. Then, integrating out N_2, N_3, the following effective Lagrangian is obtained [9, 11]

$$\mathcal{L} = \frac{1}{2}\overline{N_1}\not{\partial}N_1 - y_1\bar{\ell}\cdot\tilde{\phi}N_1 - \frac{1}{2}M_{N_1}\overline{N_1}^c N_1 - \frac{y_2^2}{2}\frac{(\overline{\ell}^c\tilde{\phi}^*)(\tilde{\phi}^\dagger\ell)}{M_2} - \frac{y_3^2}{2}\frac{(\overline{\ell}^c\tilde{\phi}^*)(\tilde{\phi}^\dagger\ell)}{M_3} + h.c.\,. \quad (2.31)$$

In this scenario, the decays of the two heavier neutrinos N_2 and N_3 are negligible, so that the $B-L$ asymmetry that they generate does not affect the final value of $B-L$. Thus leptogenesis is dominated by the CP-violating interactions of the lightest of the heavy Majorana neutrinos [88]:

- at $T > M_1$,
  right-handed neutrinos N_1 are in thermal equilibrium with the plasma

$$N_1 \leftrightarrow \ell\,\phi \quad (2.32)$$

$$N_1 \leftrightarrow \overline{\ell}\,\overline{\phi} \quad (2.33)$$

- at $T \lesssim M_1$,
  the initial thermal N_1 population decays away because the equilibrium number density is exponentially suppressed $\propto e^{-M_1/T}$ [11]. If the N_1 interactions are CP-violating, i.e. (2.13), asymmetries in all the lepton flavours can be produced. If the N_1 decay occours out-of-equilibrium for a certain period of time, the asymmetry will survive. Finally, the $B-L$ asymmetry can be converted into a baryon asymmetry by the SM $B+L$-violating processes in the range of temperature of (2.30).

The Yield of the baryon asymmetry $Y_{\Delta B}$ produced by thermal leptogenesis can be parametrized as [11]

$$Y_{\Delta B} \simeq Y_N^{eq}\, c_{sph}\, \epsilon\, \kappa_f\,, \quad (2.34)$$

where

- $Y_N^{eq} \equiv n_N^{eq}/s$ is the equilibrium Yield of RHN N_1, i.e., at $T \gg M_1$. Considering the number of relativistic degrees of freedom as in the SM i.e. $g_{*s} = g_* \simeq 106$ (see App. A), we have

$$Y_N^{eq} = \frac{3}{4}\frac{n_\gamma}{s} = \frac{135\zeta(3)}{4\pi^4 g_*} \simeq 4\cdot 10^{-3}\,, \quad (2.35)$$

  with the factor 3/4 accounting for the fermionic nature of the neutrinos;

- c_{sph} is the sphaleron conversion factor of Eq. (2.28) and in the SM [11]

$$c_{sph} \simeq 0.35\,; \quad (2.36)$$

- ϵ is the CP-asymmetry parameter and, in general, is defined as in Eq. (2.19). In the case of hierarchical Majorana masses, the expansion (2.18) holds and

$$F\left(\frac{M_k^2}{M_1^2}\right) \simeq -\frac{3}{2}\frac{M_1}{M_k}\,. \tag{2.37}$$

  Therefore the CP-asymmetry can be written as

$$\epsilon = \frac{3}{16\pi}\frac{M_1}{v_{EW}^2 (y^\dagger y)_{11}} \mathrm{Im}(y^\dagger m_\nu y^*)_{11}\,. \tag{2.38}$$

  Here, y is the Yukawa matrix, containing the CP-violating phases. Since the exact values inside this Yukawa matrix are unknown [11], the imaginary part factor of Eq. (2.38) is estimated, providing an upper bound for the CP-asymmetry in N's decays [9]

$$\epsilon < \epsilon_{\max} = \frac{3}{16\pi}\frac{m_\nu^{\max} M_1}{v_{EW}^2} \simeq 10^{-6}\left(\frac{M_1}{10^{10}\ \mathrm{GeV}}\right), \tag{2.39}$$

  where $m_\nu^{max} = \sqrt{|\Delta m_{31}^2|}$ (2.1);

- κ_f is the efficiency factor [88], accounting for washout effects, i.e. processes that erase the created lepton asymmetry, competing with the decay source term. Thus, washout processes reduce the efficiency of leptogenesis and we always have $\kappa_f \lesssim 1$.

  A relevant quantity which is useful to compute the value of the efficiency factor κ_f is the parameter K: in the following we will provide an expression of κ_f via K. The parameter K is defined as the ratio [9, 88]

$$K = \frac{\Gamma(N_1 \to \ell\phi, \overline{\ell}\,\overline{\phi})}{H(T = M_1)} = \frac{\tilde{m}_1}{m_*} \simeq \frac{(y^\dagger y)_{11} M_{\mathrm{Pl}}}{13.28\pi\sqrt{g_*}}\frac{1}{M_1}\,, \tag{2.40}$$

  where we have introduced the effective light-neutrino mass $\tilde{m}_1$ [89]

$$\tilde{m}_1 = \sum_\alpha \frac{y_{\alpha 1}^* y_{\alpha 1} v_{EW}^2}{M_1} = \frac{(y^\dagger y)_{11} v_{EW}^2}{M_1}\,, \tag{2.41}$$

  and the equilibrium neutrino mass m_* [88]

$$m_* = \frac{8\pi v_{EW}^2}{M_1^2} H(T = M_1) = \frac{16\pi^{5/2}\sqrt{g_*}}{3\sqrt{5}}\frac{v_{EW}^2}{M_{Pl}} \simeq 1.08 \cdot 10^{-3}\mathrm{eV}\,. \tag{2.42}$$

This K parameter controls whether or not N_1's decays are in equilibrium when $T = M_1$. Therefore, the following two regimes can be identified:

$$- \text{ if } \ \tilde{m}_1 > m_* \rightarrow \text{strong washout} \rightarrow \kappa_f \ll 1\,, \tag{2.43}$$

$$- \text{ if } \ \tilde{m}_1 < m_* \rightarrow \text{weak washout} \rightarrow \kappa_f \simeq 1\,. \tag{2.44}$$

Thus, $K > 1$ implies strong washout regime, while $K < 1$ weak washout regime. Then, given the experimental values of Δm^2_{21} and Δm^2_{31} (2.1), the washout is typically $K \simeq (30 \div 50)$ [88], i.e. strong washout regime. Actually, the weak washout regime can be achieved by tuning the unknown dimensionless matrix that can parametrize the lepton sector of the see-saw extension of the SM [11, 90]. In such a way, the value of K can be lowered, realizing the condition $K < 1$.
However, even though the weak washout regime is always desirable and achievable by tuning the parametrization matrix, the strong washout regime is the preferred natural one [88].

Now, we review the features of these two different regimes. In the weak washout regime, the washout processes are out-of-equilibrium when N_1 becomes non-relativistic [11] and, under these conditions, leptogenesis becomes very efficient. In this regime, κ_f strongly depends on the initial conditions [9, 88]: either thermal initial abundance for N_1 or zero initial abundance [9]. On the other hand, in the strong washout regime, the departure from thermal equilibrium is reduced and leptogenesis is less efficient. Notably, there is a period in which the washout processes are in thermal equilibrium [11] and κ_f does not depend on the initial conditions [9, 88]. In this case, κ_f is universal and can be approximated, within the theoretical uncertainties, by the simple power law [9, 88, 91]

$$\kappa_f \simeq \left(\frac{1}{2K}\right)^{1.1} \simeq (2 \pm 1) \cdot 10^{-2} \left(\frac{0.01\text{eV}}{\tilde{m}_1}\right)^{(1.1 \pm 0.1)}\,. \tag{2.45}$$

Thus, numerical calculations typically imply $\kappa_f \simeq 5 \cdot 10^{-3}$ [88].

Finally, let us note that the leptogenesis process strongly depends on the neutrino mass parameters [88]: indeed, ϵ is determined by the mass of the heavy neutrino M_1, while, in the strong washout regime, κ_f is determined by $\tilde{m}_1$ (2.41).

2.3 Integrated Boltzmann Equations

Actually, we can go beyond the approximation of expression (2.34) and carry out a more refined computation of the amount of lepton asymmetry generated by the N_1's decays.

Indeed, this is usually computed by integrating the appropriate Boltzmann Equations (BEs) [89, 92–94]. These describe the out-of-equilibrium dynamics of processes involving the heavy singlet fermions. The aim of this Section is to present the fundamental assumptions and the key steps that lead to the basic Boltzmann Equations in the case of one-flavour thermal leptogenesis, considering just the lightest neutrino N_1 involved, and to show their numerical solutions. See App. B for details about the derivation of the BEs.

As one's of Sakharov's conditions, departure from thermal equilibrium is crucial for the dynamic creation of a baryon asymmetry [29]. In the leptogenesis scenario, out-of-equilibrium conditions are achieved when interactions are no longer able to maintain the momentum distribution function of the right-handed neutrino at its equilibrium value as the Universe expands [46]. To simplify the calculation, this non-equilibrium process is traditionally studied by means of the integrated BEs [93, 95], whereby the equations of motion for the distribution functions of all particle species involved are integrated over momentum such that only the evolution of the number densities, specifically n_{N_1} and n_{B-L}, is tracked. In order for the integrated equations to be in a closed form, the following assumptions are made:

- all particles are in kinetic equilibrium, including the RHN, i.e. elastic scatterings do occur at higher rate than inelastic scatterings. Then, the phase-space distribution can be approximated as $f_i \approx f_i^{eq} n_i / n_i^{eq}$, where f_i^{eq} is the equilibrium one [46];
- all quantum statistical factors due to either Fermi-Dirac distribution for fermions and to Bose-Einstein for bosons (Pauli blocking effects/stimulated boson emissions) are neglected, i.e. $1 + f_i \approx 1$ [95], and their phase-space distribution in thermal equilibrium f_i^{eq} follows the classical Maxwell-Boltzmann distribution, $f_i^{eq} = e^{-E_i/T}$.

While these assumptions seem justifiable for particle species with gauge interactions, their validity is not immediately obvious for the RHN. However, they produce a typical magnitude of error of 20% in the asymptotic value of the lepton asymmetry produced in the weak washout regime, while $\lesssim 5\%$ in the strong washout [46].

Thus, in the following, we shall assume the aforementioned assumptions and, thanks to them, notably the one of kinetic equilibrium, the integrated BEs are obtained, i.e. involving number densities of the RHN, n_{N_1}, and of $B-L$ number, n_{B-L} (see App. B.1 for detailed derivation): first the BEs are derived with respect to the phase-space distributions f_N and f_{B-L}, then integration over the momentum phase space is performed, deriving the integrated form [46]. Eventually, a set of coupled BEs tracks the evolution of the RH neutrino Yield and $B-L$ Yield, respectively Y_{N_1} and Y_{B-L}.
In the variety of processes occurring in the hot plasma in the Early Universe, which involve the Majorana neutrinos, the simplest scenario of processes with $\mathcal{O}(y_\nu^2)$ and $\mathcal{O}(y_\nu^4)$

terms is considered, where y_ν is the neutrino Yukawa coupling (2.4). Therefore the following reactions are taken into account:

- decays: $N_1 \to \ell\,\phi$, contributing at $\mathcal{O}(y_\nu^2)$;
- inverse decays: $\ell\,\phi \to N_1$, contributing at $\mathcal{O}(y_\nu^2)$;
- $2 \leftrightarrow 2$ scatterings mediated by N_1 exchange: $\ell\,\phi \leftrightarrow \ell\,\phi$, $\ell\,\phi \leftrightarrow \overline{\ell}\,\overline{\phi}$, $\phi\,\phi \leftrightarrow \ell\,\ell$, $\phi\,\overline{\phi} \leftrightarrow \overline{\ell}\,\ell$. These $\Delta L = 2$ scattering proccesses need to be considered in the computation, otherwise decays and inverse decays would lead to generation of lepton asymmetry even in thermal equilibrium, contradicting Sakharov's conditions. However, the real intermediate states (RIS) have to be subtracted in the first two aforementioned processes in order to avoid double-counting. Indeed, the on-shell s-channel N_1 contributions are already accounted for by decays and inverse decays. The subtraction of RIS from the $2 \to 2$ is a crucial and delicate point in setting up the BEs. For a detailed discussion, see e.g. Refs. [9, 11, 88]. Let us stress that the resonant part of $2 \to 2$ scatterings contributes at order $\mathcal{O}(y_\nu^2)$, while the non-resonant one at order $\mathcal{O}(y_\nu^4)$ [11].

The $2 \to 2$ scatterings involving gauge bosons/top quarks are not considered, e.g. $N\,t \to \ell\,t$ which contributes at order $\mathcal{O}(y_\nu^2 y_t^2)$ and would lead to additional washout in the lepton asymmetry. Indeed, for thermal leptogenesis their effects are negligible in the strong washout regime ($\lesssim 5\%$ of error), because they are subleading with respect to decays and inverse decays (see Refs. [46, 96] for detailed treatment). Therefore, in the remainder of this Chapter we will solve the BEs considering only decays and inverse decays without including the aforementioned $\Delta L = 1$ processes.

Within this framework, the Boltzmann Equations valid at $\mathcal{O}(y_\nu^2)$ can be derived (see App. B.1 for details) and read [11, 88]

$$\begin{cases} \frac{dY_{N_1}}{dz} = -\frac{\gamma_D}{Hsz}\left(\frac{Y_{N_1}}{Y_{N_1}^{eq}} - 1\right) \\ \frac{dY_{B-L}}{dz} = \frac{\gamma_D \epsilon}{Hsz}\left(\frac{Y_{N_1}}{Y_{N_1}^{eq}} - 1\right) - \frac{\gamma_D}{Hsz}\frac{Y_{B-L}}{2Y_l^{eq}} \end{cases} \tag{2.46}$$

where $z = M_1/T$, $H = H(z)$ is the Hubble parameter at temperature T in a radiation-dominated Universe, $Y_{N_1}^{eq}$ and Y_l^{eq} the equilibrium Yields of RHNs and leptons considering the Maxwell-Boltzmann statistics, γ_D is the reaction density of the RHN decay $N_1 \to \ell\,\phi$ defined as [9, 46, 89]

$$\gamma_D \equiv \gamma^{eq}(N_1 \to \ell\phi) \equiv \int d\Pi_{N_1} d\Pi_\ell d\Pi_\phi f_{N_1}^{eq} (2\pi)^4 \delta^4(p_{N_1} - p_\ell - p_\phi) |\mathcal{M}_{N_1 \to \ell\phi}|^2 \,, \tag{2.47}$$

where $d\Pi_i \equiv \frac{d^3p_i}{2E_i(2\pi)^3}$.
The first equation in (2.46) tracks the evolution of Y_{N_1} and the term on the right-hand side accounts for decays and inverse decays. On the other hand, the second equation defines the evolution of the asymmetry Y_{B-L}. Let us highlight that the decays yield the source term for the generation of the asymmetry, while the second term $\frac{\gamma_D Y_{B-L}}{2Y_l^{eq} Hsz}$ quantifies the strength of the washout due to inverse decays. Finally, the second equation makes transparent that the CP-asymmetry parameter ϵ as well as the departure from thermal equilibrium of the RHN trigger the creation of the $B-L$ asymmetry.
The set of coupled Boltzmann Equations (2.46) is implemented and numerically solved, given that [11, 89]

$$\gamma_D = sY_{N_1}^{eq}\frac{K_1(z)}{K_2(z)}\Gamma_D = \frac{T^3}{\pi^2}z^2K_1(z)\Gamma_D \tag{2.48}$$

$$Y_{N_1}^{eq} = \frac{n_{N_1}^{eq}}{s} = \frac{45}{2\pi^4 g_*}z^2K_2(z)\,, \tag{2.49}$$

and

$$Y_l^{eq} = \frac{n_l^{eq}}{s} = \frac{45}{\pi^4 g_*} = \frac{2Y_N^{eq}}{z^2K_2(z)}\,, \tag{2.50}$$

where Γ_D is the decay width in the rest system of N_1 (see Eq. (2.16)), $K_1(z)$ and $K_2(z)$ are the modified Bessel functions of the second kind of first and second order. We numerically solve the BEs in the hierarchical case for $z \in [z_i, 100]$, with $z_i = 10^{-3} \ll 1$. Two different initial conditions for the RHN abundance are considered: zero initial Yield, i.e. $Y_{N_1}(z_i) = 0$, and thermal initial Yield, i.e. $Y_{N_1}(z_i) = Y_{N_1}^{eq}$, represented respectively by blue and red lines in Figs. 2.3 and 2.4. We have also plotted the RHN equilibrium Yield $Y_{N_1}^{eq}$ for reference. Moreover, both weak and strong washout regime are taken into account, with parameters $K = 0.1$ (realized by e.g. $M_N = 10^{10}$ GeV and $y_\nu = 1.88\cdot10^{-4}$) in Fig. 2.3 and $K = 10$ (realized by e.g. $M_N = 10^{10}$ GeV and $y_\nu = 1.88\cdot10^{-3}$) in Fig. 2.4. The parameter K depends on the mass and coupling of RHN through Eq. (2.40).
Eventually, in order to obtain the final baryon asymmetry, $Y_{\Delta B}$, we consider the asymptotic value of Y_{B-L} and then multiply it by the sphaleron conversion parameter c_{sph} (2.28):

$$Y_{\Delta B} = \frac{28}{79}Y_{B-L}\,. \tag{2.51}$$

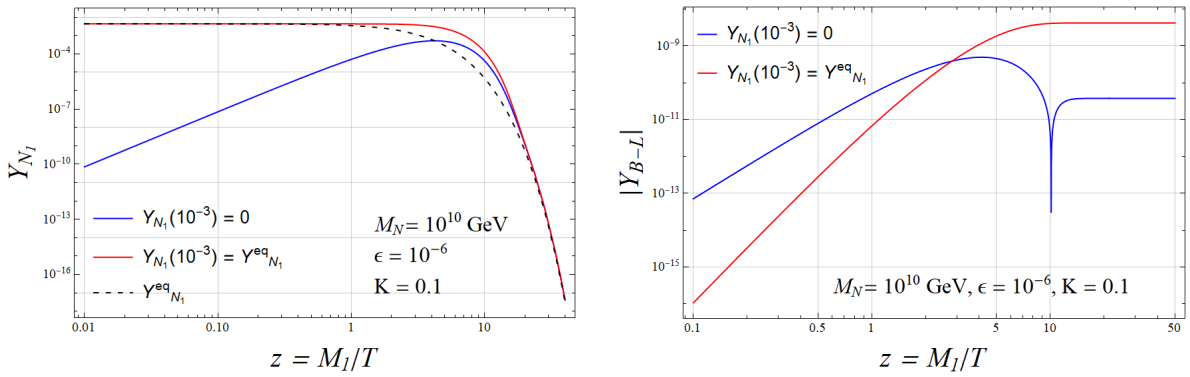

Figure 2.3: Evolution of the N_1 (left panel) and $B-L$ (right panel) Yields as function of z, in the thermal leptogenesis with one RH neutrino. Weak washout with $K = 0.1$, realized by e.g. $M_N = 10^{10}$ GeV and $y_\nu = 1.88 \cdot 10^{-4}$. Comparison zero initial abundance vs thermal initial abundance.

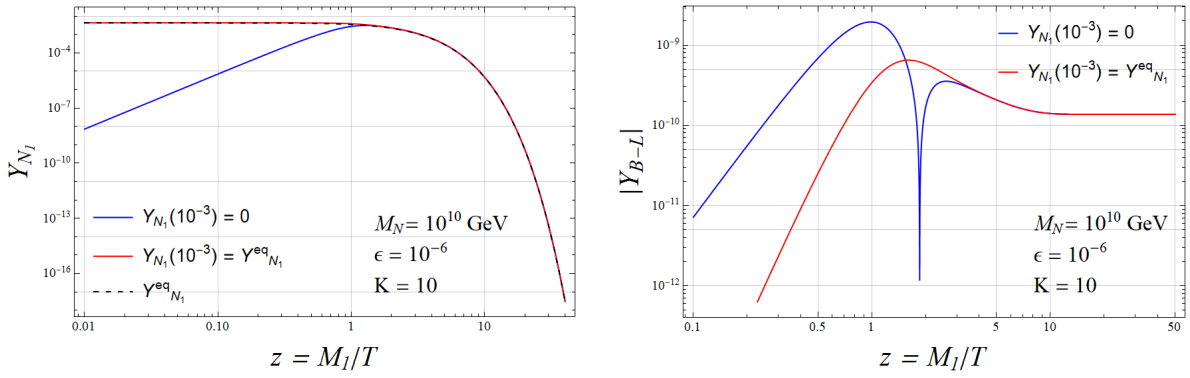

Figure 2.4: Evolution of the N_1 (left panel) and $B-L$ (right panel) Yields as function of z, in the thermal leptogenesis with one RH neutrino. Strong washout with $K = 10$, realized by e.g. $M_N = 10^{10}$ GeV and $y_\nu = 1.88 \cdot 10^{-3}$. Comparison zero initial abundance vs thermal initial abundance.

Now, let us comment the time evolution of the Majorana neutrino's Yield Y_{N_1}: comparing the left panels of Figs. 2.3 and 2.4, a stronger departure from the thermal equilibrium occurs in weak washout regime with respect to the strong washout. This is explained by the fact that, in this scenario, the production of N_1 at high temperatures, i.e. $z < 1$, is only due to inverse decays. Then, in the strong washout regime, the RHN abundance is brought to its equilibrium faster than in the weak washout case, due to the stronger coupling. A $B-L$ asymmetry is generated in the heavy neutrinos decays, since their Yield exceeds the equilibrium Yield. In both regimes, once equilibrium has been achieved, the RHN abundance falls off exponentially for $z \gtrsim 4$, as expected for all non-relativistic particle species in thermal equilibrium [46].

For what concerns the $B-L$ asymmetry, we have plotted its absolute value: indeed, a negative lepton asymmetry is produced at high temperatures by RHN production from inverse decays (in the case of zero initial RHN abundance), until the decays come to dominate over inverse decays, thus reversing the direction of the asymmetry production, and eventually flipping the sign of the asymmetry to positive. This happens at $z \sim 7$ for weak washout (see Fig. 2.3) and at $z \sim 1$ for strong washout (Fig. 2.4). As long as the washout processes are in equilibrium, the asymmetry is partly washed out again. Finally, at $z > 1$, N_1's production is kinematically suppressed, i.e. the RHN abundance begins to fall off exponentially, the washout processes eventually get out of equilibrium at some z_w in the strong washout regime and the $B-L$ asymmetry is frozen in, asymptoting to a final constant value. When $K > 1$, the washout rate plays a dominant role in determining the final asymmetry, as can be seen comparing the right panels of Figs. 2.3 and 2.4.
Now we compare the results obtained with zero (blue lines) and thermal (red lines) initial abundance for the RHNs. For thermal initial abundance, at high temperatures, $z < 1$, the RHN abundance is in equilibrium and when it approaches $z \sim 1$, it gets out-of-equilibrium (this is more evident in the weak washout regime). Moreover, for thermal initial abundance, the asymmetry $|Y_{B-L}|$ does not flip its sign and it continuously increases toward its final value [9]. In addition, we conclude that the initial conditions are significantly relevant only in the case of weak washout, while the strong washout scenario is independent of them. This is reasonable, because in the strong washout case, the RHN abundance is quickly brought to its equilibrium value, thus it is not particularly affected by the initial conditions (either zero or thermal abundance). As motivated in Sect. 2.2, the strong washout regime is the most natural and, in the following, we will assume zero abundance of N_1 as initial condition.

In order to gain a comprehensive understanding of the non-equilibrium process of thermal leptogenesis, it is useful to compare the reaction rates per particles [9],

$$\tilde{\Gamma}_D = \frac{\gamma_D}{Y_{N_1}^{eq} s} \tag{2.52}$$

for decays, and

$$\tilde{\Gamma}_W = \frac{\gamma_D}{2Y_\ell^{eq} s} \tag{2.53}$$

for washout processes. The latters are due to inverse decays and they partially destroy the $B-L$ asymmetry produced, as can be explicitly seen from the second term in the right-hand side of the BE (2.46) describing Y_{B-L}. Plotting the ratio $\tilde{\Gamma}/H$ shows when those processes are in equilibrium, i.e. $\tilde{\Gamma}/H > 1$, and when they are not, i.e. $\tilde{\Gamma}/H < 1$ (see Fig. 2.5). The main difference between the weak and strong washout regime is that in the former, the washout processes are always out-of-equilibrium and the asymmetry produced is not washed out. On the other hand in the latter, both decay

and washout processes are out-of-equilibrium for $z < 0.15$, while at $z \sim 0.15$ the decay comes into equilibrium and, right after (i.e. at larger z), the washout processes come into equilibrium, too. For $1 \lesssim z \lesssim 10$, we have $\tilde{\Gamma}_W > H$: washout processes affect the production of the $B - L$ asymmetry. Eventually, at $z \sim 10$ the washout processes go out-of-equilibrium and the asymmetry is frozen in.

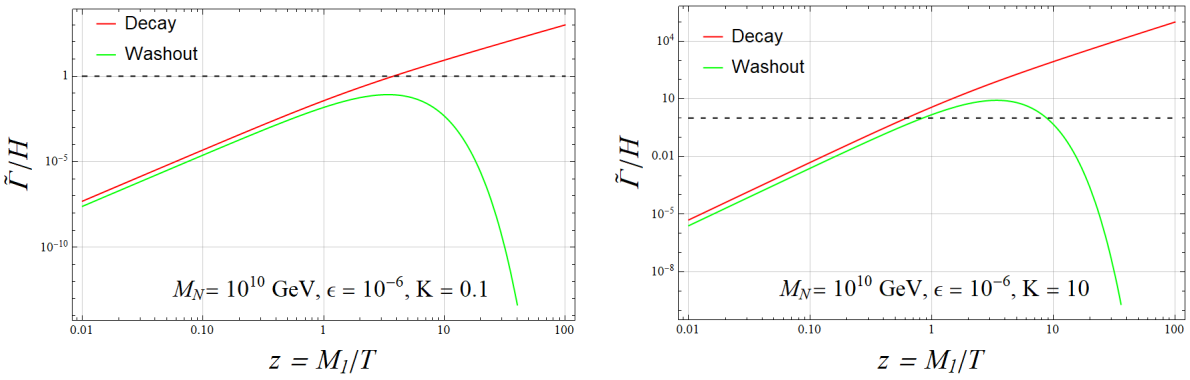

Figure 2.5: Left panel: weak washout with $K = 0.1$, the washout processes are always out-of-equilibrium. Right panel: strong washout with $K = 10$, the washout processes are in equilibrium for $1 \lesssim z \lesssim 10$.

2.4 Resonant leptogenesis

In the simplest leptogenesis scenario, the right-handed Majorana neutrinos are really heavy particles, having hierarchical masses, i.e., $M_1 \gtrsim 10^9$ GeV and $M_{2,3} \gg M_1$. Then, the effects of N_2 and N_3 are neglected, because either $T_{RH} < M_{2,3}$ or N_2, N_3 decouple when N_1 is still in thermal equilibrium [11]. This case was treated previously in the Sect. 2.2. Instead, in this Section we consider the case of resonant RHN masses: the mass difference between two heavy RHN is small (quasi-degeneracy) and comparable to the heavy neutrino decay width Γ_D (see e.g. [94, 97] for reviews). This condition leads to an enhancement of the CP-asymmetry ϵ and, consequently, leptogenesis temperatures of order of TeV are possible [94].
It is useful to analyze the resonant leptogenesis mechanism because we will consider relatively small masses for Majorana neutrinos in the scenario of ALP leptogenesis in Chapt. 4.

We study, for simplicity, the case where only N_2 is quasi-degenerate with N_1. For small mass differences $|M_1 - M_2| \ll \frac{1}{2}(M_1 + M_2)$, the CP-asymmetry is dominated by the self-energy contribution [94]. Specifically, the resonant effect is related to the propagator of N_2 in the third Feynman diagram of Fig. 2.1. A resummation of self-

energy effects is necessary to solve the singularity in the last term of Eq. (2.17). Then, considering the approach based on an expansion of full resummed propagators around their poles developed in the literature [9, 11, 94, 97], the CP-asymmetry parameter ϵ_1 can be expressed as [11, 94]

$$\epsilon_1 = \frac{Im[(y_\nu^\dagger y_\nu)^2_{12}]}{(y_\nu^\dagger y_\nu)_{11}(y_\nu^\dagger y_\nu)_{22}} \frac{(M_1^2 - M_2^2) M_1 \Gamma_{N_2}}{(M_1^2 - M_2^2)^2 + M_1^2 \Gamma_{N_2}^2}\,, \tag{2.54}$$

where

$$\Gamma_{N_2} = \frac{(y_\nu^\dagger y_\nu)_{22}}{8\pi} M_2 \tag{2.55}$$

is the decay width of N_2 at tree-level. Besides the CP-violating parameter due to the decay of N_1, a second CP-asymmetry ϵ_2 coming from the decay of N_2 also contributes to generate the final $B-L$ asymmetry. This ϵ_2 is determined by an expression similar to Eq. (2.54), where the subscripts '1' and '2' are exchanged.
The term $M_1^2\Gamma_{N_2}^2$ in the denominator on the right-hand side of (2.54) can be considered as a regulator, that arises from the fact that Majorana neutrinos are not strictly on-shell because of their finite lifetime [97]. Indeed, in finite-order perturbation theory, this absorptive term $M_1^2\Gamma_{N_2}^2$ is absent, thereby leading to a singular behaviour for ϵ_1 in the mass degenerate limit $M_1 \to M_2$. However, the appearance of this regulating absorptive term due to the finite width of the heavy Majorana neutrinos should be expected on physical grounds and emerges naturally within the resummation approach [94, 98].
Thus, the CP-violating parameter (2.54) depends on the mass splitting between the two RHNs and a resonant enhancement of ϵ_1 (as well as ϵ_2) occurs when the mass difference between N_1 and N_2 is of the order of their decay widths. In particular, the resonance condition reads [97]

$$M_1^2 - M_2^2 \simeq M_1 \Gamma_{N_2}\,, \tag{2.56}$$

and hence,

$$\epsilon_1 \simeq \frac{1}{2} \frac{|Im[(y_\nu^\dagger y_\nu)^2_{12}]|}{(y_\nu^\dagger y_\nu)_{11}(y_\nu^\dagger y_\nu)_{22}}\,. \tag{2.57}$$

Since the following relation holds [98]

$$\frac{|Im[(y_\nu^\dagger y_\nu)^2_{12}]|}{(y_\nu^\dagger y_\nu)_{11}(y_\nu^\dagger y_\nu)_{22}} \leq 1\,, \tag{2.58}$$

if the maximal case of CP-violation was considered, i.e.

$$\frac{|Im[(y_\nu^\dagger y_\nu)^2_{12}]|}{(y_\nu^\dagger y_\nu)_{11}(y_\nu^\dagger y_\nu)_{22}} \simeq 1\,, \tag{2.59}$$

the CP-asymmetry would be of the order of unity, specifically [11]

$$\epsilon_1 \simeq \frac{1}{2}\,. \tag{2.60}$$

Actually, some rather generic scenarios minimally satisfying (2.56) and (2.59), and still having sufficient freedom to describe the light neutrino data (2.1), have been studied in the literature [9, 94]. Thus, it has been proved that an efficient thermal leptogenesis can be achieved at low-scale, e.g. TeV-scale, in presence of a resonance amplification [94]. For instance, if we consider a TeV-scale Majorana neutrino, such low-scale leptogenesis would produce an amount of baryon asymmetry of order

$$Y_{\Delta B} \simeq 10^{-19}\,, \tag{2.61}$$

estimated as in Eq. (2.34), with $\epsilon \simeq 10^{-13}$. Nevertheless, if we apply resonant leptogenesis with two quasi-degenerate RHN masses,

$$M_1 \simeq M_2 \simeq 10^3\,\text{GeV}\,, \tag{2.62}$$

eventually we obtain a value of $Y_{\Delta B}$ which reproduces the experimental value (1.5) with mass degeneracy [94]

$$\frac{M_2 - M_1}{M_1} = 8 \cdot 10^{-10}\,, \tag{2.63}$$

thereby satisfying the resonance condition (2.56).
Let us stress that, in the framework of resonant leptogenesis, we are able for instance to increase the value of the CP-asymmetry ϵ_1 up to the order of unity (2.60) by tuning the mass degeneracy between Majorana neutrino masses. Therefore, resonant leptogenesis allows to obtain a sizable amount of baryon asymmetry, even considering small Majorana masses. The price of this mechanism is to require a considerable fine-tuning of the RHN masses.

Chapter 3

ALP in the Early Universe

In this Chapter, the cosmology of the ALP is investigated. The ALP is considered to be coupled to gluons, top quarks and, in addition, Majorana heavy neutrinos Ns. First, we discuss the ALP production in the Early Universe in Sect. 3.1, focusing in particular on its thermal production in 3.1.1, taking into account the coupling to Majorana neutrinos in 3.1.2 and eventually computing the cosmological ALP Yield coming from either freeze-in or freeze-out is evaluated in Sect. 3.1.3. In Sect. 3.2 the ALP's decay channels are studied.
This Chapter is mainly based on Refs. [99, 100], to which we add the phenomenology due to the ALP couplings to Ns.

3.1 ALP production in the Early Universe

In the Early Universe a generic ALP can be produced either thermally, i.e. from scatterings with particles in the thermal bath, or non-thermally [50, 101]. In particular, the non-thermal production can be due to global cosmic strings [102], i.e. closed string loops shrinking with emitting ALP (spontaneous breaking of approximate $U(1)$ symmetry produces cosmic strings by the Kibble-Zurek mechanism [103, 104]), and string-wall systems, whose stored energy turns into ALP particles [105, 106].
In the following, the non-thermally production is assumed to be negligible with respect to the thermal one, by considering the ALP decay constant greater than the reheating temperature of the Universe after inflation ends: $f_a > T_{RH}$. This condition allows to neglect the ALP production from cosmic strings and domain walls, because topological defects are not produced [50, 101].
Thus, in the following, the thermal production of ALPs is evaluated in order to compute the ALP relic abundance.

3.1.1 Thermal ALP production

We consider the following effective Lagrangian that describes the ALP's couplings at first order in the ALP field a [99]

$$\begin{aligned}\mathcal{L}_a = &\frac{1}{2}\partial_\mu a \partial^\mu a - \frac{1}{2}m_a^2 a^2 - \frac{\alpha_s}{8\pi} C_g \frac{a}{f_a} G^b_{\mu\nu}\tilde{G}^{b,\mu\nu} + \frac{\partial_\mu a}{f_a} C_t \bar{t}_R \gamma^\mu t_R + \\ &+ \frac{\partial_\mu a}{f_a} C_{Q_3} \overline{Q}_3 \gamma^\mu Q_3 + \frac{\partial_\mu a}{f_a} \overline{N}_R \gamma^\mu N_R\end{aligned} \tag{3.1}$$

where $G^b_{\mu\nu}$ is the gluon field strength with its dual $\tilde{G}_{\mu\nu} = \frac{1}{2}\epsilon_{\mu\nu\alpha\beta}G_{\alpha\beta}$, Q_3 is the Weyl spinor of left-handed doublet of the third quark generation, $\alpha_s = g_s^2/(4\pi)$, t_R and N_R are the right-handed top quark and neutrino, the coupling constants C_g, C_{Q_3} and C_t are dimensionless coefficients.
Therefore, thermal scatterings with gluons and top quarks in the primordial plasma unavoidably produce a population of hot ALP. The thermal ALP production rate will be computed in terms of strong interactions and top Yukawa coupling. In order to clarify the top Yukawa coupling, it is convenient to perform a phase redefinition of the SM fields

$$t_R \to e^{i\frac{C_t a}{f_a}} t_R\,, \quad Q_3 \to e^{i\frac{C_{Q_3} a}{f_a}} Q_3\,. \tag{3.2}$$

This redefinition removes the derivative couplings to quarks but it implies a shifting of the gluon coupling $C_g \to C'_g = C_g + C_t - 2C_{Q_3}$, as well as the generation of couplings with electroweak gauge bosons that we will neglect in the following (see Ref. [99] for the detailed expressions). In addition, this transformation induces an ALP phase in the top Yukawa coupling

$$y_t \to y_t e^{iC'_t \frac{a}{f_a}} \tag{3.3}$$

with coupling $C'_t = C_{Q_3} - C_t$. Then, the Lagrangian interaction

$$iC'_t y_t \frac{a}{f_a} \bar{Q}_3\, \phi\, t_R + h.c. \tag{3.4}$$

is generated, which will control the ALP production in the Early Universe.

In order to evaluate the thermal ALP production rate [107], we will follow Ref. [99], which provides an improved computation with respect to previous works.
Let us first discuss the ALP production due to the coupling with gluons. ALPs are produced in the plasma through scatterings involving gluons: $gg \to ag$, $q\overline{q} \to ag$ and $qg \to aq$. The results obtained for these processes point to potential infrared divergences associated with exchange of soft (massless) gluons in the t and u channels. Actually, in the Early Universe the screening effects of the plasma become relevant and, in order to account for such effects, a thermal mass for gluons is introduced [107]. Previous

computations rely on the Hard Thermal Loop (HTL) [108, 109] approximation to treat the thermal gluons [110]: in this method a momentum scale κ_{cut} is introduced such that $g_s T \ll \kappa_{cut} \ll T$, in order to separate soft gluons with momentum transfer of order $g_s T$ from hard gluons with momentum transfer of order T. Therefore, in the region $\kappa < \kappa_{cut}$ the leading order soft contribution is the imaginary part of the thermal axion self-energy with ultraviolet cutoff κ_{cut}, where only one effective HTL-resummed gluon propagator is needed (see Ref. [110]). On the other hand, in the region $\kappa > \kappa_{cut}$, bare gluon propagators can be used since κ_{cut} provides an IR cutoff. Actually, the HTL approximation suffers from limitations: it is only valid in the weak coupling limit $g_s \ll 1$.
This computation made by using the HTL approximation was improved in Ref. [99] by employing the thermal field theory formalism [111]. In this framework, there is no need to introduce the arbitrary splitting scale κ_{cut}. In the general formalism of thermal field theory, the thermal production rate γ_{prod} of a weakly interacting scalar a is equivalently computed from the imaginary part of its propagator π_a as

$$\gamma_{prod} = \frac{dN_a}{dV dt} = -2 \int d\overrightarrow{\Pi} f_B(E) Im\pi_a \tag{3.5}$$

with $\overrightarrow{\Pi} = \frac{d^3p}{2E(2\pi)^3}$. Thermal field theory cutting rules allow to see that, at leading order in strong coupling, Eq. (3.5) is equivalent to the usual summing of all rates for the various tree-level processes that lead to axion production, i.e. S, T, U, X processes in Fig. 3.1 [99]. Thus, instead of computing $|S + T + U + X|^2$, we can calculate the production rate as

$$\gamma_{prod} = \gamma_A + \gamma_B + \gamma_C + \gamma_D \,. \tag{3.6}$$

Since this computation still gives IR divergent results, the thermal effects are resummed by substituting the two-loop thermal diagram D with the one-loop 'Decay' diagram in Fig. 3.2, where the tree-level gluon propagator is replaced by the full thermal gluon propagator at leading order in the strong coupling. This 'Decay' diagram physically describes the decay process of the thermal gluon g_T: $g_T \to g_T a$.

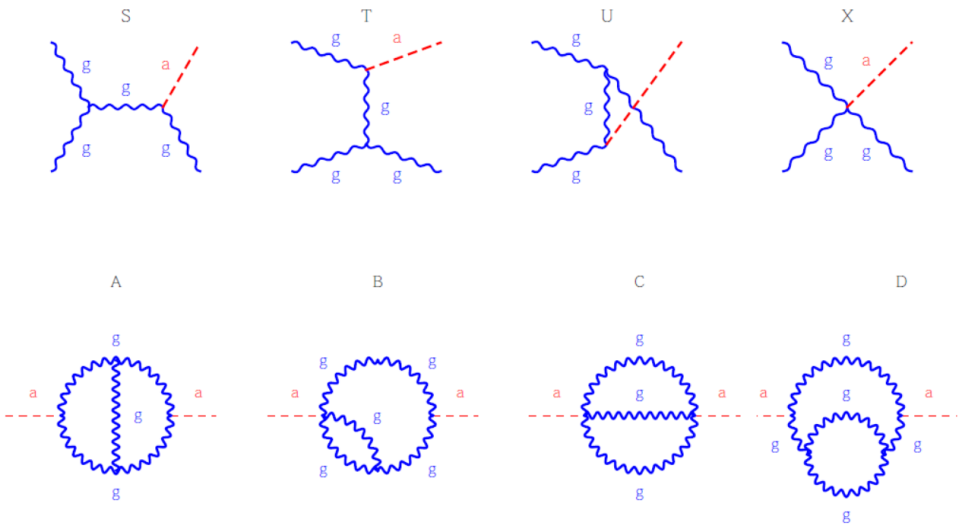

Figure 3.1: The $g\,g \to g\,a$ scattering rate at leading order in the thermal plasma can be obtained either by summing the Feynman diagrams, S,T,U,X, in the upper row, or, equivalently, by summing the imaginary parts of the two-loop thermal diagrams in the lower row. In both cases, the result is infrared divergent, such that proper inclusion of higher order effects is needed [99].

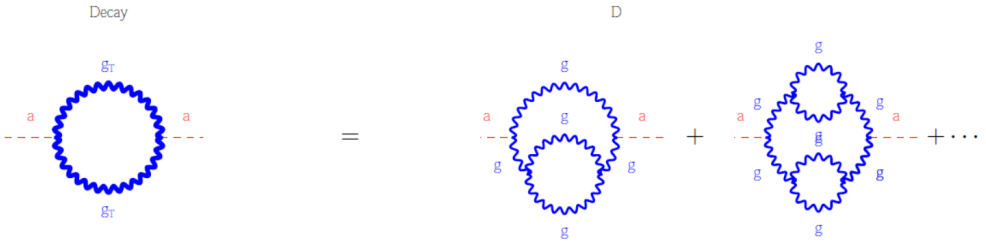

Figure 3.2: Thermal diagram 'Decay' is equivalent to diagram D plus the resummation of higher order diagrams with corrections to gluon propagator. Thick lines denote propagator of the thermal gluon g_T [99].

Going beyond the anomalous ALP coupling to gluons, the interaction in (3.1) also generates a top Yukawa contribution to the ALP thermal production, with processes like $\phi\,t \to a\,t$. Following the computation in [99], the total axion production rate becomes

$$\gamma_{prod} = \frac{T^6\zeta(3)}{(2\pi)^5 f_a^2}\left[37C_t'^2 y_t^2 + 8C_g'^2\alpha_s^2 F_3\left(\frac{m_g}{T}\right)\right], \tag{3.7}$$

where $F_3(m_g/T)$ is a function that parameterizes the axion production rate due to gauge interactions. We conventionally consider $C_t' = C_g' = 1$ and 1-loop approximation for the running of the strong and Yukawa couplings, g_s and y_t.

Finally, we conclude that the top Yukawa ALP production rate dominates the ALP production with respect to the gluon contribution, because it arises at tree-level, while the anomalous ALP couplings arise at loop level [99].

3.1.2 ALP production via coupling to Majorana neutrinos

In Sect. 3.1.1, we have only considered the production of ALP due to the gluon coupling and the top Yukawa coupling. In this Section, we show that the ALP production via coupling to Majorana neutrinos Ns is a subdominant contribution to the total production. The rough estimates of this Section are refined by computing the corresponding ALP Yields in App. C.

Let us consider the last interaction term of the Lagrangian (3.1), which after integrating by parts can be written as $\frac{M_N}{f_a} a \overline{N}_R N_R$: thus, the ALP could be frozen in via interactions with Majorana neutrinos Ns. In particular, the ALP can be produced by the following processes:

1. $NN \to aa$ t-channel:
$$|\mathcal{M}_1|^2 \propto \left(\frac{M_N}{f_a}\right)^4 \tag{3.8}$$

2. $NN \to aa$ s-channel with ALP trilinear vertex:
$$|\mathcal{M}_2|^2 \propto \left(\frac{M_N}{f_a}\right)^2 \left(\frac{T}{f_a}\right)^2 \tag{3.9}$$

3. $\phi N \to \ell a$ t-channel:
$$|\mathcal{M}_3|^2 \propto \left(\frac{M_N}{f_a}\right)^2 y_\nu^2 \tag{3.10}$$

4. $NN \to a$ inverse N decays:
$$\Gamma_N \propto \left(\frac{M_N}{f_a}\right)^2 \frac{T}{8\pi} \tag{3.11}$$

where we have estimated their matrix elements squared and the decay width of the inverse decay. We can evaluate the relevance of these processes by comparing their production of the ALP with the production coming from the top quark interaction. Then, we have to consider the process $\phi\, t \to t\, a$ with matrix element squared

$$|\mathcal{M}_t|^2 \propto \left(\frac{T}{f_a}\right)^2 y_t^2 \tag{3.12}$$

and

$$\Gamma_t \propto \frac{T^3}{8\pi}\left(\frac{y_t}{f_a}\right)^2 . \tag{3.13}$$

As will be explained in Sect. 4.1, only a portion of the parameter space yields results which are suitable for successful ALP leptogenesis. Let us then consider the following benchmark of parameters belonging to the viable parameter space: $y_\nu \simeq 10^{-5}$ GeV, $M_N \simeq 10^4$ GeV, $f_a \simeq 10^{12}$ GeV, $m_a \simeq 10^5$ GeV, $T_R \simeq 10^8$ GeV (this choice will be motivated in 4.1). In that point, ALP production through processes 1, 2, 3, listed above can be estimated as subdominant with respect to the one via top Yukawa coupling:

$$(|\mathcal{M}_1|^2 \simeq 10^{-32}, |\mathcal{M}_2|^2 \simeq 10^{-24}, |\mathcal{M}_3|^2 \simeq 10^{-26}) \ll |\mathcal{M}_t|^2 \simeq 10^{-8} . \tag{3.14}$$

Actually, we can also consider the gluon production of the ALP. We can estimate the matrix element as

$$|\mathcal{M}_g|^2 \propto g_s^6\left(\frac{T}{f_a}\right)^2 \tag{3.15}$$

which at $T = T_{RH}$ turns out to be $|\mathcal{M}_g|^2 \simeq 10^{-9}$. Thus, the squared matrix elements of the processes we are considering are also subdominant with respect to the gluon production of the ALP. It will turn out that ALP production via processes 1, 2, 3 is subdominant with respect to ALP production via top and gluon in the entire parameter space of interest.

Now, we examine the process 4: the inverse decay $N\,N \to a$. We have

$$\frac{\Gamma_t}{\Gamma_N} \propto y_t^2\left(\frac{T}{M_N}\right)^2 \gg 1 \tag{3.16}$$

at $T = T_{RH}$, since $T_{RH} > M_N$. Thereby, we conclude that the top Yukawa coupling freeze-in dominates over the freeze-in coming from the inverse decay at high temperatures, and becomes of the same order when $T \simeq M_N$. Overall, we can then expect that the production of the ALP from the $N\,N \to a$ decays is negligible with respect to the one from the top quark interaction. Therefore, the major contribution to the ALP production comes from the top Yukawa coupling, while the others coming from processes 1, 2, 3, 4 are subdominant and their ALP production is negligible.

Furthermore, we can show that the inverse decays do not re-equilibrate the ALP a, because $\frac{\Gamma_N}{H} > 1$ implies $T < M_N$. Indeed, the ratio $\frac{\Gamma_N}{H}$ is IR dominated and we have

$$\frac{\Gamma_N}{H} \simeq \frac{1}{8\pi}\left(\frac{M_N}{f_a}\right)^2\frac{M_{Pl}}{T} < 1 \quad \text{for} \quad T > \frac{1}{8\pi}\left(\frac{M_N}{f_a}\right)^2 M_{Pl} \simeq \left(\frac{M_N}{10^{-9} f_a}\right)^2 \text{GeV} \tag{3.17}$$

and for our parameter choice we get $\Gamma_N/H < 1$ for $T > 10^2$ GeV. Then, when the inverse decays $N\,N \to a$ come into equilibrium with the thermal bath, Ns are already

non-relativistic and the inverse decays are kinematically forbidden: inverse decays cannot bring the ALP in equilibrium with the primordial plasma.

3.1.3 Cosmological ALP Yield

Once we have computed the thermal production rate γ_{prod} (3.7), we need to evaluate the relic abundance of ALP, i.e. cosmological ALP Yield Y_a, which will be crucial for the following discussion about ALP leptogenesis. We consider the usual scenario of reheating after inflation, where Φ is the inflaton with energy density ρ_Φ and decay width Γ_Φ. Defining the reheating temperature T_{RH} as the temperature at which Γ_Φ equals H_{RH}, we obtain

$$T_{RH} = \left(\frac{45}{4\pi^3 g_*}\Gamma_\Phi^2 M_{Pl}^2\right)^{1/4}, \tag{3.18}$$

where $M_{Pl} = 1.22{\cdot}10^{19}$ GeV is the Planck mass and g_* is the number of relativistic degrees of freedom as defined in (A.3). Let us note that T_{RH} is the starting temperature of the radiation-dominated epoch and effectively the maximal temperature of the Universe, even though $T_{max} > T_{RH}$. Indeed, while higher temperatures exist, particles produced at $T > T_{RH}$ are diluted by the entropy released by inflaton decays, as described by the term $(Z-1) = -\frac{\Gamma_\Phi \rho_\Phi}{4H\rho_R}$ in the Boltzmann Equations for the evolution of the inflaton energy density ρ_Φ and the ALP Yield Y_a [99]

$$\begin{cases} HZz\frac{d\rho_\Phi}{dz} = -3H\rho_\Phi - \Gamma_\Phi\rho_\Phi \\ sHZz\frac{dY_a}{dz} = 3sH(Z-1)Y_a + \gamma_{prod}\left(1 - \frac{Y_a}{Y_{eq}}\right) \end{cases} \tag{3.19}$$

with in this case $z = T_{RH}/T$, $Y_a = \frac{n_a}{s}$, $Y_a'^{eq} = \frac{n_a'^{\,eq}}{s} \simeq 0.00258$, $n_a'^{\,eq} = \zeta(3)T^3/\pi^2$ which accounts for the bosonic nature of the ALP. Actually, in the following we will ignore the statistical quantum factors, approximating the ALP momentum distribution with the classical Maxwell-Boltzmann one. Thus, we will consider the following value for the equilibrium Yield of the ALP: $Y_a^{eq} = \frac{Y_a'^{eq}}{\zeta(3)} \simeq 2.15 \cdot 10^{-3}$. The solution to the BEs (3.19) for the ALP abundance at $T \ll T_{RH}$ is [99]

$$\frac{Y_a}{Y_a^{eq}} = \left(1 + r^{-3/2}\right)^{-2/3} \simeq \begin{cases} r \text{ for } r \ll 1 \\ 1 \text{ for } r \gg 1 \end{cases} \tag{3.20}$$

with

$$r = \frac{2.4}{Y_a^{eq}}\frac{\gamma_{prod}}{Hs}\bigg|_{T=T_{RH}} = 1.7\frac{T_{RH}}{10^7\text{GeV}}\left(\frac{10^{11}\text{GeV}}{f_a}\right)^2 \frac{\gamma_{prod}}{T^6\zeta(3)/((2\pi)^5 f_a^2)}\bigg|_{T=T_{RH}}. \tag{3.21}$$

This means that the ALP, once it is produced, either can be in thermal equilibrium with the plasma ($r \gg 1$) and later it is frozen out at T_d, with relic abundance given by

$Y_a = Y_a^{eq} \simeq 2.15 \cdot 10^{-3}$ (relativistic freeze-out), or it can be produced out of equilibrium with abundance $Y_a = rY_a^{eq}$ ($r \ll 1$), i.e. the ALP is frozen in. In the case of freeze-out, the decoupling temperature can be derived by equaling $r = 1$. In Fig. 3.3, the parameter space of f_a and T_{RH} for ALP's freeze-out and freeze-in is plotted, where the white area corresponds to the freeze-in, with different Yields Y_a depending on the parameters, and the blue one to the freeze-out, with constant Yield $Y_a = Y_a^{eq}$. Fig. 3.4 shows the decoupling temperature T_d in the freeze-out case (dashed lines), which only depends on the value of f_a. Let us note that when the interaction strength increases, i.e. f_a decreases, the freeze-out happens later in time and the decoupling temperature is lower.

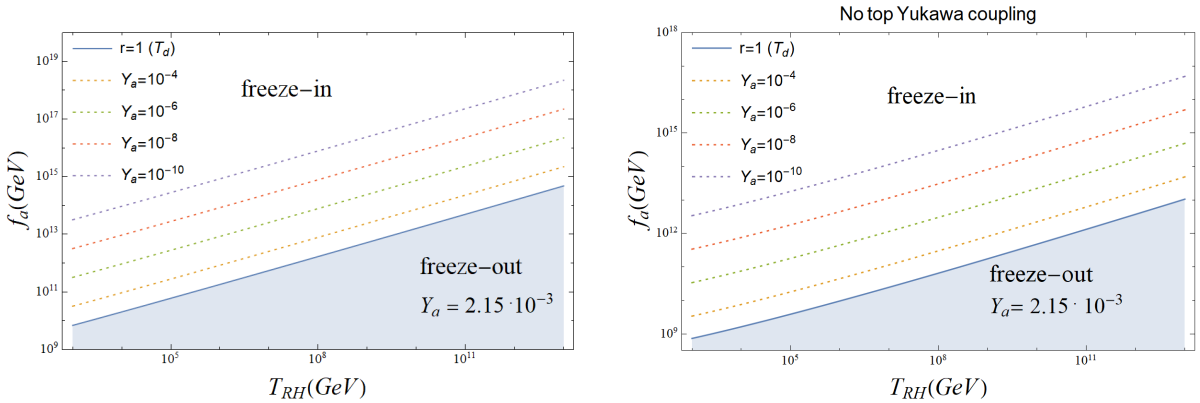

Figure 3.3: Cosmological ALP Yield. Blue area: freeze-out with $Y_a = Y_a^{eq} \simeq 2.15 \cdot 10^{-3}$. White area: freeze-in with $Y_a = rY_a^{eq}$, represented by the dashed lines. Left panel: ALP coupled to both top and gluon. Right panel: ALP coupled to gluon only.

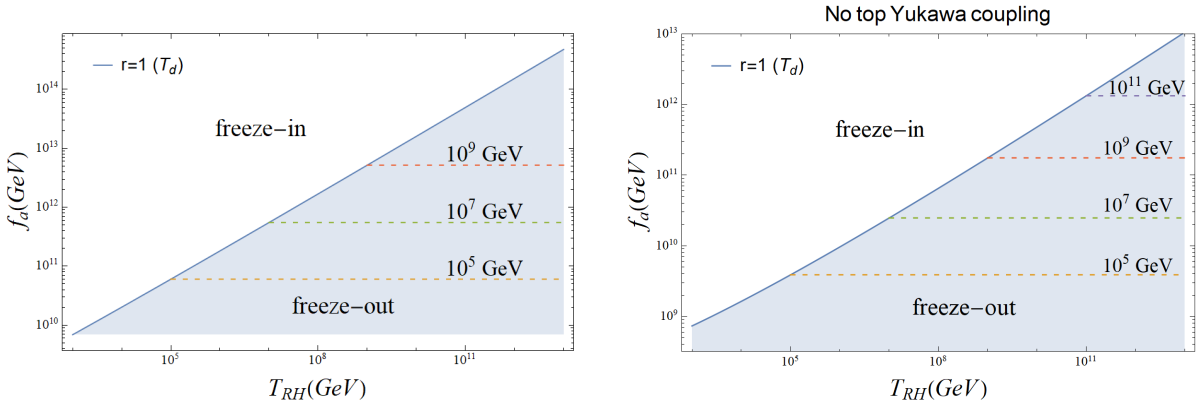

Figure 3.4: Dashed lines represent different values of decoupling (i.e. freeze-out) temperature T_d in the freeze-out case. Blue area: freeze-out with $Y_a = Y_a^{eq} \simeq 2.15 \cdot 10^{-3}$. White area: freeze-in with $Y_a = rY_a^{eq}$. Left panel: ALP coupled to both top and gluon. Right panel: ALP coupled to gluon only.

3.2 ALP's decay

In Sect. 3.1, the ALP production in the Early Universe has been investigated. Now, we study the possible decay channels for the ALP. Due to the interaction terms we are considering (see Eq. (3.1)), it can decay via different channels, see e.g. [72, 100]:

- $a \to g\,g$:
$$\Gamma(a \to gg) = C_g'^2 \frac{\alpha_s^2}{32\pi^3} \frac{m_a^3}{f_a^2}\,; \tag{3.22}$$
- $a \to NN$:
$$\Gamma(a \to N\,N) = \frac{m_a M_N^2}{8\pi f_a^2} \sqrt{1 - 4\frac{M_N^2}{m_a^2}}\,; \tag{3.23}$$
- $a \to \bar{t}\,t$:
$$\Gamma(a \to t\,\bar{t}) = C_t'^2 \frac{m_a m_t^2}{8\pi f_a^2} \sqrt{1 - 4\frac{m_t^2}{m_a^2}}\,. \tag{3.24}$$

We consider as benchmark $M_N = m_a/3$. We have computed the branching ratios of the decay channels
$$Br_g = \frac{\Gamma(a \to gg)}{\Gamma_a}\,, \tag{3.25}$$
$$Br_N = \frac{\Gamma(a \to NN)}{\Gamma_a}\,, \tag{3.26}$$

$$Br_t = \frac{\Gamma(a \to t\,\bar{t})}{\Gamma_a}\,, \tag{3.27}$$

with

$$\Gamma_a = \Gamma(a \to g\,g) + \Gamma(a \to NN) + \Gamma(a \to t\,\bar{t})\,. \tag{3.28}$$

The results are plotted in Fig. 3.5. The dominant channel is $a \to N\ N$.

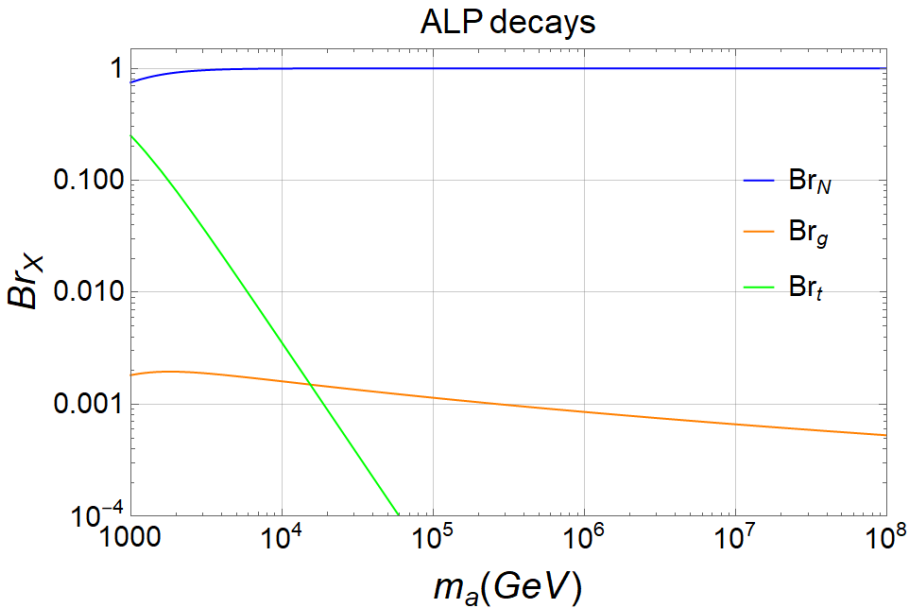

Figure 3.5: Branching ratios of ALP decay channels. Benchmark: $M_N = m_a/3$.

Chapter 4

Non-thermal leptogenesis via ALP

In this Chapter, we investigate how the ALP could affect leptogenesis. Indeed, besides the standard leptogenesis sourced by a thermal population of Majorana neutrinos Ns, non-thermal leptogenesis takes place thanks to Ns produced via ALP decays. Therefore, two different populations of heavy neutrinos are involved in the generating process of the $B-L$ asymmetry.
This Chapter mainly contains the original results of this thesis: in Sect. 4.1 the suitable parameter space for ALP leptogenesis is identified, in Sect. 4.2 the ALP leptogenesis is studied by means of Boltzmann Equations, providing numerical solutions, and in Sect. 4.3 the case of matter-dominating ALP is addressed.

4.1 Parameter space for ALP leptogenesis

We consider the scenario in which the interactions of right-handed neutrinos N_1s are described by the usual Lagrangian (2.31) and the interactions of the ALP by (3.1). Here, we are considering hierarchical Majorana masses (in the following we will denote $N_1 \equiv N$ to simplify the notation), while at the end of Sect. 4.2.3 the resonant case will be taken into account. Let us stress that, after integrating by parts the last term of the ALP Lagrangian (3.1), the interaction term becomes $\frac{M_N}{f_a} a\, \overline{N}_R N_R$.
Before computing the processes that contribute to generate the $B-L$ asymmetry, we identify the parameter space (m_a, f_a) available for a successful ALP leptogenesis:

1. the first constraint is
$$T_d^a < \frac{M_N}{20}\,, \tag{4.1}$$
where T_d^a is defined as the freeze-out temperature of the decay $a \to NN$
$$T_d^a = \frac{M_N}{f_a}\sqrt{\frac{m_a}{8\pi}\frac{M_{Pl}}{1.66\sqrt{g_*}}\sqrt{1-4\frac{M_N^2}{m_a^2}}} \tag{4.2}$$

and it is computed by imposing $\Gamma(a \to NN) = H(T = T_a^d)$.
We require that (4.1) is satisfied in order to have Ns out-of-equilibrium, once they are produced via ALP decay, because this implies that the washout processes are out-of-equilibrium when the ALPs begin to produce the RHNs;

2. the second condition is
$$m_a > 2M_N \,, \tag{4.3}$$
in order to realize the decay $a \to NN$. In the following computations, we take $M_N = m_a/3$ as a benchmark;

3. the last constraint is
$$T_d^a > v_{EW} \simeq 246\text{GeV} \,, \tag{4.4}$$
because the decay of neutrinos has to happen mostly before the electroweak phase transition, when the sphaleron processes are in thermal equilibrium and so induce a baryon asymmetry from the lepton asymmetry generated in our model.

These constraints can be seen in Figs. 4.1 and 4.2, where the available parameter space is the white area. In the case of ALP freeze-in, we have also indicated in the plots the values of T_{RH}, corresponding for instance to $Y_a \simeq 10^{-4}$ (dashed lines). Eventually, let us remind that $T_{RH} > m_a$ in order to produce thermally the ALPs. Then, including the top Yukawa coupling contribution to the ALP production (Fig. (4.1)), we deduce that a favourable range of parameters can be for instance:

- $f_a = (10^{12} \div 10^{13})$ GeV
- $m_a = (10^5 \div 10^6)$ GeV
- $T_R > 10^6$ GeV
- $M_N = (10^4 \div 10^5)$ GeV

and, consequently, $y_\nu = (10^{-5} \div 10^{-5.5})$ (see Eq. (2.7)).

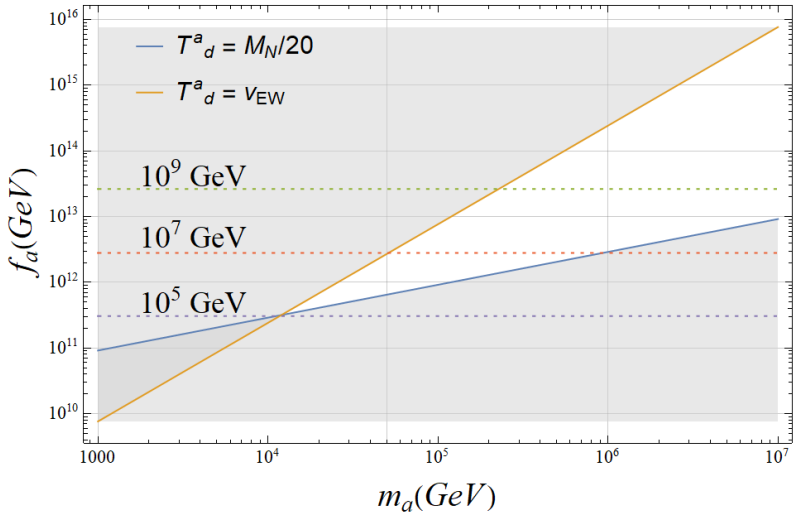

Figure 4.1: Parameter space for ALP leptogenesis: the area where ALP leptogenesis is possible is the white one. Below the orange line ($T^a_d = v_{EW}$), sphalerons are active. Above the blue line ($T^a_d = M_N/20$), the washout processes are estimated to be out-of-equilibrium when the ALP decay $a \to N\,N$ becomes efficient. The dashed lines represent values of reheating temperature such that $Y_a \simeq 10^{-4}$ in the freeze-in case.

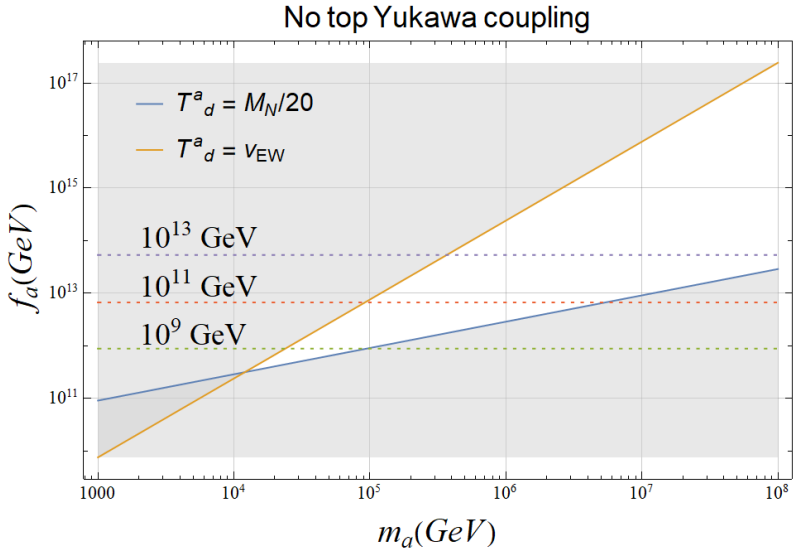

Figure 4.2: Parameter space without considering the top Yukawa coupling for ALP production: the area where ALP leptogenesis is possible is the white one. The dashed lines represent values of reheating temperature T_{RH} such that $Y_a \simeq 10^{-4}$ in the freeze-in case. Other lines as in Fig. 4.1.

4.1.1 Dilution factor

Until now, we have not considered the scenario in which the ALP induces a matter-dominated period in the Universe: indeed, if they are sufficiently heavy and their lifetime is long enough, the ALPs after becoming non-relativistic may temporarily dominate the energy density of the Universe. Usually, when a cold relic decays into SM particles, its energy density is transferred to the SM bath and the non-relativistic degrees of freedom of the decaying particle are converted into relativistic degrees of freedom of the SM. That may inject significant entropy in the SM bath and dilute any pre-existing relic. Let us stress that this changes the behaviour of the scale factor a with respect to the temperature T of the thermal bath. Indeed, the standard scaling

$$a \propto T^{-1} \tag{4.5}$$

is only valid under that assumption that entropy is conserved [112]. Instead, in presence of large entropy injection into the plasma, there can be an epoch during which a grows faster than the standard scaling, i.e. $a \propto T^{-\alpha}$ with $\alpha > 1$.
The evolution of Yields and energy densities of radiation, ALPs and Ns, and the scaling of bath temperature will be studied in Sect. 4.3 by means of BEs. Now let us estimate for which values of the parameter space the ALP may dominate. We consider the dilution factor [113]

$$D_{SM} \equiv \frac{S_{SM}^{aft}}{S_{SM}^{bef}}\,, \tag{4.6}$$

where S refers to the comoving entropy, related to the entropy density s through $S = sa^3$. The superscripts 'bef' and 'aft' denote the times before and after the ALP decay $a \to N\,N$. Thus, for instance the Yield Y_N of the RHN after the decay can be related to the one before via this dilution factor:

$$Y_N^{aft} = \frac{n_N^{aft}}{s^{aft}} = \frac{N_N^{aft}}{S_{SM}^{aft}} = \frac{1}{D_{SM}}\frac{N_N^{bef}}{S_{SM}^{bef}} = \frac{1}{D_{SM}}\frac{n_N^{bef}}{s^{bef}} = \frac{Y_N^{bef}}{D_{SM}}\,, \tag{4.7}$$

where N is the comoving number density ($N = na^3$) and $N_N^{aft} = N_N^{bef}$ because the RHNs are decoupled from the bath when the ALP decays. The dilution factor can be also written as [113]

$$D_{SM} = \left[1 + \left(0.23\frac{Y_a}{Y_a^{FO}}(g_{SM})^{1/4}\frac{g_a}{g_{SM}}\frac{m_a(8\pi)^{1/4}}{\sqrt{\Gamma_a M_{Pl}}}\right)^{4/3}\right]^{3/4} \tag{4.8}$$

where $g_a = 1$, $g_{SM} = 106.75$, Y_a is the ALP yield and Y_a^{FO} is the freeze-out abundance of the ALP.
We now employ the expression in Eq. (4.8) to estimate the region of the parameter space where the dilution induced by the matter-dominated period will be significant in the final

abundance of RHNs (and hence of the $B - L$ asymmetry). We consider as threshold a representative value for the dilution factor, chosen to be $D_{SM} = 1.2$. We then estimate that:

- if
$$D_{SM} \ll 1.2\,, \tag{4.9}$$
the ALP does not dominate the energy content of the Universe and the resulting abundance for the Majorana neutrinos produced via ALP decays is $Y_N = 2Y_a$ at $T = T_d^a$;

- if
$$D_{SM} > 1.2 \tag{4.10}$$
the ALP dominates and $Y_N \neq 2Y_a$. In particular Y_N gets significantly diluted by the factor D_{SM}, obtaining that $Y_N^{aft} = \frac{Y_N^{bef}}{D_{SM}}$.

Then, we can constrain the parameter space by using the dilution factor. Thus, Figs. 4.3, 4.4 and 4.5 show that the parameter space gets divided into two regions: above the green line, matter-domination induced by ALP occurs, below the green line, the ALP does not dominate.

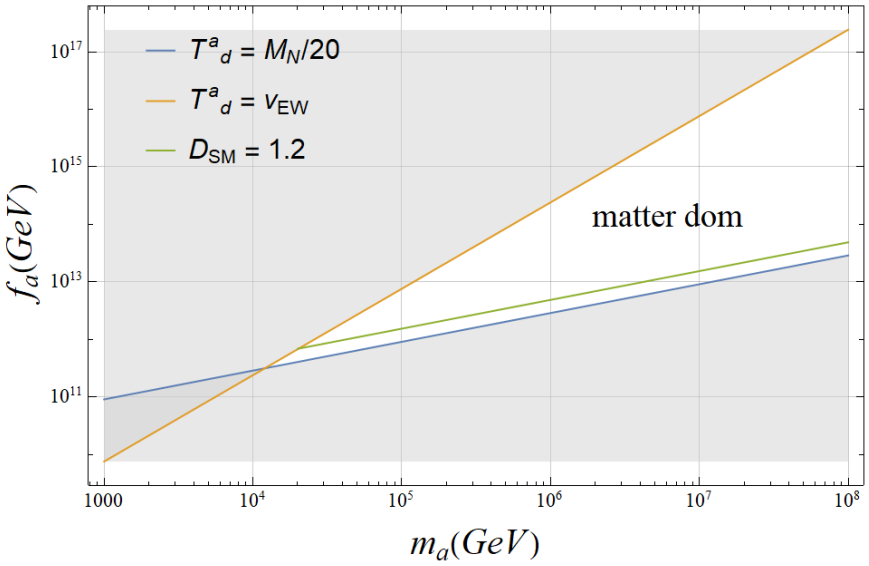

Figure 4.3: The area between the orange and the green lines denotes where dilution significantly occurs (matter-dominated phase). Other lines as in Fig. 4.1. ALP is mainly produced via the top Yukawa coupling and it is frozen out with $Y_a = 2.15 \cdot 10^{-3}$.

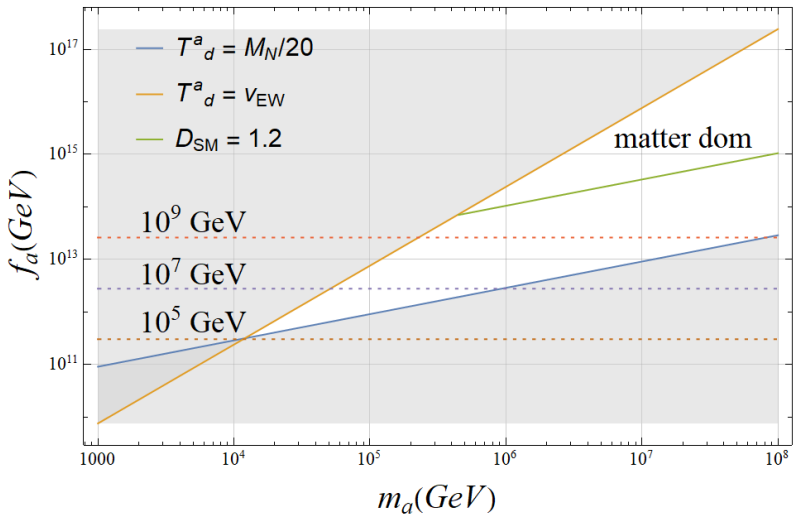

Figure 4.4: The area between the orange and the green lines denotes where dilution significantly occurs (matter-dominated phase). The dashed lines show the reheating temperature values for which the ALP is frozen-in with $Y_a = 10^{-4}$. The ALP is coupled to both top quarks and gluons. Other lines as in Fig. 4.1.

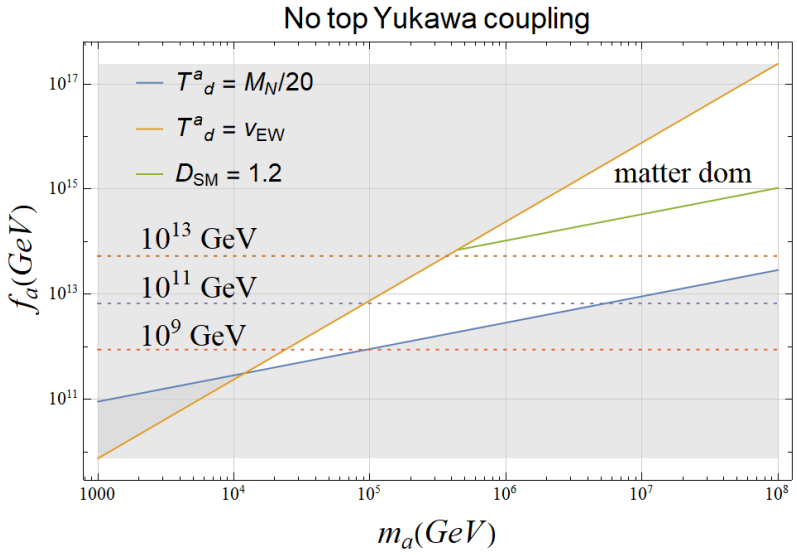

Figure 4.5: Parameter space without considering the top Yukawa coupling for ALP production.The area between the orange and the blue lines denotes where dilution significantly occurs (matter-dominated phase). The dashed lines show the reheating temperature values for which the ALP is frozen-in with $Y_a = 10^{-4}$. Other lines as in Fig. 4.1.

4.2 Boltzmann Equations

Once we have identified the parameter space for the ALP to possibly realize this non-thermal leptogenesis, we need to study this process more in detail and investigate its features. Thus, let us enlighten the differences with respect to thermal leptogenesis:

- the initial Yield of N is not provided by the thermal number density, but by ALP decays such that
$$Y_N^{in} = 2Y_a \,, \tag{4.11}$$
knowing that each ALP dominantly decays to two RHNs;[1]
- in some regions of the parameter space, strong washout effects can be avoided: that happens if, when the ALP decays into two RHNs, the washout processes are already out-of-equilibrium. This can be estimated as first approximation with the condition $T_a^d < M_N/20$. Thus, we can consider
$$\kappa_f \simeq 1 \,. \tag{4.12}$$

Therefore, we first estimate the amount of baryon asymmetry generated in this case via Eq. (2.34) and later evaluate the kinetic equations. Taking into account that the ALP can be frozen out with a Yield (see Sect. 3.1.3)

$$Y_a \simeq 10^{-3} \,, \tag{4.13}$$

and since c_{sph} and ϵ have the same value as in the thermal leptogenesis, we can gain the washout factor with respect to standard case. Indeed, we have in ALP leptogenesis

$$Y_{\Delta B} \simeq 2 \cdot 10^{-3} c_{sph} \epsilon_{max} \,, \tag{4.14}$$

while in thermal leptogenesis usually

$$Y_{\Delta B} \simeq 2 \cdot 10^{-5} c_{sph} \epsilon_{max} \,. \tag{4.15}$$

Thus, overall we can gain a factor ~ 100 with ALP leptogenesis.

Before moving to the precise analysis of ALP leptogenesis by solving numerically the BEs (Sect. 4.2.3), we discuss now some relevant aspects of the dynamics of ALP leptogenesis, such as whether the ALP and the RHN are in kinetic equilibrium with the plasma (Sect. 4.2.1) and whether there is an enhancement of the washout due to boosted Ns (Sect. 4.2.2). The resulting implications will be fundamental in constructing the BEs (see App. B.2 for a detailed derivation).

[1] Note we will have $Y_N^{in} > 2Y_a$ if e.g. one has flavour violating ALP couplings and mass splittings so that processes like $a \to N_1 N_2 (\to 2N_1 a^* \to 4N_1)$ are allowed. For simplicity, we will not consider this possibility in this thesis.

4.2.1 Kinetic equilibrium

Let us start to evaluate the kinetic equations in the scenario of ALP leptogenesis. One crucial assumption in the derivation of the integrated form of the BEs in thermal leptogenesis case is that all the particles are in kinetic equilibrium with the plasma (see App. B.1). Indeed, if this condition is verified, the relation for their phase-space distribution

$$f(k) \approx \frac{n}{n^{eq}} f^{eq}(k)\,, \tag{4.16}$$

can be used [21] and, consequently, the BEs for the total number density can be solved. In the scenario we are considering, the ALP decouples from the plasma and, afterwards, it decays into the Ns. The ALP can undergo either freeze-in or relativistic freeze-out. In both cases, the shape of the phase-space momentum distribution $f(\mathbf{k}, t)$ remains untouched after the freeze-in/freeze-out of the particles [21]. This ensures that the ALP momentum distribution has the same shape of the kinetic equilibrium distribution and Eq. (4.16) can be applied.
For what concerns the N's population, their momentum distribution is due to the ALP decay and, in principle, it will be different from the equilibrium kinetic distribution: since $T_d^a < m_a$ (satisfied by requiring $T_a^d < M_N/20$), the kinetic distribution of Ns is expected to be peaked around $m_a/2$, i.e. all the particles have the same energy

$$E_N \simeq \frac{m_a}{2}\,, \tag{4.17}$$

and so Eq. (4.16) cannot be used. We now discuss some implications of the non-thermal energy of the Ns.

4.2.2 Extra washout due to boosted Ns

In the scenario of ALP leptogenesis, the second population of Ns produced via ALP decays is boosted, i.e. with $E_N \gg T$ (in particular, let us assume that (4.17) holds). This boost could in principle enhance the following $\Delta L = 1$ washout process

$$N + t \to \ell + t\,, \tag{4.18}$$

that proceeds via a ϕ in t-channel. This scattering depletes the population of Ns. Its matrix element squared goes as

$$|\mathcal{M}|^2 \sim y_\nu^2 y_t^2 \frac{E_N T}{m_{\phi,th}^2} \sim y_\nu^2 y_t^2 \frac{E_N}{g_w^2 T}\,, \tag{4.19}$$

where the Mandelstam variable s is $s = E_N T$, g_w is the weak coupling and $m_{\phi,th}$ is the thermal mass of the Higgs boson. This washout process is usually subleading with

respect to the N's decay in standard leptogenesis [11, 46, 96], i.e. assuming that the Ns have $E_N \sim T$. Its cross section can be estimated as

$$\sigma \sim \frac{|\mathcal{M}|^2}{E_N T} \sim \frac{y_\nu^2 y_t^2}{4\pi m_{\phi,th}^2} \sim \frac{y_\nu^2 y_t^2}{4\pi g_w^2 T^2}\,. \tag{4.20}$$

Then, the interaction rate is

$$\Gamma_{Nt\to\ell t} \sim n_t \sigma \sim \frac{y_\nu^2 y_t^2}{16\pi^2 \alpha_w} T\,, \tag{4.21}$$

with $n_t \sim T^3$. Now, we need to verify whether the process (4.18) dominates over the RHN decay. Comparing Eq. (4.21) with the decay width of N's decay

$$\Gamma_{N\to\ell\,\phi} = \frac{y_\nu^2 M_N}{8\pi}\frac{2M_N}{m_a}\,, \tag{4.22}$$

where $\frac{2M_N}{m_a}$ is the Lorentz-boost factor due to the ALP's decay, one obtains

$$\frac{\Gamma_{Nt\to\ell t}}{\Gamma_{N\to\ell\phi}} \sim \frac{y_t^2 T m_a}{4\pi\alpha_w M_N^2}\,, \tag{4.23}$$

with the temperature T of the decay $Nt \to \ell t$. Being conservative, let us assume T to be at most the temperature of the decay $a \to NN$, therefore we arrive at the estimate

$$\frac{\Gamma_{Nt\to\ell t}}{\Gamma_{N\to\ell\phi}} \lesssim \frac{y_t^2}{4\pi\alpha_w}\frac{m_a}{20 M_N}\,. \tag{4.24}$$

We conclude that the process $N\,t \to \ell\,t$ is not dominating over the RHN decay considering the benchmark $M_N = m_a/3$, for which

$$\frac{\Gamma_{Nt\to\ell t}}{\Gamma_{N\to\ell\phi}} \lesssim 0.3\,, \tag{4.25}$$

and it can be neglected in the kinetic equations.

4.2.3 Numerical solution of Boltzmann Equations and computation of baryon asymmetry

In the previous sections, we have discussed the kinetic equilibrium of ALPs and RHNs and estimated the relevance of $\Delta L = 1$ washout processes (4.18) involving boosted RHNs, concluding that the momentum distribution of the Majorana neutrinos cannot be approximated as the equilibrium one and that we can ignore the process (4.18) because its washout effect is negligible with respect to N's decays. Now, we can move on and

implement numerically the derived BEs in order to obtain a more precise computation of the asymptotic value of the $B-L$ asymmetry.

We first consider the simplest case of ALP leptogenesis: we take into account hierarchical heavy neutrino masses and a region of the parameter space corresponding to the case when the ALP does not dominate the energy content of the Universe (leptogenesis from matter-dominating ALP will be treated in 4.3). Therefore, the following set of coupled BEs, for the Yields of the ALP, RHN and $B-L$ asymmetry, can be obtained (we refer the reader to App. B.2 for a complete computation):

$$\begin{cases} \frac{dY_a}{dz} = -Br_N \frac{\gamma_a}{Hsz}\frac{Y_a}{Y_a^{eq}} - Br_g \frac{\gamma_a}{Hsz}\left(\frac{Y_a}{Y_a^{eq}} - 1\right) - Br_t \frac{\gamma_a}{Hsz}\left(\frac{Y_a}{Y_a^{eq}} - 1\right) \\ \frac{dY_N}{dz} = -\frac{\gamma_D}{Hsz}\left(\frac{2M_N}{m_a}\frac{Y_N}{Y_N^{eq}} - 1\right) + \frac{Br_N \gamma_a}{Hsz}\frac{Y_a}{Y_a^{eq}} \\ \frac{dY_{B-L}}{dz} = \frac{\gamma_D \epsilon}{Hsz}\left(\frac{2M_N}{m_a}\frac{Y_N}{Y_N^{eq}} - 1\right) - \frac{\gamma_D}{Hsz}\frac{Y_{B-L}}{2Y_l^{eq}} \end{cases} \tag{4.26}$$

where $z = M_N/T$, s is the entropy density, Br_i are the branching ratios defined in (3.25), (3.26) and (3.27), the reaction density γ_a is

$$\gamma_a = sY_a^{eq}\frac{K_1\left(\frac{m_a}{T}\right)}{K_2\left(\frac{m_a}{T}\right)}\Gamma_a = \frac{T^3}{2\pi^2}\left(\frac{m_a}{T}\right)^2 K_1\left(\frac{m_a}{T}\right)\Gamma_a = \frac{m_a^2 M_N K_1\left(z\frac{m_a}{M_N}\right)\Gamma_a}{2\pi^2 z} \tag{4.27}$$

with Γ_a the total decay width of the ALP defined in (3.28) and

$$Y_a^{eq} = \frac{n_a^{eq}}{s} = \frac{45}{4\pi^4 g_*}\left(\frac{m_a}{T}\right)^2 K_2\left(\frac{m_a}{T}\right) = \frac{45 m_a^2 z^2 K_2\left(z\frac{m_a}{T}\right)}{4\pi^4 M_N^2 g_*}\,. \tag{4.28}$$

In this set of BEs (4.26), the equation for the ALP Yield Y_a has been added on top of the BEs (2.46) describing the thermal leptogenesis. We consider as initial condition for Y_a its freeze-out/freeze-in value so that, in the right-hand side of the differential equation, only the decay processes of the ALP into RHNs, gluons and top-quarks, have been taken into account. Moreover, we have a new source term for Y_N due to ALP decays in the right-hand side.

The factor $2M_N/m_a$ that multiplies the decay interaction rate γ_D is the Lorentz boost factor: it captures the effects of the fact that the momentum distribution of the Majorana neutrinos Ns is not the equilibrium one, but it is peaked around $m_a/2$. Indeed, in the RHN population generated via the ALP decays, the Ns are boosted by the aforementioned factor, which means that they decay later in time and thus, they can generate more $B-L$ asymmetry, being further away from thermal equilibrium and thus less prone to washout effects.

Let us point out that in (4.26), we have not considered the terms due to the inverse reaction $N\,N \to a$, because they are negligible with respect to the Ns decays for our benchmark parameters. Indeed, estimating the rates, we obtain

$$\frac{\Gamma_{N\,N\to a}}{\Gamma_{N\to \ell\,\phi}} \simeq \frac{v_{EW}^2 m_a}{f_a^2 m_\nu} \simeq 10^{-4}\,. \tag{4.29}$$

In order to properly compute the final $B-L$ asymmetry by means of kinetic equations, we need to consider that the first thermal population of Ns undergoes the standard thermal leptogenesis, while a second non-thermal population, consisting of boosted Ns, is created by the ALP's decay and it is the source for ALP leptogenesis. Thus, in order to account for the different evolution of these two population of RHNs, it is convenient to use two different sets of BEs.
We implement the BEs (2.46) describing thermal leptogenesis (i.e. with thermal population of Ns) for $z \in [10^{-3}, 13]$, with initial conditions $Y_N(10^{-3}) = Y^{th}_{B-L}(10^{-3}) = 0$, and the BEs (4.26) describing ALP leptogenesis (i.e. with boosted population of Ns) for $z \in [13, 150]$, with initial conditions $Y_a(13) = Y^{eq}_a$ (ALP is relativistically frozen out), $Y_N(13) = Y^{eq}_N$ and $Y_{B-L}(13) = Y^{th}_{B-L}(13)$. Then, gluing these different solutions, we find the behaviour of Y_N and Y_{B-L} with respect to z.
We checked that the juncture point can be chosen in the range $z \in [10, 14]$, without affecting the results. It is important to stress that it cannot be considered a value of z greater than the one corresponding to the moment when the ALP decay comes into equilibrium (i.e. $z \sim 14$), becoming efficient (see Fig. 4.9). In addition, it is convenient not to choose $z < 10$, because at that time the ALP leptogenesis BEs (4.26) do not properly model the production of thermal population of Ns coming from inverse decays: indeed, we would have a greater abundance of Ns due to the boost factor. Thus, we have chosen a value lying in the aforementioned range, e.g. $z = 13$, as juncture point and we have verified that the final asymptotic value of Y_{B-L} does not depend on the choice of the juncture point. Eventually, at $z = 13$, the thermal population of Ns can be considered as negligible, i.e. $Y_N \simeq 10^{-7}$.
In Fig. 4.6, the ALP Yield Y_a has been plotted, starting from $z = 10^{-3}$, where we see that after $z \simeq 20$ it is exponentially suppressed, i.e. it decays as non-relativistic matter. Fig. 4.7 shows the evolution of the RHNs, where the bump due to the ALP decay is visible at $z \simeq 20$. In Fig. 4.8, the solution tracking the $B-L$ asymmetry is plotted: the gain with respect to thermal leptogenesis for the same choice of parameters is manifest.

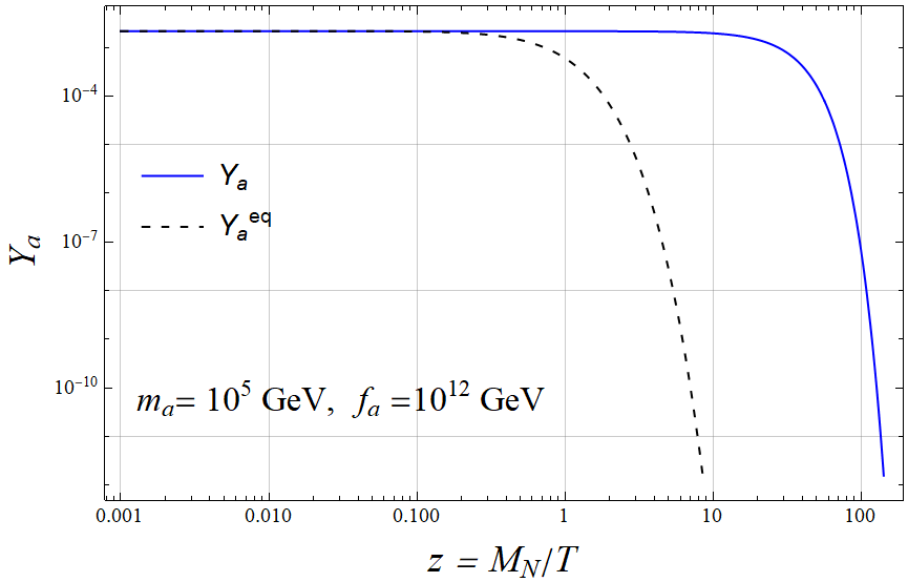

Figure 4.6: ALP Yield as function of z. It is frozen out with initial abundance $Y_a = Y_a^{eq} = 2.15 \cdot 10^{-3}$.

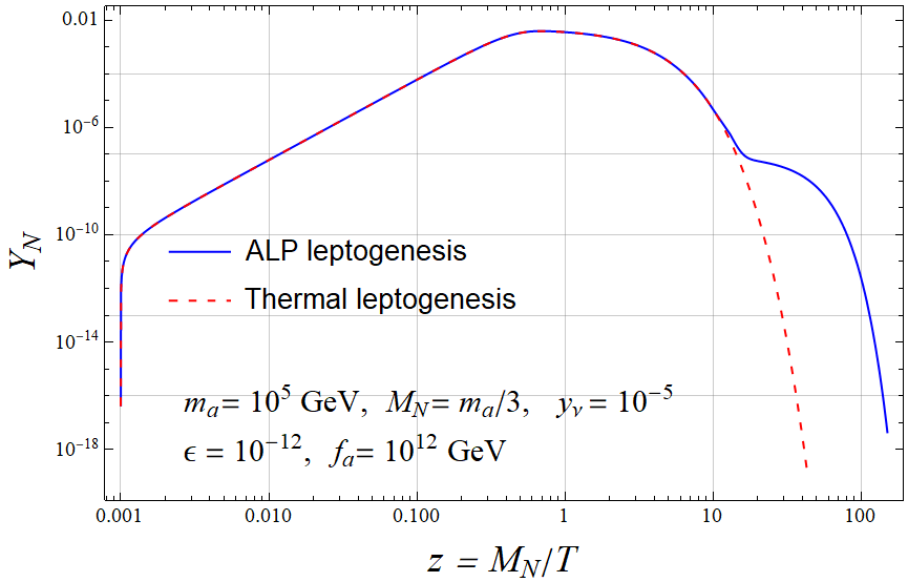

Figure 4.7: ALP leptogenesis: Majorana neutrino Yield as function of z. Comparison between thermal and ALP leptogenesis with same parameters.

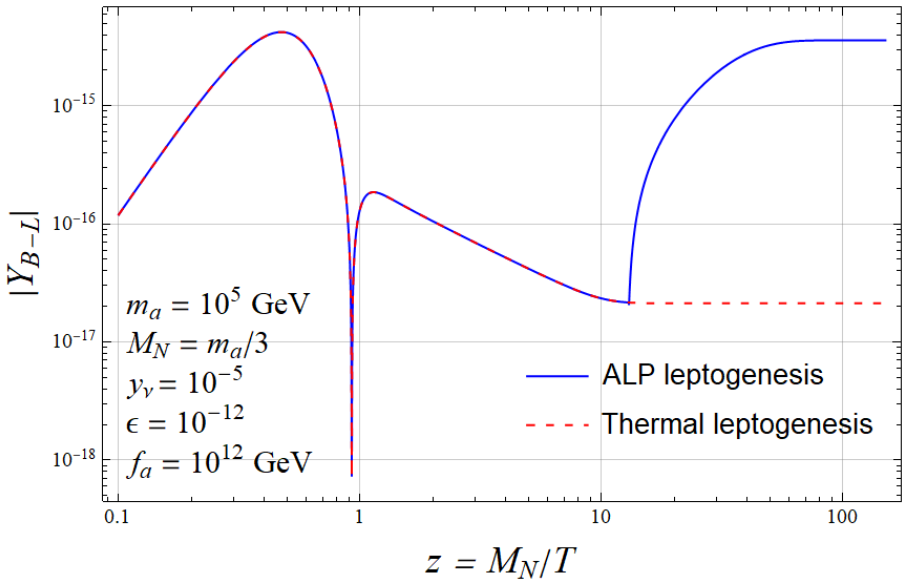

Figure 4.8: ALP leptogenesis: $B-L$ Yield as function of z. Comparison between thermal and ALP leptogenesis: one sees that ALP leptogenesis avoids the strong washout effects of standard thermal leptogenesis, and thus allows to obtain a baryon asymmetry larger than more than two orders of magnitude for the same values of parameters.

To understand better the physical origin of the difference between our proposed ALP leptogenesis and the standard one, in Fig. 4.9 the ratios $\tilde{\Gamma}/H$ are plotted as functions of $z = \frac{M_N}{T}$, with:

$$\tilde{\Gamma}_{N\to\ell\phi} = \frac{\gamma_D}{sY_N^{eq}}, \tag{4.30}$$

$$\tilde{\Gamma}_{a\to NN} = \frac{\gamma_{a\to NN}}{sY_a^{eq}}, \tag{4.31}$$

$$\tilde{\Gamma}_W = \frac{\gamma_D}{2sY_l^{eq}} = \frac{\gamma_D}{4sY_N^{eq}} z^2 K_2(z)\,. \tag{4.32}$$

As long as washout processes are in equilibrium ($\tilde{\Gamma}_W > H$), the $B-L$ asymmetry is partially washed out again. The crucial point of ALP leptogenesis is that, for some regions of parameter space, the washout processes go out of equilibrium ($\tilde{\Gamma}_W < H$) before the ALP decay comes into equilibrium ($\tilde{\Gamma}_{a\to N\,N} > H$). This means that, when the ALP decay starts producing RHNs, the washout processes are already ineffective. This explains the gain that ALP leptogenesis mechanism can achieve.

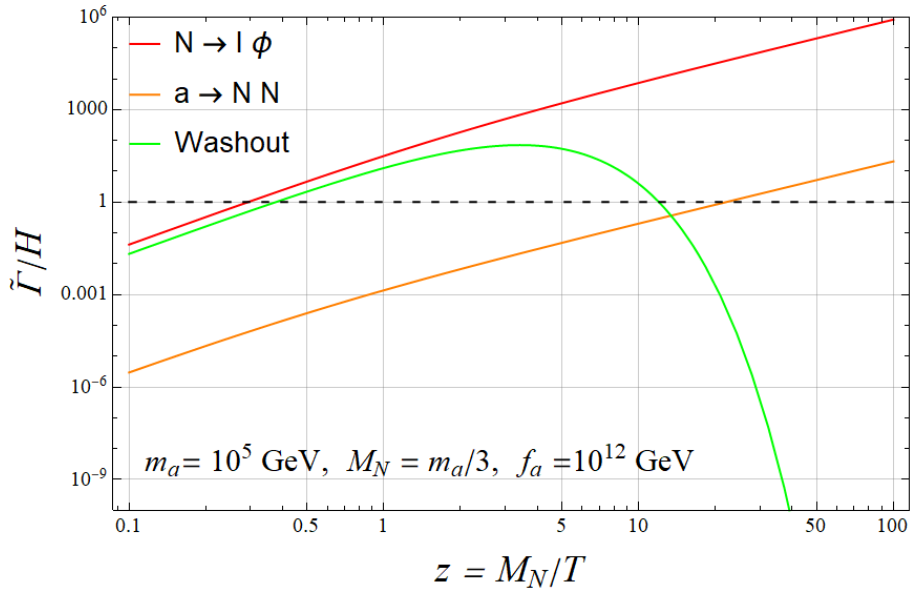

Figure 4.9: ALP leptogenesis: the rates $\tilde{\Gamma}$ of N's decay (red line), ALP's decay (orange line) and washout processes,i.e. inverse decay of N(green line), are compared to Hubble parameter H. The dashed black line corresponds to $\tilde{\Gamma}/H = 1$. Above that line, processes are in thermal equilibrium with the plasma. Below that line, processes are out-of-equilibrium. The advantage of ALP leptogenesis is that we can avoid washout effects for some regions of parameter space. This is explicated by this plot: washout processes are out-of-equilibrium when the ALP's decay comes into equilibrium.

From Fig. 4.8, we see that, despite the gain of a factor ~ 100 with respect to thermal leptogenesis, the amount of $B-L$ asymmetry produced, $Y_{B-L} \simeq 2 \cdot 10^{-15}$, is still not enough to reproduce the observed value of baryon asymmetry (1.5). We can apply to ALP leptogenesis the resonant formalism, addressed in Sect. 2.4, in order to generate the observed value of $Y_{\Delta B}$. Indeed, in this case we are dealing with the benchmark parameter $M_N \simeq 10^4$ GeV, and successful resonant leptogenesis allows to consider Majorana neutrino masses down to $\mathcal{O}(100)$ GeV-scale (see e.g. Refs. [9, 94, 114]). This ensures that, if we consider in our scenario of ALP leptogenesis two RHNs, N_1 and N_2, supposing that the ALP democratically couples to them, i.e. same coupling strength[2] ,

$$\Gamma(a \to N_1\, N_1) \simeq \Gamma(a \to N_2\, N_2)\,, \tag{4.33}$$

there exist a parameter space where N_1 and N_2 have quasi-degenerate masses, i.e. $|M_1 - M_2| \ll \frac{1}{2}(M_1 + M_2)$, and thereby that produces a resonantly enhancement of the CP-violating parameter e.g. ϵ_1, for a certain value of mass splitting comparable

[2] This is motivated e.g. in scenario of supersymmetry breaking and gauge-mediation, where the couplings of the R-axion are flavour-diagonal, since gauge interactions are flavour-blind.

with their decay widths. Thus, the value of $Y_{\Delta B} \simeq 10^{-10}$ can be obtained, reproducing the experimental data (1.5), and ALP resonant leptogenesis turns out to be successful. A proper treatment of ALP resonant leptogenesis would imply to keep track in the BEs of the evolution of the two RHNs, N_1 and N_2, whose decays produce a total CP-asymmetry $\epsilon = \epsilon_1 + \epsilon_2$. However, the detailed study of resonant aspects of ALP leptogenesis is beyond the scope of this thesis and it is left for future works. Nevertheless, we can provide a rough estimate making some simplifying assumptions. Indeed, the resulting Y_{B-L} asymmetry in resonant leptogenesis can be analytically approximated to depend only on one CP-asymmetry parameter in case of strong washout regime (see Ref. [115] for the precise analytic approximation). Thus, we assume to simplify the picture and solve the BEs (4.26) considering effectively only one RHN with CP-violating parameter ϵ_{eff}. Hence, as first approximation, we can estimate that a value of

$$\epsilon_{eff} \simeq 10^{-7} \tag{4.34}$$

can produce the observed BAU. Numerical results of ALP resonant leptogenesis are plotted in Figs. 4.10 and 4.11.

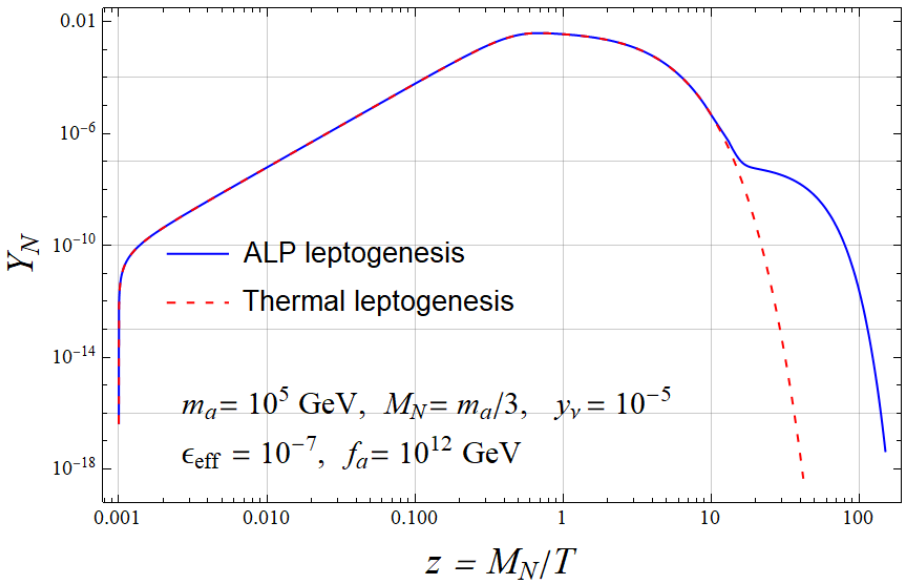

Figure 4.10: Resonant ALP leptogenesis with $M_{1,2} \simeq 10^4$ GeV. RHN Yield as function of z, with zero initial abundance for RHNs, $Y_N(10^{-3}) = 0$, as initial condition.

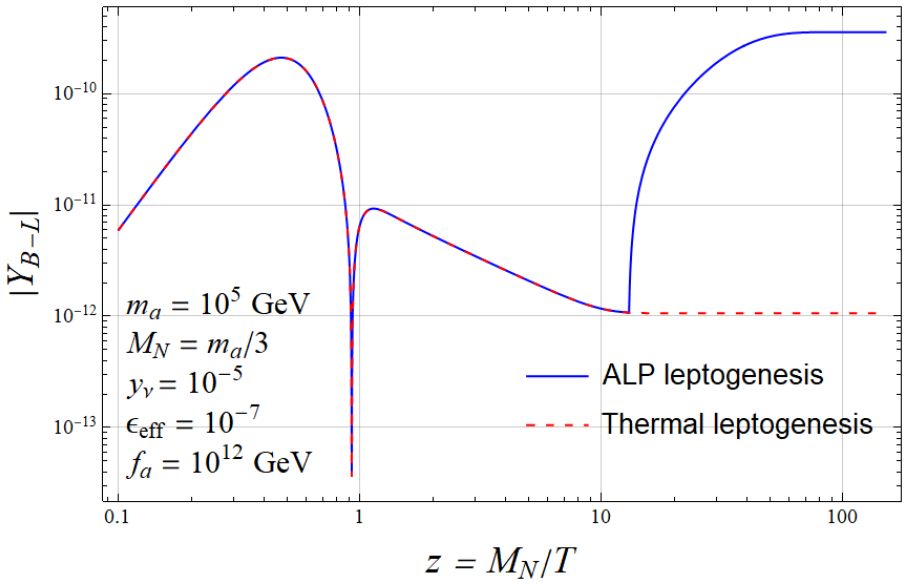

Figure 4.11: Resonant ALP leptogenesis with $M_{1,2} \simeq 10^4$GeV. $B-L$ Yield as function of z, with zero initial abundance for RHNs, $Y_N(10^{-3}) = 0$, as initial condition. The advantages of ALP resonant leptogenesis are manifest: one sees that this mechanism can avoid the strong washout effects of standard thermal leptogenesis, and thus allows to obtain a baryon asymmetry larger than more than two orders of magnitude for the same values of parameters. Therefore, we expect that a smaller resonant enhancement is needed with respect to thermal leptogenesis with same parameter values. Eventually, the asymptotic value of the $B-L$ asymmetry, for the ALP resonant leptogenesis (blue solid line), reproduces successfully the experimental data of the BAU (1.5).

4.3 Leptogenesis from a matter-dominating ALP

In the previous Section, we have considered a region of parameter space corresponding to a non-dominating ALP. Instead, in this Section, we explore the region of parameter space where the ALP, once it becomes non-relativistic, induces an early epoch of matter-domination and investigate how it could affect the ALP leptogenesis. Intuitively, we expect that the $B-L$ asymmetry will get diluted as well as the population of Ns coming from the ALP's decay.
We assume that the total energy density of the Universe consists of three components

$$\rho_{tot} = \rho_R + \rho_a + \rho_N \,, \tag{4.35}$$

where the relativistic component is ρ_R, containing all the SM relativistic particles, while the non-relativistic one is made up of ρ_a and ρ_N. We consider that, initially, the Universe

is radiation-dominated ($\rho_R \gg \rho_{a,N}$), i.e. $T \propto a^{-1}$ [112]. Let us highlight here that the Hubble parameter $H(t)$, with cosmic time t, depends on the energy content of the Universe via the first Friedmann equation [21]

$$H(t) = \frac{\dot{a}(t)}{a(t)} = \frac{1}{M_{Pl}}\sqrt{\frac{8\pi\rho_{tot}}{3}} \tag{4.36}$$

with $M_{Pl} = 1.2 \cdot 10^{19}$ GeV. In order to follow the evolution of the energy densities ρ_i of the different components, we have to solve the following set of BEs

$$\begin{cases} \dot{\rho}_a = -3\rho_a - \frac{\Gamma_a}{H}\rho_a \\ \dot{\rho}_N = -3\rho_N + \frac{Br_N\Gamma_a}{H}\rho_a - \frac{\Gamma_D}{H}\rho_N \\ \dot{\rho}_R = -4\rho_R + \frac{(Br_g+Br_t)\Gamma_a}{H}\rho_a + \frac{\Gamma_D}{H}\rho_N \end{cases} \tag{4.37}$$

where the derivatives are computed with respect to the natural logarithm of the scale factor a, $\dot{\rho} = \frac{d\rho}{d(lna)}$, and the factor $-4\rho_R$ ($-3\rho_{a,N}$) accounts for the scaling behaviour of radiation (matter). This set of equations (4.37) is modelled in a similar way as the simplest case of BEs mostly studied in the literature (e.g. Ref. [112]), in which dark matter (non-relativistic component) directly decays into radiation (relativistic component). In this basic case, during the matter-dominated phase induced by dark matter, the temperature of the thermal bath scales as [112]

$$T \propto a^{-3/8}\,. \tag{4.38}$$

However, our case of interest has some peculiar characteristics: indeed, the ALP can decay into radiation both directly, via the term

$$\frac{(Br_g + Br_t)\Gamma_a}{H}\rho_a\,, \tag{4.39}$$

and indirectly, decaying first into RHNs through

$$\frac{Br_N\Gamma_a}{H}\rho_a\,, \tag{4.40}$$

and then, the RHNs decay into radiation via the term

$$\frac{\Gamma_D}{H}\rho_N\,. \tag{4.41}$$

In order to solve the system (4.37), the energy densities are expressed as functions of the ratio $\frac{a}{a_0}$, where a_0 corresponds to the temperature value T_0 of the plasma at which the ALP is deeply non-relativistic, i.e. $T_0 = m_a/10$. Thus, the following initial conditions are considered

- $\rho_a(a_0/a_0) = \rho_a(1) = m_a Y_a s = m_a Y_a \frac{2\pi^2}{45} g_{*s}(T_0) T_0^3$;
- $\rho_N(1) = 0$;
- $\rho_R(1) = \frac{\pi^2}{30} g_*(T_0) T_0^4$.

4.3.1 Temperature scaling

We first study the scaling behaviour of the temperature during the early matter-dominated epoch in this scenario. In order to highlight the possible differences with respect to the standard case in which the ALP (e.g. dark matter) decays directly into radiation, we consider a long matter-dominated phase with high values for f_a, m_a and Y_a, e.g. $f_a = 10^{16}$ GeV, $m_a = 10^7$ GeV and $Y_a = 10^{-1}$. Thus, we numerically solve the BEs (4.37) and plot the temperature of the plasma

$$T = \left(\frac{30}{\pi^2 g_*}\rho_R\right)^{1/4}, \tag{4.42}$$

in Fig. 4.12, with $g_* = g_*^{SM} = 106.75$. For comparison, we also plot the results coming from the case most often considered in the literature (see e.g. Ref. [112])

$$\begin{cases} \dot{\rho}_a = -3\rho_a - \frac{\Gamma_a}{H}\rho_a \\ \dot{\rho}_N = 0 \\ \dot{\rho}_R = -4\rho_R + \frac{\Gamma_a}{H}\rho_a \end{cases} \tag{4.43}$$

In Fig. 4.12 we compare the two cases, Eqs. (4.43) and (4.37) with initial conditions as specified in the text. One sees that the matter-dominated epoch induces a change of the slope of temperature T. In particular, we see that the two cases provide same results: the temperature of the bath goes as $T \sim a^{-3/8}$ during the matter-dominated epoch, while it scales as $T \sim a^{-1}$ during the radiation-dominated period.

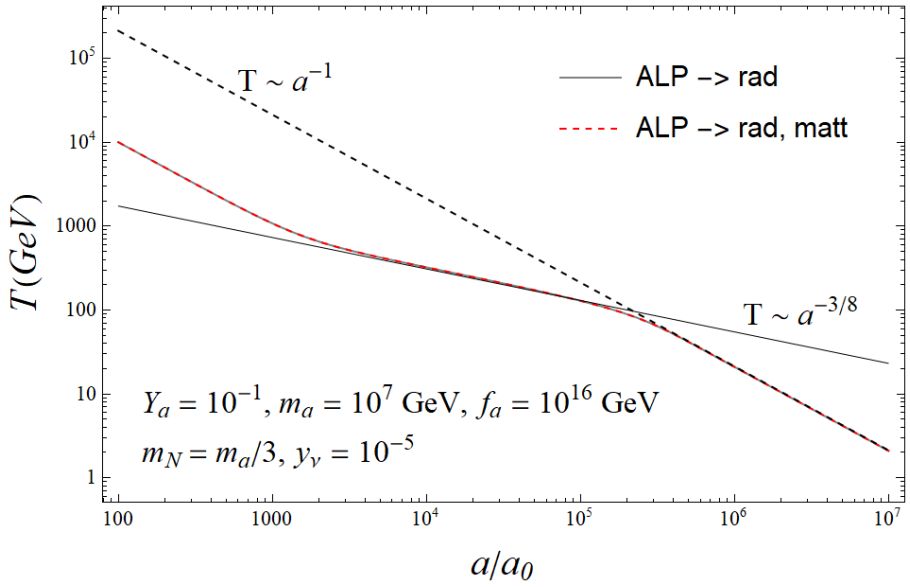

Figure 4.12: Bath temperature scaling with respect to scale factor in scenarios of early matter-domination induced by the ALP. The gray line denotes the standard case, in which the ALP only decays directly into radiation, while the dashed red one the case in which it also decays into non-relativistic matter, i.e. RHNs (dominant channel), that is relevant for ALP leptogenesis. The gray line and the dashed red line actually overlap.

Since the ALP mostly decays into RHNs, in order to explore its matter-domination phase in a more general way, we can also take into account the case in which the dominant channel is $\Gamma_{a\to SM}$ (ALP decays into top/antitop and gluons), e.g.

$$\Gamma_{a\to SM} = 20\,\Gamma_{a\to NN}\,. \tag{4.44}$$

Thus, the ALP mostly decays into radiation. As shown in Fig. 4.13, in this case the ALP decays earlier and, hence, the slope of the temperature T changes from $T \propto a^{-1}$ to $T \propto a^{-3/8}$ earlier with respect to the case in which the ALP mostly decays into non-relativistic RHNs. However, the slope of T turns out to be the same as the basic case. For completeness, the energy densities are shown in Fig. 4.14, where the results in the case defined by Eq. (4.44) are represented by dashed lines. Let us stress that the matter-dominated period occurs when

$$\rho_a > \rho_R\,. \tag{4.45}$$

Having understood how early matter-domination by the ALP affects the evolution of the various cosmological quantities in a benchmark case that made this task easy to visualize, we now turn to study its impact on the parameter space relevant for ALP leptogenesis.

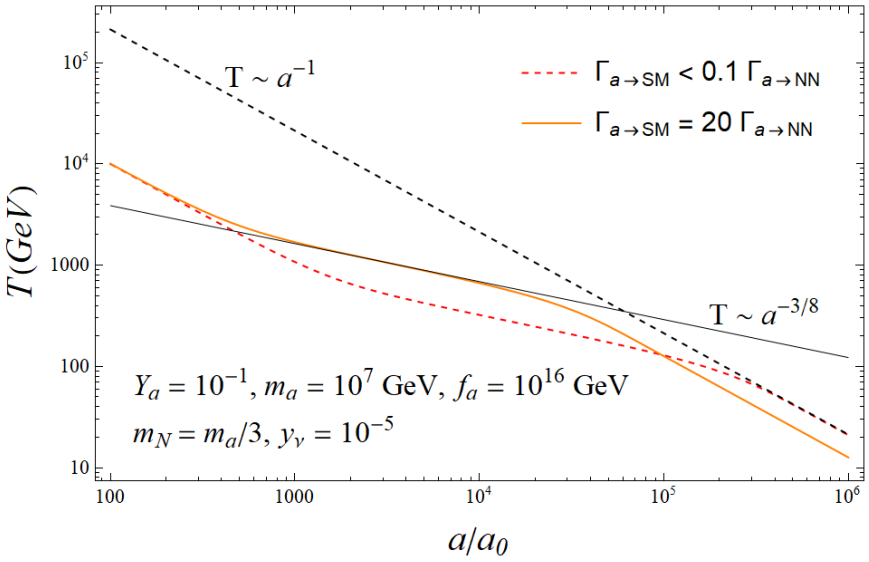

Figure 4.13: Temperature as a function of scale factor a/a_0 in scenarios of early matter-domination induced by the ALP. The cases in which the dominant channel is either $\Gamma_{a\to NN}$ (relevant for ALP leptogenesis) or $\Gamma_{a\to SM}$ are plotted respectively as dashed red and orange lines.

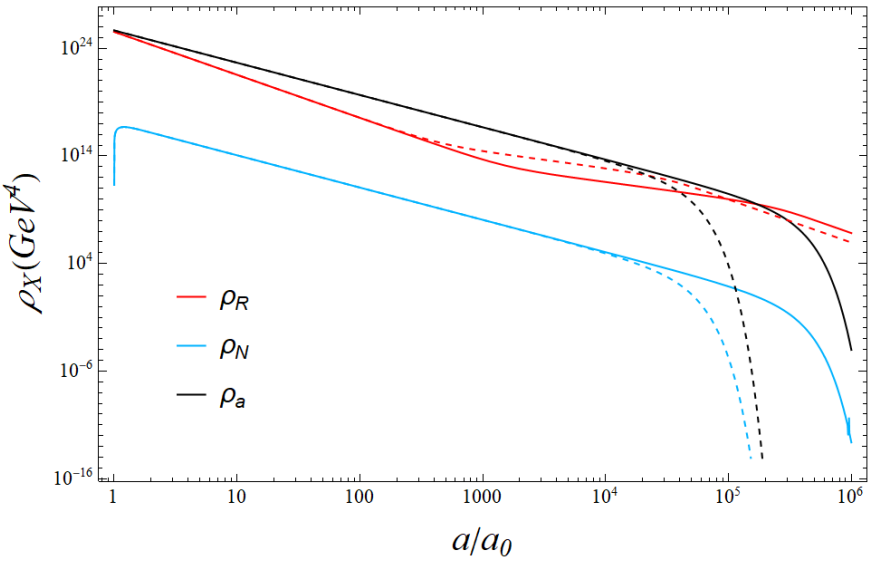

Figure 4.14: Energy densities of radiation, Majorana neutrinos and ALP as functions of a/a_0 in scenarios of early matter-domination induced by the ALP. Solid and dashed lines refers to cases $\Gamma_{a\to SM} < 0.1\Gamma_{a\to NN}$ (relevant for ALP leptogenesis) and $\Gamma_{a\to SM} = 20\Gamma_{a\to NN}$, respectively.

4.3.2 Dilution in ALP leptogenesis

We now explore how the period of matter-domination induced by the ALP may affect the ALP leptogenesis. In order to achieve this goal, we can consider to plot the Yields $Y_i = n_i/s$ of a, N and radiation, with number densities

$$n_a = \frac{\rho_a}{m_a}\,, \qquad n_N = \frac{\rho_N}{m_N}\,, \qquad n_R = \frac{\zeta(3) g_*}{\pi^2} T^3 \tag{4.46}$$

and entropy density

$$s = \frac{2\pi^2}{45} g_{*s} T^3\,, \tag{4.47}$$

where the radiation temperature T is defined by Eq. (4.42). It is also enlightening to compute the total comoving entropy $S = sa^3$, before and after the matter-dominated period, in order to evaluate the entropy injection and identify the exact value of the dilution factor D_{SM}, which is proportional to the ratios of entropies before and after the period of matter-domination (see Eq. (4.6)) and was previously estimated via Eq. (4.8) in Sect. 4.1.1. For instance, we choose a region of parameter space where matter-domination is expected: $f_a = 10^{15}$ GeV, $m_a = 10^7$ GeV and $Y_a = 2.15 \cdot 10^{-3}$. Thus, after implementing the set of equations (4.37), the energy densities, the Yields and the comoving entropy S can be plotted as functions of a/a_0, as shown in Figs. 4.15, 4.16 and 4.17. In particular, Fig. 4.15 shows the period of matter-domination induced by the ALP using the aforementioned parameters. From Fig. 4.16, we can see that the ALP's decay dilutes the Ns Yield as well as its Yield when $a/a_0 \in [5 \cdot 10^2, 2 \cdot 10^3]$. Then, we conclude that the diluter not only dilutes its decay products, but also dilutes itself. The dilution factor in this case is $D_{SM} \simeq 10^2$. Furthermore, as shown in Fig. 4.17, this damping factor can be computed looking at the increment of the total entropy after that the ALP decays away. Eventually, comparing this value with the estimate of Sect. 4.1.1, we find that D_{SM} is well calculated by Eq. (4.8), with an error which is less than 5%.
Let us stress that the total entropy injection can be seen as a consequence of the different scaling of the temperature during a matter-dominated epoch. On the other hand, in a radiation-dominated phase, the total entropy is constant because $T \propto a^{-1}$ leads to

$$S = sa^3 \propto constant\,, \tag{4.48}$$

where $s \sim T^3$.

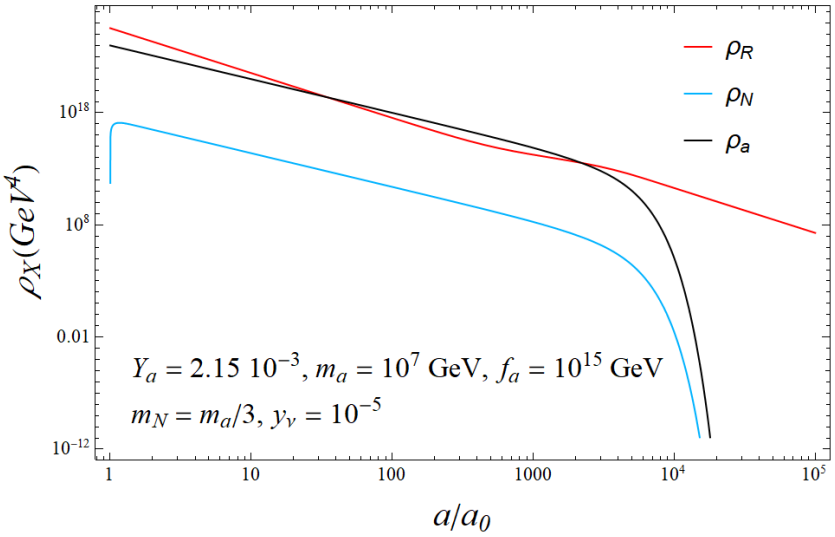

Figure 4.15: Energy density of ALP, RHN and radiation for a benchmark choice of parameters where early matter-domination is realised. The ALP dominates the energy content of the Universe for $a/a_0 \in [26, 2 \cdot 10^3]$. The temperature slope is affected by matter-dominated phase for $a/a_0 \in [5 \cdot 10^2, 2 \cdot 10^3]$.

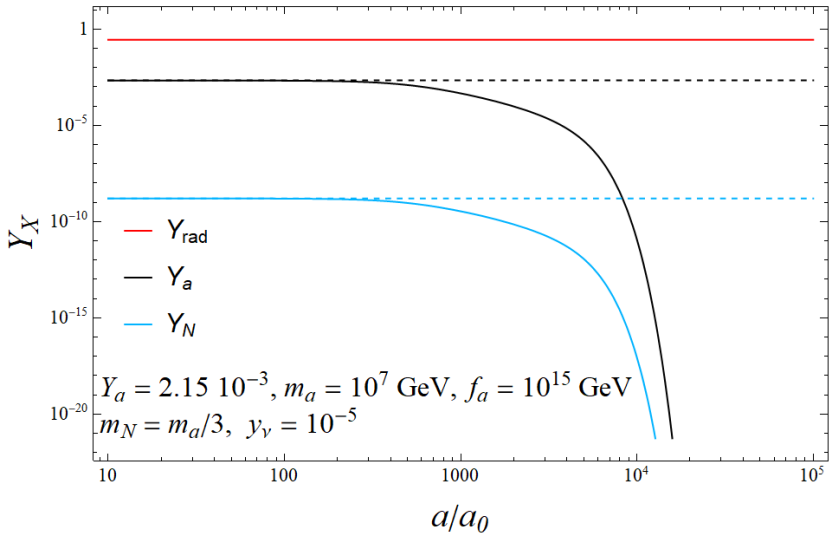

Figure 4.16: Yields of ALP, RHN and radiation for a benchmark choice of parameters where early matter-domination induced by the ALP is realized. Y_a and Y_N get diluted for $a/a_0 \in [5 \cdot 10^2, 2 \cdot 10^3]$ by a factor $\sim 10^2$. The dashed lines represent the constant initial values of the Yields and they are plotted as a reference to enlighten the dilution. The exponential drop of Y_a and Y_N for $a/a_0 \gtrsim 2 \cdot 10^3$ is due to their decay.

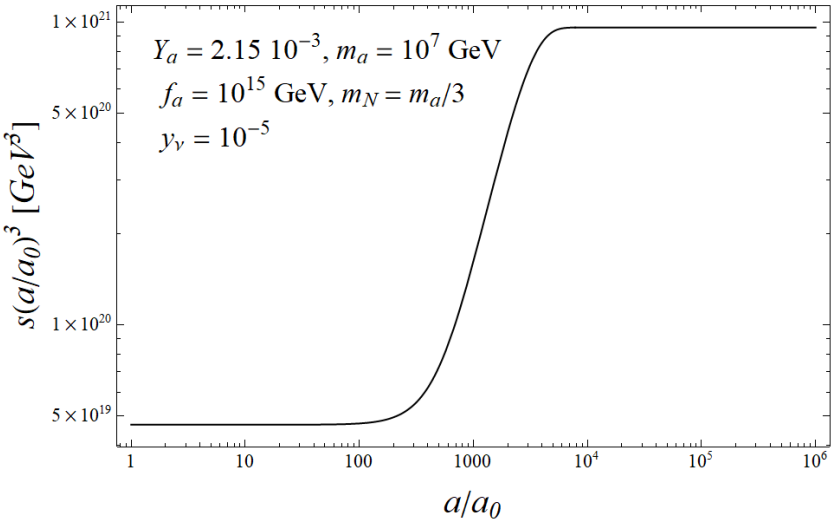

Figure 4.17: Comoving entropy $S = sa^3$ as function of a/a_0 for a benchmark choice of parameters where early matter-domination induced by the ALP is realized. During the radiation-domination its value is constant, while in matter-domination one finds a huge increase, corresponding to a significant entropy injection due to the ALP's decay.

Thus, in the simplest scenario and as first estimate, we expect that the $B-L$ asymmetry gets diluted by the factor $D_{SM} \simeq 10^2$ as well as the ALP's Yield and RHN's Yield in Fig. 4.16. Then, the dilution induced by the decay of the matter-dominating ALP should also be taking into account when considering ALP leptogenesis, since it works against the generation of the baryon asymmetry. In particular, we can estimate that above the red line in Fig. 4.18,

$$D_{SM} \gtrsim 10^2\,. \tag{4.49}$$

Thus the amount of Y_{B-L} that can be gained by the mechanism of ALP leptogenesis, i.e. a factor of $\sim 10^2$, is lost because of dilution, indeed the resulting $B-L$ asymmetry is

$$Y_{B-L}^{aft} = \frac{Y_{B-L}^{bef}}{D_{SM}}\,. \tag{4.50}$$

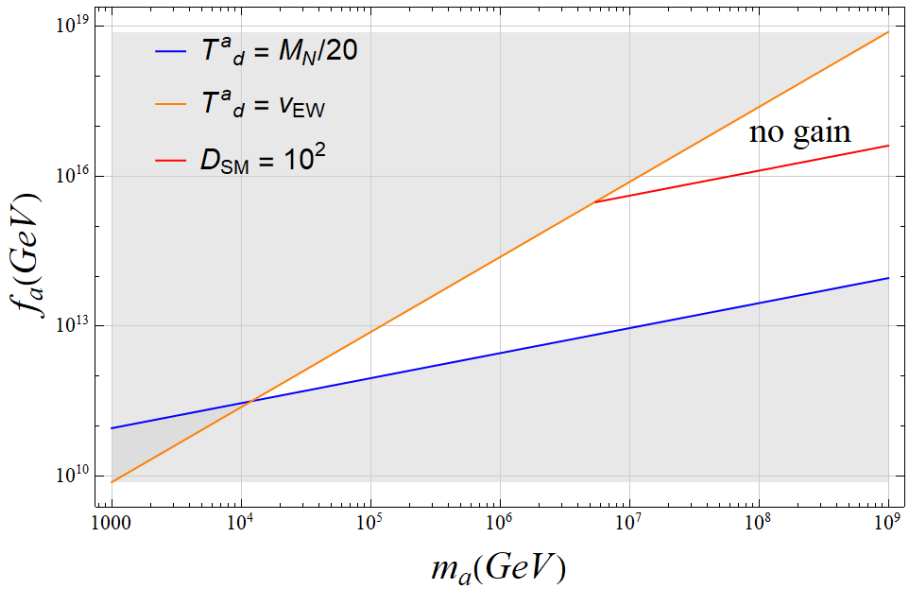

Figure 4.18: Parameter space of ALP leptogenesis, where the red line corresponds to a dilution factor $D_{SM} = 10^2$. Thus, above the red line, the factor 10^2 in baryon asymmetry, gained by ALP leptogenesis with respect to standard leptogenesis, is diluted away due to the ALP matter-domination. Meanwhile, below the red line, ALP leptogenesis allows to gain some factors with respect to thermal leptogenesis.

Chapter 5

Conclusion

This thesis dealt with one of the most striking shortcomings of the Standard Model: the lack of a proper explanation to the Baryon Asymmetry of the Universe, whose experimental value measured by CMB is $Y_{\Delta B} = (8.69 \pm 0.22) \cdot 10^{-11}$ [7]. In particular, this work explored how baryogenesis could be affected by a new pseudo-scalar particle, the axion-like particle (ALP), predicted by many UV extensions of the SM and thus a natural target to search for new physics.
The main goal of this project was to study ALP leptogenesis: a non-thermal leptogenesis sourced via axion-like particle's decay into right-handed Majorana neutrinos, which can be considered as alternative to the standard thermal leptogenesis.

In Chapt. 2, we provided an overview of thermal leptogenesis, which is one of the solutions to the Baryon Asymmetry of the Universe proposed in the literature [10], focusing on the implementation of the Boltzmann Equations (2.46) describing the dynamics of the process in the case of hierarchical Majorana neutrino masses, i.e. $M_1 \ll M_{2,3}$. Usually, this standard leptogenesis features heavy right-handed neutrinos, where the lightest one satisfies the so-called Davidson-Ibarra bound $M_1 \geq 10^9$ GeV [116] in a weak washout regime, while for strong washout $M_1 \geq 10^{11}$ GeV holds. Generally, thermal leptogenesis is considered to undergo the strong washout regime, which is achievable without a tuning of parameters and, thus, is the natural preferred one: in this regime, the initially produced $B - L$ asymmetry is reduced by the following cosmic thermal evolution. Furthermore, in Sect. 2.4, we reviewed the mechanism of resonant leptogenesis, which allows to perform a successful low-scale leptogenesis with Majorana neutrino masses down to $\mathcal{O}(100)$ GeV-scale [9, 94, 114]. Indeed, the CP-asymmetry parameter affecting the computation of the resulting Y_{B-L} can be resonantly enhanced by considering quasi-degenerate masses of the two lightest Majorana neutrinos, i.e. $|M_1 - M_2| \ll \frac{1}{2}(M_1 + M_2)$, where the mass splitting is comparable with the Majorana neutrino decay widths.
Then, we turned to investigate the ALP cosmology in Chapt. 3, including its thermal production in the Early Universe and its decay. On top of its couplings to gluons and top

quarks, already treated in the literature [99], we also considered its interaction with the Majorana neutrinos via the term $\frac{\partial_\mu a}{f_a}\overline{N}_R\gamma^\mu N_R$. Hence, the ALP production is mainly due to the top Yukawa coupling and the ALP abundance via relativistic freeze-out turned out to be $Y_a = 2.15 \cdot 10^{-3}$, while smaller values can be achieved via freeze-in, e.g. $Y_a = 10^{-4}$. The dominant decay channel of the ALP is found to be $a \to N\,N$, with benchmark $M_N = m_a/3$.

Chapt. 4 exposed the main novelty of this thesis: we presented the mechanism of ALP leptogenesis, where a non-thermal population of Ns is generated via ALP decays thanks to its coupling to the Majorana neutrinos. First, the parameter space (f_a, m_a) has been constrained in order to achieve successful ALP leptogenesis (Sect. 4.1). Thus, results favour values of $f_a > 10^{11}$ GeV, $m_a > 10^4$ GeV and $M_N > 1$ TeV. After estimating the viable parameter space, we derived the Boltzmann Equations (4.26) for ALP leptogenesis and implement them numerically. The solutions of the Boltzmann Equations are shown in Figs. 4.7 and 4.8, where we have considered e.g. $f_a = 10^{12}$ GeV, $m_a = 10^5$ GeV and $M_N = m_a/3$ as benchmarks.
In particular the main advantage of ALP leptogenesis is visible in Fig. 4.8: a factor $\sim 10^2$ can be gained in the final $B - L$ asymmetry with respect to the standard thermal leptogenesis. The physical reason behind this increment in the resulting abundance Y_{B-L} is that, when the ALP decays into two right-handed neutrinos, $a \to N\,N$, the washout processes are already out-of-equilibrium and thus, they cannot affect the ALP leptogenesis process anymore. Thereby, the secondary non-thermal population of Majorana neutrinos produced via the ALP decays is able to fuel the generating process of the $B - L$ asymmetry. Thus, for some regions of parameter space, ALP leptogenesis can successfully avoid strong washout effects.
Eventually, the value of Y_{B-L} resulting from ALP leptogenesis can reproduce the observed one if we consider to deal with two Majorana neutrinos N_1 and N_2 with a small Majorana mass splitting, able to satisfy the resonance condition (2.56). The resonant enhancement in the CP-asymmetry parameter, due to a quasi-degeneracy of Majorana masses comparable with their decay widths, allows to successfully perform low-scale leptogenesis. Indeed, resonant leptogenesis procedure ensures that there exist a parameter space for Majorana neutrino masses $M_1 \simeq M_2 \simeq 10^4$ GeV, where the amount of baryon asymmetry produced is comparable with the experimental data (1.5). Moreover, thanks to the factor $\sim 10^2$ that can be gained in ALP leptogenesis by avoiding the strong washout regime, we expect that our ALP leptogenesis does not require a tuning of the Majorana masses as severe as the one in thermal leptogenesis, for the same choice of parameter values. Even though a detailed study of numerical results of the resonant leptogenesis formalism applied to our proposed ALP leptogenesis is beyond the scope of this thesis, we can roughly estimate the final Y_{B-L}, solving the BEs for the simplified scenario in which we assume that the baryon asymmetry in ALP resonant leptogenesis only depends on an effective CP-asymmetry parameter ϵ_{eff} and we keep track of only

one effective heavy Majorana neutrino. The solutions to BEs, which for simplicity have been parametrized in the aforementioned way, are shown in Figs. 4.10 and 4.11.
In the previous computations, we have chosen to work in a region of parameter space where the ALP does not induce a matter-dominated period. In other regions of the ALP parameter space suitable for ALP leptogenesis, a period of matter-domination from the ALP inevitably occurs: we have analysed it in Sect. 4.3. First of all, we have investigated how the temperature of the primordial bath scales with respect to the scale factor a during the matter-domination, in the case in which the ALP can decay both directly into radiation (antitops, tops and gluons) and into Ns, which in turn decay in radiation. Thus, solving the differential equations (4.37) for the energy densities of radiation, ALPs and Majorana neutrinos, we found that in this scenario the temperature scales as $T \propto a^{-3/8}$ during the decays of the ALP and RHNs, to be compared with the more standard $T \propto a^{-1}$ cosmological evolution. $T \propto a^{-3/8}$ is the same scaling as the basic matter-dominating case studied in literature [112], where matter (e.g. ALP) only decays directly into radiation. Moreover, in Figs. 4.16 and 4.17 we have shown the evolution of the Yields Y_i and the comoving entropy $S = sa^3$. Thus, we have discovered that the diluter (i.e. ALP) dilutes itself as well as its decay products (i.e. Ns) and we have computed the dilution factor D_{SM} due to the entropy injection, which turns out to be the same as the one (4.8) used to constrain the parameter space in 4.1.1. We have estimated that this dilution factor also affects the abundance Y_{B-L}, reducing in this way the efficiency of ALP leptogenesis. Thus, we have identified the region of parameter space where the dilution completely cancels the gain obtained via introducing the decay $a \to N\,N$ into the leptogenesis mechanism: this happens for values $f_a \gtrsim 10^{15}$ GeV and $m_a \gtrsim 10^7$ GeV, as shown in Fig. 4.18.

5.1 Outlook

Now, we address some possible future developments that could expand and improve the work that has been done in this thesis.
A possible outlook is to consider values for the masses of Majorana neutrinos and ALPs different from $M_N = m_a/3$, to gain a more complete understanding of the parameter space. In this case, we could study in depth the topic about the kinetic equilibrium of the Majorana neutrinos and the resulting Lorentz boost factor, which should be applied to this population of Ns generated from the ALP's decay. Thus, one future direction can be to improve the computation of the N and $B-L$ Yields in ALP leptogenesis by solving the Boltzmann Equations with respect to the phase-space distributions $f(k)$, since Ns are not in kinetic equilibrium and, if $M_N \neq m_a/3$, the approximations we have done in App. B.2 to derive (4.26) are not valid anymore. Furthermore, in this scenario, scattering processes e.g. $N\,t \to t\,\ell$, which contribute to deplete the N's population, could become relevant and even dominate over Majorana neutrino's decays. Hence, the

effects of these processes should be implemented into the BEs, in order to compute the final asymmetry.

Another possible future direction consists of rigorously applying the resonant leptogenesis formalism to our proposed scenario of ALP leptogenesis, and thereby improving the rough estimate made by assuming to solve the BEs taking into account only one Majorana neutrino which produces an effective CP-asymmetry parameter ϵ_{eff}.

Another interesting framework to be explored is the one where the ALP dominates the energy content of the Universe, inducing a significant dilution of the other species relics. Indeed, we have simply estimated its effect on the $B-L$ asymmetry in Sect. 4.3.2 by applying the dilution factor D_{SM} to Y_{B-L} (4.50). However, the picture could be more complicated than that, because the Majorana neutrinos Ns have been diluting while they are performing the usual leptogenesis. Therefore, we could solve numerically a set of BEs that implement both the ALP matter-domination (4.37) and the ALP leptogenesis (4.26), in order to better compute the resulting $B-L$ asymmetry in the case in which the ALP induces an early matter-dominated epoch.

In addition, a future direction could be to specify a possible model realizing the scenario of ALP leptogenesis. Indeed, in this thesis, we studied generically model-independent axion-like particles. Thus, we could refer to a particular ALP, e.g. R-axion, whose existence is motivated in a supersymmetric theory with an R-symmetry breaking.

Finally, the phenomenology of ALP leptogenesis could be explored. In this thesis, we have shown that the viable parameter space for ALP leptogenesis can include lighter Majorana neutrinos, $M_N \simeq (10 \div 100)$ TeV, with respect to the ones used in standard thermal leptogenesis. Thus, from a phenomenological point of view, ALP leptogenesis is favorable because its Majorana neutrinos could be testable. In particular, one could search for N's signatures in lepton flavour violating observables [117] and at future facilities such as high-energy muon colliders [118–120].

Acknowledgements

I would like to thank my supervisor, Dr. Filippo Sala, and co-supervisors, Prof. Alberto Mariotti and Prof. Silvia Pascoli, first for proposing me to work with them on this project, and then for providing me their fundamental expertise and guidance. I am really grateful for their constant dedication, support and availability. In particular, I feel to express my gratitude to Prof. Mariotti, who enthusiastically accepted to co-supervise my thesis, hosting me at VUB University in Brussels.
Then, I also want to thank both the University of Bologna and the VUB University that gave me the precious chance to travel abroad and stay in Brussels for the preparation of my master thesis.
I would also like to thank Dr. Miguel Vanvlasselaer, who worked with me on this project during the past months, providing his fundamental expertise as well as essential help and precious advice. Eventually, I want to mention the whole phenomenological VUB group led by Prof. Mariotti, that kindly welcomed me into their team.

Appendices

Appendix A

Cosmology

We summarize in this Appendix some features, conventions and definitions about the cosmological history of the Universe, used throughout this thesis. This appendix is mainly based on the textbook [21].

In the standard cosmological model the Universe expands from an initially hot and dense state. The expanding Universe is described by the Friedmann-Lemaitre-Robertson-Walker (FLRW) metric, where the physical length scales are proportional to the scale factor $a(t)$. The expansion rate is quantified via the Hubble parameter $H(t)$, which is defined by the energy content of the Universe through the first Friedmann equation

$$H(t) \equiv \frac{\dot{a}(t)}{a(t)} = \sqrt{\frac{8\pi\rho_{tot}}{3}}\frac{1}{M_{Pl}}\,, \tag{A.1}$$

with the Planck mass $M_{Pl} = 1.22 \cdot 10^{19}$ GeV and ρ_{tot} is the total energy density. The various species composing the Universe at different times are considered as perfect fluids, characterized by the energy density ρ and the pressure p.
We consider the usual scenario of reheating after an initial inflationary phase of the Universe: the inflaton Φ, with energy density ρ_Φ, decays with width Γ_Φ into SM particles. Defining the reheating temperature T_{RH} as the temperature at which Γ_Φ equals H, T_{RH} becomes effectively the maximal temperature of the Universe. Indeed, while higher temperatures exist, particles produced at $T > T_{RH}$ are diluted by the entropy released by inflaton decays. Then, T_{RH} is the starting temperature of the primordial thermal bath of relativistic particles dominating the energy content of the Early Universe. Indeed, after inflation, the Universe contains a plasma of particles in thermal equilibrium with temperature T. This initially coincides with a period of radiation-domination. In particular, during a radiation-dominated epoch, the Hubble parameter can be approximated as

$$H(t) \simeq 1.66\sqrt{g_*(T)}\frac{T^2}{M_{Pl}}\,, \tag{A.2}$$

where $g_*(T)$ accounts for the effective number of relativistic degrees of freedom in the primordial plasma at the temperature T, including both bosons and fermions. The general expression for $g_*(T)$ reads

$$g_*(T) = \frac{7}{8}\sum_F g_i^F \left(\frac{T_i^F}{T_\gamma}\right)^4 + \sum_B g_i^B \left(\frac{T_i^B}{T_\gamma}\right)^4 , \tag{A.3}$$

where T_γ is the photon temperature and $T_i^{F(B)}$, $g_i^{F(B)}$ are the temperature and the number of degrees of freedom of each fermionic (bosonic) particle i. The Eq. (A.3) is applicable for both relativistic species in themal equlibrium with the photons, i.e. $T_i = T_\gamma \gg m_i$, and decoupled relativistic species, i.e. $T_\gamma \neq T_i \gg m_i$. $g_*(T)$ remains roughly constant away from paricle mass thresholds $T \sim m_i$ and, for temperatures much higher than the electroweak scale, $T \gtrsim 1$ TeV, all the SM particles are relativistic and in equilibrium, resulting in $g_*^{SM} = 106.75$.

A.1 Thermal history of the Universe

In the very Early Universe most particles were in thermal equilibrium with photons, forming the primordial plasma. Therefore, the notion of thermal equilibrium is extremely important in determining how temperature, energy density and entropy density of the Universe evolve with the Hubble expansion. Thus, in this Section some basic aspects of systems of both relativistic and non-relativistic particles in thermal equilibrium are reviewed.

Local thermal equilibrium is achieved for species which are both in kinetic and chemical equilibrium. In order to study the evolution of particles in the primordial Universe, it is convenient to use the phase-space distribution function $f(\mathbf{k}, t)$, which depends on the momentum $\mathbf{k}$ and time t. In kinetic equilibrium, f is given by either the Fermi-Dirac $(+)$ or Bose-Einstein $(-)$ distributions at temperature T:

$$f^{eq}(k,t) = \left(e^{\frac{E-\mu}{T}} \pm 1\right)^{-1} , \tag{A.4}$$

with particle energy E and chemical potential μ. Moreover, in a process of the form

$$A + B \leftrightarrow C + D , \tag{A.5}$$

the chemical equilibrium implies $\mu_A + \mu_B = \mu_C + \mu_D$.
Other associated quantities for a dilute and weakly-interacting gas of particles, such as the number density n and the energy density ρ, can be computed thanks to the phase-space distribution:

$$n = \frac{g}{(2\pi)^3}\int d^3k f(\mathbf{k}, t) , \tag{A.6}$$

$$\rho = \frac{g}{(2\pi)^3} \int d^3k E(\mathbf{k}) f(\mathbf{k}, t) \,, \tag{A.7}$$

with internal degrees of freedom g.
Let us now show the above expressions in two asymptotic limits, assuming $|\mu| \ll T$ [21]:

- **Relativistic species**
  For $T \gg m$, we can approximate for bosons

$$n_B = \frac{g}{\pi^2}\zeta(3)T^3 \,, \qquad \rho_B = \frac{\pi^2}{30} g T^4 \tag{A.8}$$

  while for fermions,

$$n_F = \frac{3}{4} n_B \,, \qquad \rho_F = \frac{7}{8}\rho_B \,; \tag{A.9}$$

- **Non-relativistic species**
  For $T \ll m$, the bosonic and fermionic nature of particles becomes indistinguishable because the exponential factor dominates the denominator in Eq. (A.4), and

$$n \simeq g\left(\frac{mT}{2\pi}\right)^{3/2} e^{-m/T} \,, \qquad \rho = mn \tag{A.10}$$

Denoting T_γ as the temperature of the photon bath in the Early Universe, the total energy density of radiation in presence of other relativistic species is given by:

$$\rho_r = \frac{\pi^2}{30} g_*(T) T^4 \tag{A.11}$$

with $g_*(T)$ defined in Eq. (A.3).

Other useful quantities can be defined, such as the comoving entropy of the Universe

$$S = \frac{E + pV}{T} \,, \tag{A.12}$$

where p and V indicate pressure and volume, and the entropy density $s = S/V$, which is thus given by

$$s = \frac{\rho + p}{T} \,. \tag{A.13}$$

The total entropy density of radiation in the Early Universe is given by the sum over all relativistic species:

$$s = \frac{2\pi^2}{45} g_{*s}(T) T^3 \,, \tag{A.14}$$

where g_{*s} is the effective number of relativistic degrees of freedom contributing to the entropy. If the species are in thermal equilibrium, $g_* = g_{*s}$, but for decoupled species we have

$$g_{*s}(T) = \frac{7}{8}\sum_F g_i^F \left(\frac{T_i^F}{T_\gamma}\right)^3 + \sum_B g_i^B \left(\frac{T_i^B}{T_\gamma}\right)^3 , \tag{A.15}$$

which differs from the expression of $g_*(T)$ in Eq. (A.3). Therefore, at high temperature we can assume $g_* = g_{*s}$, while at low temperatures, after the neutrino decoupling, $g_* \neq g_{*s}$. Thus, at leptogenesis temperatures, we have $g_* = g_{*s}$.
Note that entropy conservation implies that $S = a^3 s = g_{*s} a^3 T^3 = const.$ Thus, far away from particle mass thresholds, g_{*s} is approximately constant and the temperature scales as

$$T \propto a^{-1} . \tag{A.16}$$

Finally, let us notice that g_{*s} accounts for particles becoming non-relativistic and exponentially decaying away. Thus, their entropy is transferred into the species that remain in the plasma, the so-called entropy injection, which makes the radiation temperature decreases more slowly than $T \propto a^{-1}$.
Another useful cosmological parameter to denote the abundance of a species i is the Yield, defined as

$$Y_i = \frac{n_i}{s} , \tag{A.17}$$

which remains constant if no particles are being created or destroyed.
Before proceeding in the discussion of the equilibrium thermodynamics, we explain the relation between the entropy density and the photon number density at present time T_0, stated in Sect. 1.1. Using Eq. (A.8), we obtain

$$n_{\gamma,0} = \frac{g_\gamma \zeta(3)}{\pi^2} T_0^3 \tag{A.18}$$

with $g_\gamma = 2$ degrees of freedom for photons, while using (A.14),

$$s_0 = \frac{2\pi^2}{45} g_{*s}(T_0) T_0^3 . \tag{A.19}$$

At T_0, the only relativistic species are photons and neutrinos and the latter are decoupled. Thus, the contribution to the present entropy density s_0 comes from the photons at T_γ and from the neutrinos at $T_\nu = \frac{4}{11} T_\gamma^3$. From Eq. (A.15) we derive

$$g_{*s}(T_0) = g_\gamma + \frac{7}{8} g_\nu \left(\frac{T_\nu}{T_0}\right)^3 = 2 + \frac{7}{8} \cdot 6 \cdot \frac{4}{11} = 3.91 . \tag{A.20}$$

Then, combining Eqs. (A.18) and (A.19), the relation

$$s(T_0) = 7.04\, n_\gamma(T_0) \tag{A.21}$$

is obtained.

Now, we focus on the mechanism that makes particles decouple from the thermal bath. The Universe is expanding and getting colder and colder over time. The departure from thermal equilibrium allows species to acquire a significant cosmological abundance and different particle species decouple at different epochs. In particular, the condition to be satisfied by a species to get out-of-equilibrium compares its interaction rate, Γ, with expansion rate H of the Universe. As long as

$$\Gamma > H\,, \tag{A.22}$$

a species i is kept in thermal equilibrium with the plasma, for instance via annihilation processes like $A + \overline{A} \leftrightarrow i + \bar{i}$. In this case, the particles are being created and destroyed within a Hubble time and the equilibrium is maintained. But, when

$$\Gamma < H\,, \tag{A.23}$$

the system departs from thermal equilibrium because the interactions can no longer keep up with the Hubble expansion: for instance, the process $i + \bar{i} \to A + \overline{A}$ becomes inefficient, the species cannot be produced back by the bath and decouples, i.e., the particle is *frozen out*. Thus, the abundance of the species i will remain constant after the decoupling. This mechanism is called *freeze-out* and the decoupling temperature T_D is computed by equalling Γ to H. Furthermore, the freeze-out can be either relativistic, if $m \ll T$ with m the particle's mass, or non-relativistic, if $m \gtrsim T$, resulting in a certain abundance, expressed by the Yield Y_i, for that species i. In both cases the phase-space distribution $f(\mathbf{k}, t)$ remains untouched after decoupling, while the scaling behaviour of the temperature for relativistic and non-relativistic species after freeze-out is different:

$$T(t) = T_D \frac{a(t_D)}{a(t)} \qquad \text{for} \qquad m \ll T \tag{A.24}$$

where the energy of the particle is simply redshifted by expansion, $E(t) = E(t_D)\frac{a(t_D)}{a(t)}$, and in particular $E/T = const$, and

$$T(t) = T_D \left(\frac{a(t_D)}{a(t)} \right)^2 \qquad \text{for} \qquad m \gtrsim T \tag{A.25}$$

where the momentum of the particle redshifts and consequently its kinetic energy scales as $E \propto |\mathbf{k}|^2 \propto a^{-2}$, and in particular $(E - \mu)/T = const$.
An alternative mechanism with respect to the freeze-out is the so-called freeze-in (see Ref. [121] for a review). First studied as possible mechanism of dark matter genesis, it assumes that a certain species has a negligible initial abundance and it interacts so feebly with the thermal bath that it never attains thermal equilibrium. The particle is said to be *frozen in* through decays and two-to-two scatterings and its Yield is infrared dominated by low temperatures near its mass.

Appendix B

Boltzmann Equations

The Boltzmann Equations are kinetic equations treating out-of-equilibrium processes. For instance, the non-equilibrium process of baryogenesis is usually studied by means of Boltzmann Equations [95, 122]. In the same way, leptogenesis has been studied in the last decades [11, 12, 46, 74, 89, 92, 94].
In this Appendix, the steps of the derivation of the BEs relevant for standard leptogenesis are reviewed in B.1and the new set of BEs for ALP leptogenesis is derived in B.2.

Generally, the Boltzmann Equation for the phase-space distribution $f_i = f(t, \mathbf{p}_i)$ of the particles species i can be written as [15, 46]

$$\frac{\partial f_i}{\partial t} - |\mathbf{p}_i| H \frac{\partial f_i}{\partial |\mathbf{p}_i|} = C[f_i] \tag{B.1}$$

where the left-hand side corresponds to the Liouville operator with momentum $\mathbf{p}_i$. On the right-hand side, the collision integral $C[f_i]$ encodes the interactions of the particle i,

$$\begin{aligned} C[f_i] = & \frac{1}{2E_i} \sum_{i \to XY} \int d\Pi_X d\Pi_Y (2\pi)^4 \delta^4(p_i - p_X - p_Y) \cdot \\ & \cdot \left[f_X f_Y (1 \pm f_i) |\mathcal{M}_{XY \to i}|^2 - f_i (1 \pm f_X)(1 \pm f_Y) |\mathcal{M}_{i \to XY}|^2 \right] \end{aligned} \tag{B.2}$$

with $d\Pi_n = \frac{d^3 p_n}{2E_n (2\pi)^3}$, E_n and p_n respectively the energy and the 4-momenta of the particles species n, $\mathcal{M}_A$ the matrix element for the process A. The sign + accounts for bosons, while − for fermions.
The left-hand side of Eq. (B.1) is usually expressed as a derivative with respect to the dimensionless coordinate $z = M_i/T$. Thus, using the relation $dT/dt = -HT$ [46], the differential operator becomes

$$\frac{\partial}{\partial t} - |\mathbf{p}_i| H \frac{\partial}{\partial |\mathbf{p}_i|} = z H(z) \frac{\partial}{\partial z} \,. \tag{B.3}$$

Therefore, (B.1) assumes the simpler form

$$\frac{\partial f_i(z\,,y)}{\partial z} = \frac{1}{H(z)z} C[f_i(z,y)] \tag{B.4}$$

with $y_i = |\mathbf{p}_i|/T$.

In the following, the spacetime densities γ^{eq} of decays in thermal equilibrium (e.g. see (2.47)) will be used, then it is convenient to define them here. Generally for a decay, the reaction density is defined as

$$\gamma^{eq}(a \to i+j) = \int d\Pi_a d\Pi_i d\Pi_j f_a^{eq} (2\pi)^4 \delta^4(p_a - p_i - p_j) |\mathcal{M}(a \to i+j)|^2 \,, \tag{B.5}$$

where $|\mathcal{M}|^2$ is summed (not averaged) over the internal degrees of freedom of the initial states. Eq. (2.47) can also take the following form [92]

$$\gamma := \gamma^{eq}(i \to j\, k) = n_i^{eq} \frac{K_1(z_i)}{K_2(z_i)} \Gamma \,, \tag{B.6}$$

with $z_i = m_i/T$, Γ the usual decay width in the rest frame of the decaying particle, $K_1(z)$, $K_2(z)$ the modified Bessel functions of second kind of first and second order and the number density n_i^{eq} of particle i at equilibrium is approximated to follow the classical Maxwell-Boltzmann distribution, [11]

$$n_{i,MB}^{eq} = \frac{g_i}{2\pi^3} \int d^3p f_{i,MB}^{eq} = \begin{cases} \frac{g_i T^3}{2\pi^2} z_i^2 K_2(z_i) & \text{for } z_i = \frac{m_i}{T} \neq 0,\ \mu = 0\,, \\ \frac{g_i T^3}{\pi^2} & \text{for } m_i = 0\,. \end{cases} \tag{B.7}$$

Then, inserting (B.7) into (B.6) in the case of massive particle, the reaction rate becomes

$$\gamma = \frac{g_i m_i^3}{2\pi^2 z_i} K_1(z_i) \Gamma \,. \tag{B.8}$$

B.1 Standard thermal leptogenesis

In standard leptogenesis, two coupled BEs for the RHN and for the $B-L$ asymmetry are derived. We consider that decays, $N_1 \to \ell\,\phi$, and inverse decays, $\ell\,\phi \to N_1$, dominate leptogenesis, as motivated in Sect. 2.3. Then, the kinetic equation for N_1 is

$$\frac{\partial f_{N_1}}{\partial t} - |\mathbf{p}_{N_1}| H \frac{\partial f_{N_1}}{\partial |\mathbf{p}_{N_1}|} = C_D[f_{N_1}] \tag{B.9}$$

with

$$C_D[f_{N_1}] = \frac{1}{2E_{N_1}} \int d\Pi_\ell d\Pi_\phi (2\pi)^4 \delta^4(p_{N_1} - p_\ell - p_\phi) \big[f_\phi f_\ell (1 - f_{N_1})(|\mathcal{M}_{\phi\ell\to N_1}|^2 + \\ + |\mathcal{M}_{\bar{\phi}\,\bar{\ell}\to N_1}|^2) - f_{N_1}(1 - f_\ell)(1 + f_\phi)(|\mathcal{M}_{N_1\to\phi\ell}|^2 + |\mathcal{M}_{N_1\to\bar{\phi}\,\bar{\ell}}|^2) \big] \tag{B.10}$$

Using CPT invariance, the neutrino decay amplitudes can be written as

$$|\mathcal{M}_{N_1\to\ell\phi}|^2 = |\mathcal{M}_{\bar{\phi}\,\bar{\ell}\to N_1}|^2 = \frac{(1+\epsilon)}{2}|\mathcal{M}_0|^2\,, \;\; |\mathcal{M}_{N_1\to\bar{\phi}\,\bar{\ell}}|^2 = |\mathcal{M}_{\phi\,\ell\to N_1}|^2 = \frac{(1-\epsilon)}{2}|\mathcal{M}_0|^2 \tag{B.11}$$

where $|\mathcal{M}_0|^2 = \frac{m_D^\dagger m_D}{v_{EW}}\, p_\ell\, p_{N_1}$ [46] is the (CP-conserving) squared matrix element at tree-level, and ϵ is the CP-asymmetry parameter (2.19). We work in the approximation of thermal equilibrium for all SM particles, i.e.

$$f_\ell = f_\ell^{eq}\,, f_\phi = f_\phi^{eq}\,, \tag{B.12}$$

and we neglect quantum statistical factors due to Pauli blocking for fermions and induced emission for bosons, i.e. [95]

$$1 + f_i \approx 1\,, \tag{B.13}$$

adopting the classical Maxwell-Boltzmann distribution function

$$f_i^{eq} = e^{-E_i/T}\,. \tag{B.14}$$

Thus, using these assumptions and energy conservation, the following relation holds

$$f_\phi f_\ell = e^{-\frac{(E_\phi + E_\ell)}{T}} = e^{-E_N/T} = f_{N_1}^{eq}\,. \tag{B.15}$$

Therefore, the collision operator (B.10) gets simplified as follows [46]

$$C_D[f_{N_1}] = \frac{M\Gamma_D}{E_{N_1} p_{N_1}} \int_{(E_{N_1} - p_{N_1})/2}^{(E_{N_1} + p_{N_1})/2} dp_\phi (f_{N_1}^{eq} - f_{N_1})\,, \tag{B.16}$$

where Γ_D has been defined in (2.16). Performing the integration over the momenta p_ϕ, from Eq. (B.4) we obtain

$$\frac{\partial f_{N_1}(z\,, y)}{\partial z} = \frac{M_N \Gamma_D}{z H(Z) E_{N_1}} (f_{N_1}^{eq} - f_{N_1})\,. \tag{B.17}$$

Assuming kinetic equilibrium for the RHN neutrinos, i.e. $f_{N_1} \approx \frac{n_{N_1}}{n_{N_1}^{eq}} f_{N_1}^{eq}$, where the number density is defined as (A.6) with $g_{N_1} = 2$, and integrating Eq. (B.17) over the RHN phase-space, we find

$$\frac{\partial n_{N_1}(z\,, y)}{\partial z} = -\frac{n_{N_1}^{eq}}{z H(z)} \Gamma_D < \frac{M_N}{E_{N_1}} > \left(\frac{n_{N_1}}{n_{N_1}^{eq}} - 1 \right), \tag{B.18}$$

where [46]

$$\Gamma_D < \frac{M_N}{E_{N_1}} > \equiv \frac{\Gamma_D}{n_{N_1}^{eq}} \int \frac{d^3 p_{N_1}}{2\pi^3} f_{N_1}^{eq} \frac{M_N}{E_N} \tag{B.19}$$

is the thermal average of the decay rate and [95]

$$< \frac{M}{E_{N_1}} > = \frac{K_1(z)}{K_2(z)} \,. \tag{B.20}$$

Eq. (B.18) is the integrated form of the BE, i.e. the time evolution of number densities n_i are tracked in favour of the phase-space distributions f_i. Therefore, in the integrated approach, which is conventionally used in the literature, the BE (B.17) is integrated over the momentum Majorana neutrino phase space.

Since Eq. (B.20) holds, Eq. (B.18) can be written in a handy way, making use of the space time density γ^{eq} of decays in thermal equilibrium in the form of (B.6). Eventually, the BE for the RHN evolution has the following form

$$\frac{\partial Y_{N_1}(z\,, y)}{\partial z} = -\frac{\gamma_D}{H(z) s z} \left(\frac{Y_{N_1}}{Y_{N_1}^{eq}} - 1 \right) , \tag{B.21}$$

where we have divided by the entropy density s to obtain the yield Y_{N_1}.

Now, we derive the BE for the $B - L$ asymmetry's evolution. The BE for leptons (antileptons) with phase-space distribution f_ℓ ($f_{\overline{\ell}}$) is built similarly to (B.9). The collision integral includes decays $N_1 \to \ell\,\phi$, inverse decays $\ell\,\phi \to N_1$ and $\Delta L = 2$ scattering processes, such as $\ell\,\phi \to \overline{\ell}\,\overline{\phi}$ and $\ell\,\ell \to \phi\,\phi$. Since all the particles species are assumed to be in kinetic equilibrium, the BE for the number density n_ℓ is obtained by integrating over the lepton phase-space. Thus, using the reaction densities defined as (B.5), we have the following expression

$$\begin{aligned} \frac{\partial n_\ell}{\partial t} + 3Hn_\ell =& \frac{n_{N_1}}{n_{N_1}^{eq}} \gamma(N_1 \to \ell\phi) - \frac{n_\ell}{n_\ell^{eq}} \gamma(\ell\,\phi \to N_1) + \frac{n_{\overline{\ell}}}{n_\ell^{eq}} \gamma_{sub}(\overline{\ell}\,\overline{\phi} \to \ell\,\phi) + \\ & - \frac{n_\ell}{n_\ell^{eq}} \gamma_{sub}(\ell\,\phi \to \overline{\ell}\,\overline{\phi}) + \gamma(\phi\,\overline{\phi} \to \ell\,\ell) \left(\frac{n_\ell}{n_\ell^{eq}} \right)^2 \gamma(\ell\,\ell \to \phi\,\phi) \,. \end{aligned} \tag{B.22}$$

Here, the Higgs doublets ϕ are assumed to be in thermal equilibrium and γs are the reaction densities in thermal equilibrium.
The $\Delta L = 2$ scattering processes mediated by N_1, e.g. $\ell\,\phi \to \overline{\ell}\,\overline{\phi}$, have to be taken into account, otherwise a lepton asymmetry would be generated even in thermal equilibrium [88]. However, the real intermediate state (RIS) contribution from these $2 \to 2$ scatterings needs to be subtracted in order to avoid double counting [11, 95]. Thus,

in (B.22) the subtracted reaction density are denoted as γ_{sub}. This procedure is a delicate and crucial point in setting up the BEs for leptogenesis. The explicit calculation of $\Delta L = 2$ processes, including one-loop self-energy and vertex corrections in the resonance region is carried out in Ref.[88]. Therefore, the following expression holds

$$\gamma_{sub}(\overline{\phi}\,\overline{\ell} \to \ell\,\phi) = \gamma_{\Delta L=2,+} - \frac{\epsilon}{2}\gamma_{N_1}\,, \tag{B.23}$$

$$\gamma_{sub}(\phi\,\ell \to \overline{\ell}\,\overline{\phi}) = \gamma_{\Delta L=2,+} + \frac{\epsilon}{2}\gamma_{N_1}\,, \tag{B.24}$$

$$\gamma(\overline{\phi}\,\overline{\phi} \to \ell\,\ell) = \gamma(\overline{\ell}\,\overline{\ell} \to \phi\,\phi) = \gamma_{\Delta L=2,t}\,. \tag{B.25}$$

where $\gamma_{\Delta L=2,+}$ is the unsubtracted reaction density, which, contrary to the subtracted one, preserves the CP symmetry [88]. Let us stress that, to leading order in the coupling, γ_{sub} contributes only on-shell, at order $\mathcal{O}(y_\nu^2)$.
Expressing the lepton-number densities in terms of the $B-L$ number density as follows

$$n_\ell = n_\ell^{eq} - \frac{1}{2}n_{B-L}\,, \qquad n_{\overline{\ell}} = n_\ell^{eq} + \frac{1}{2}n_{B-L}\,, \tag{B.26}$$

assuming $n_{B-L} = n_{\overline{\ell}} - n_\ell = \mathcal{O}(\epsilon)$ and keeping only $\mathcal{O}(\epsilon)$ terms, the BE for $B-L$ asymmetry becomes [88]

$$\frac{\partial n_{B-L}}{\partial t} + 3Hn_{B-L} = \epsilon\gamma_{N_1}\left(\frac{n_{N_1}}{n_{N_1}^{eq}} - 1\right) - \frac{n_{B-L}}{n_\ell^{eq}}\left(\frac{\gamma_{N_1}}{2} + \gamma_{\Delta L=2}\right), \tag{B.27}$$

where

$$\gamma_{\Delta L=2} = 2\gamma_{\Delta L=2,+} + 2\gamma_{\Delta L=2,t}\,. \tag{B.28}$$

Let us highlight that the CP-violating part of γ_{sub} yields the term $+\epsilon\gamma_{N_1}$, which guarantees that in thermal equilibrium, i.e. $n_{N_1} = n_{N_1}^{eq}$, no $B-L$ asymmetry is generated. The off-shell contribution $\gamma_{\Delta L=2}$ is subleading, indeed it is a $\mathcal{O}(y_\nu^4)$-term. Thus, by neglecting all these non-resonant terms, BE valid at $\mathcal{O}(y_\nu^2)$ is derived [11, 88]. Eventually, performing the coordinate transformation that leads to (B.4) and rewrite in terms of Yields, the BE for the $B-L$ asymmetry becomes:

$$\frac{\partial Y_{B-L}}{\partial z} = \frac{\epsilon\gamma_D}{H(z)sz}\left(\frac{Y_{N_1}}{Y_{N_1}^{eq}} - 1\right) - \frac{\gamma_D Y_{B-L}}{2Y_\ell^{eq}Hsz}\,, \tag{B.29}$$

with

$$Y_\ell^{eq} = \frac{2Y_{N_1}^{eq}}{z^2K_2(z)}\,. \tag{B.30}$$

Thus, Eqs. (B.21) and (B.29) are the ultimate form of BEs for thermal leptogenesis, which have been numerically implemented in Sect. 2.3.

B.2 ALP leptogenesis

In this Appendix, the Boltzmann Equations describing the dynamics of ALP leptogenesis are derived. Let us stress that this non-thermal leptogenesis takes place besides the standard thermal one. Thus, two different populations of RHN are generated: the first one due to inverse decays and scatterings occurring in the thermal bath, and the second one due to the ALP's decays $a \to N\,N$. Then, looking at the ratios $\tilde{\Gamma}/H$ of Fig. 4.9, thermal leptogenesis is approximated to take place until $z = M_N/T \sim 13$, and it is described by the usual BEs derived previously in App. B.1, Eqs. (B.21) and (B.29). For higher values of z, the ALP's decays begin to create the second non-thermal population of N_1. Therefore, on top of the kinetic equations for the RHN and the $B-L$ asymmetry, the BE for the ALP needs to be computed.

For what concerns the ALP, its frozen-in/frozen-out Yield obtained in Sect. 3.1.3 is taken as initial value for the abundance, and then the collision integral is modelled on Eq. (B.2) considering only its decays into Majorana neutrinos, top quarks and gluons. Therefore, we have

$$\frac{\partial f_a}{\partial z} = \frac{1}{H(z)z} C[f_a]\,, \tag{B.31}$$

with

$$C[f_a] = C_{a\to N_1\,N_1}[f_a] + C_{a\to g\,g}[f_a] + C_{a\to t\,\bar{t}}[f_a]\,. \tag{B.32}$$

Neglecting statistical quantum numbers and assuming the same matrix element squared for decay and inverse decay, the collision operator simplifies with

$$C_{a\to N_1\,N_1}[f_a] = -\frac{1}{2E_a}\int d\Pi_{N_1} d\Pi_{N_1} (2\pi)^4 \delta^4(p_a - p_{N_1} - p_{N_1}) |\mathcal{M}_{a\to N_1\,N_1}|^2 f_a\,, \tag{B.33}$$

$$C_{a\to g\,g}[f_a] = \frac{1}{2E_a}\int d\Pi_g d\Pi_g (2\pi)^4 \delta^4(p_a - p_g - p_g) |\mathcal{M}_{a\to g\,g}|^2 (f_g^2 - f_a)\,, \tag{B.34}$$

$$C_{a\to t\,\bar{t}}[f_a] = \frac{1}{2E_a}\int d\Pi_t d\Pi_{\bar{t}} (2\pi)^4 \delta^4(p_a - p_t - p_{\bar{t}}) |\mathcal{M}_{a\to t\,\bar{t}}|^2 (f_t f_{\bar{t}} - f_a)\,, \tag{B.35}$$

where, in the first collision integral, we have not considered the term concerning the back reaction $N_1\,N_1 \to a$. Since the SM particles are approximated to be in thermal equilibrium, i.e. $f_g = f_g^{eq}$ and $f_{t(\bar{t})} = f_{t(\bar{t})}^{eq}$, and since

$$f_a^{eq} = f_{N_1,eq}^2 = f_{g,eq}^2 = f_t^{eq} f_{\bar{t}}^{eq} \tag{B.36}$$

because of energy conservation, the collision operators can be rewritten as

$$C_{a\to N_1\,N_1}[f_a] = -\frac{1}{2E_a}\int d\Pi_{N_1} d\Pi_{N_1} (2\pi)^4 \delta^4(p_a - p_{N_1} - p_{N_1}) |\mathcal{M}_{a\to N_1\,N_1}|^2 f_a^{eq} \frac{f_a}{f_a^{eq}}\,, \tag{B.37}$$

$$C_{a\to g\,g}[f_a] = \frac{1}{2E_a}\int d\Pi_g d\Pi_g (2\pi)^4\delta^4(p_a - p_g - p_g)|\mathcal{M}_{a\to g\,g}|^2 f_a^{eq}\left(1-\frac{f_a}{f_a^{eq}}\right), \tag{B.38}$$

$$C_{a\to t\,\bar{t}}[f_a] = \frac{1}{2E_a}\int d\Pi_t d\Pi_{\bar{t}} (2\pi)^4\delta^4(p_a - p_t - p_{\bar{t}})|\mathcal{M}_{a\to t\,\bar{t}}|^2 f_a^{eq}\left(1-\frac{f_a}{f_a^{eq}}\right), \tag{B.39}$$

where we have factored out f_a^{eq}. Assuming that the ALP is in kinetic equilibrium, i.e. $f_a/f_a^{eq} \approx n_a/n_a^{eq}$, as motivated in 4.2.1, and integrating over the ALP phase-space, the BE becomes

$$\frac{dn_a}{dz} = -\frac{1}{H(z)z}\left[Br_{N_1}\gamma_a\frac{n_a}{n_a^{eq}} - Br_g\gamma_a\left(\frac{n_a}{n_a^{eq}}-1\right) - Br_t\gamma_a\left(\frac{n_a}{n_a^{eq}}-1\right)\right], \tag{B.40}$$

where Br_i are the branching ratios of the ALP's decay and γ_a the total decay density. Furthermore, Eq. (B.40) can be rewritten by dividing for the entropy density s as

$$\frac{dY_a}{dz} = -Br_N\frac{\gamma_a}{Hsz}\frac{Y_a}{Y_a^{eq}} - Br_g\frac{\gamma_a}{Hsz}\left(\frac{Y_a}{Y_a^{eq}}-1\right) - Br_t\frac{\gamma_a}{Hsz}\left(\frac{Y_a}{Y_a^{eq}}-1\right). \tag{B.41}$$

Now, we derive the BE describing the time evolution of RHNs. Due to the ALP's decay acting as new source of N_1 and to the fact that the Majorana neutrinos produced via decay are not in kinetic equilibrium, Eqs. (B.21) gets modified. The first modification appears as a new term in the right-hand side of the BE: it has the same expression of the first term in (B.41) but opposite sign.
Then, we need to review the steps of the BE's derivation, dropping the assumption of kinetic equilibrium for the non-thermal population of N_1. Integrate Eq. (B.17), we obtain

$$\frac{\partial n_{N_1}}{\partial z} = \frac{M_N\Gamma_D}{zH(z)}\left(\int\frac{d^3p_{N_1}}{E_{N_1}(2\pi)^3}f_{N_1}^{eq} - \int\frac{d^3p_{N_1}}{E_{N_1}(2\pi)^3}f_{N_1}\right), \tag{B.42}$$

where in the first integral, the RHN's energy for the thermal population can be approximated as

$$E_{N_1} \simeq M_N\,, \tag{B.43}$$

since the RHN are non-relativistic, while in the second integral

$$E_{N_1} \simeq \frac{m_a}{2} \tag{B.44}$$

is the energy of the Majorana neutrinos produced via ALP's decays. Then, the integrals in Eq. (B.42) are the number densities $n_{N_1}^{eq}$ and n_{N_1}, respectively, and

$$\frac{\partial n_{N_1}}{\partial z} = \frac{\Gamma_D}{zH(z)}\left(n_{N_1}^{eq} - \frac{2M_N}{m_a}n_{N_1}\right). \tag{B.45}$$

Factoring out $n_{N_1}^{eq}$ and dividing by the entropy density, we obtain

$$\frac{\partial Y_{N_1}}{\partial z} = -\frac{\gamma_D}{H(z)sz}\left(\frac{2M_N}{m_a}\frac{Y_{N_1}}{Y_{N_1}^{eq}} - 1\right), \tag{B.46}$$

where the ratio of Bessel functions is reasonably approximated as $K_1(z)/K_2(z) \simeq 1$. Thus, the fact that the RHNs produced via ALP's decays are not in kinetic equilibrium can be modelled in the BEs by the boost factor $2M_N/m_a$. The effect is that the RHNs decay slower, due to the energy inherited from the ALP. Therefore, the BE for N_1 can be written as

$$\frac{dY_{N_1}}{dz} = -\frac{\gamma_D}{Hsz}\left(\frac{2M_N}{m_a}\frac{Y_{N_1}}{Y_{N_1}^{eq}} - 1\right) + \frac{Br_N\gamma_a}{Hsz}\frac{Y_a}{Y_a^{eq}}\,. \tag{B.47}$$

Following the same reasoning as above, the BE for the $B-L$ asymmetry is modified by multiplying by the boost factor as follows

$$\frac{dY_{B-L}}{dz} = \frac{\gamma_D\epsilon}{Hsz}\left(\frac{2M_N}{m_a}\frac{Y_{N_1}}{Y_{N_1}^{eq}} - 1\right) - \frac{\gamma_D}{Hsz}\frac{Y_{B-L}}{2Y_l^{eq}}\,. \tag{B.48}$$

Eventually, the coupled system of Eqs. (B.41), (B.47) and (B.48) can be solved numerically with respect to z, with $z \in [13, 200]$.

Appendix C

ALP production via Majorana neutrino coupling

In this Appendix, we improve the estimates of the ALP production due to the coupling with the Majorana neutrinos Ns, which have been carried out in Sect. 3.1.2. Here, we precisely check that those contributions are subdominant by computing the resulting ALP Yields (see Ref. [121]).

We assume that the ALP abundance right after reheating is approximately zero, i.e., $f_a \approx 0$, that the bath particles are in thermal equilibrium and therefore are Maxwell-Boltzmann distributed, i.e., $f_i \approx e^{-E_i/T}$, and let us neglect Pauli blocking/stimulated emission effects, i.e., $(1 \pm f_i \approx 1)$. Then, under these assumptions, the general form of the BE for a $2 \to 2$ scattering becomes [121]

$$\dot{n}_a + 3Hn_a \approx \int d\Pi_1 d\Pi_2 d\Pi_3 d\Pi_a (2\pi)^4 \delta^4(p_1 + p_2 - p_3 - p_a) |\mathcal{M}_{12\to 3a}|^2 f_1 f_2 \,. \tag{C.1}$$

Now, we consider the processes arising from the RHN's coupling with the ALP, that could contribute to the ALP production:

1. $NN \to aa$ t-channel:
   This can be seen as a $2 \to 2$ scattering with an effective quartic interaction term: $\lambda_{eff} aaNN = \frac{M_N}{f_a^2} aaNN$. This is a non-renormalizable operator and, from Eq. (C.1), we get

   $$\dot{n}_a + 3Hn_a \approx \int d\Pi_a d\Pi_N d\Pi_N d\Pi_a (2\pi)^4 \delta^4(p_N + p_N - p_a - p_a) |\mathcal{M}|^2_{NN\to aa} f_N^2 \,. \tag{C.2}$$

   Following the computation in Ref. [121], this equation can be manipulated, obtaining

   $$\dot{n}_a + 3Hn_a \approx \frac{T}{2048\pi^6} \int ds d\Omega \sqrt{s} |\mathcal{M}|^2_{NN\to aa} K_1(\sqrt{s}/T) \,, \tag{C.3}$$

where s is the center of mass energy at temperature T, considering all the masses negligible with respect to the temperature at which we are working. In this limit, $|\mathcal{M}|^2_{NN\to aa} = \frac{M_N^2}{f_a^4} s$ which means

$$\dot{n}_a + 3Hn_a \approx \frac{TM_N^2}{512\pi^5 f_a^4} \int_0^\infty ds s^{3/2} K_1(\sqrt{s}/T)\,. \tag{C.4}$$

Using the definition of $Y = n/s$, switching variables from t to T and performing the final integral

$$\frac{dY_a}{dT} \approx \frac{-1}{sHT} \frac{T^6 M_N^2}{16\pi^5 f_a^4}\,. \tag{C.5}$$

Computing the integral from T_{RH} to $T_0 \simeq 0$

$$Y_a \approx \frac{0.4 T_{RH} M_{Pl} M_N^2}{\pi^7 f_a^4 g_{*s}\sqrt{g_*}} \approx 10^{-20}\,, \tag{C.6}$$

with $T_{RH} \simeq 10^8$GeV, $M_N \simeq 10^4$GeV, $f_a = 10^{12}$GeV, $g_{*s} = g_* = 106.75$ (here we are inserting values of the parameters, based on considerations about the suitable parameter space for ALP leptogenesis, see 4.1);

2. $NN \to aa$ s-channel with ALP trilinear vertex:
This case is similar to the previous one, but now the effective coupling is $\lambda_{eff} = \frac{M_N T}{f_a^2 m_a}$. Following the same steps as above, we get $|\mathcal{M}|^2_{NN\to aa} = (\frac{M_N T}{m_a f_a^2})^2 s$ and

$$\dot{n}_a + 3Hn_a \approx \frac{T^3 M_N^2}{512\pi^5 m_a^2 f_a^4} \int_0^\infty ds s^{3/2} K_1(\sqrt{s}/T)\,. \tag{C.7}$$

Thus,

$$\frac{dY_a}{dT} \approx \frac{-1}{sHT} \frac{T^8 M_N^2}{16\pi^5 m_a^2 f_a^4}\,. \tag{C.8}$$

Computing the integral over the temperature and inserting the aforementioned values of the parameters, we obtain

$$Y_a \approx \frac{0.4 T_{RH}^3 M_{Pl} M_N^2}{3\pi^7 m_a^2 f_a^4 g_{*s}\sqrt{g_*}} \approx 10^{-14}\,, \tag{C.9}$$

with $m_a = 10^5$GeV;

3. $\phi\, N \to \ell\, a$ t-channel:
It is the same as process 1, but now the effective coupling is $\lambda_{eff} = \frac{y_\nu}{f_a}$. Then, we obtain

$$Y_a \approx \frac{0.4 T_{RH} M_{Pl} y_\nu^2}{\pi^7 f_a^2 g_{*s}\sqrt{g_*}} \approx 10^{-14}\,; \tag{C.10}$$

4. $NN \to a$ inverse N decays:
   The interaction term is a renormalizable operator which means we are dealing with an IR freeze-in production [121]. We have $m_a > M_N + M_N$. At high temperatures ($T \gg m_a$):

$$\dot{n}_a + 3Hn_a \approx \int d\Pi_a d\Pi_N d\Pi_N (2\pi)^4 \delta^4(p_a - P_N - P_N) |\mathcal{M}|^2_{NN\to a} f_N^2 \,. \tag{C.11}$$

   Assuming $|M|^2_{a\to NN} = |M|^2_{NN\to a}$, and energy conservation,

$$\dot{n}_a + 3Hn_a \approx \int d\Pi_a d\Pi_N d\Pi_N (2\pi)^4 \delta^4(p_a - P_N - P_N) |\mathcal{M}|^2_{a\to NN} f_a^{eq} \,. \tag{C.12}$$

   Then, after some manipulations (see Ref. [121]), converting the integral over momentum space into an integral over energy

$$\dot{n}_a + 3Hn_a \approx \frac{g_a \Gamma_N m_a^2}{2\pi^2} T K_1(m_{B_1}/T) \,. \tag{C.13}$$

   Writing $Y = \frac{n}{s}$, $x = \frac{m_a}{T}$ and using $\frac{dT}{dt} \approx -HT$, we get

$$Y_a \approx \frac{45 g_a \Gamma_N M_{Pl}}{1.664 \pi^4 m_a^2 g_{*s} \sqrt{g_*}} \int_{x_{min}}^{x_{max}} K_1(x) x^3 dx \,. \tag{C.14}$$

   Setting $x_{max} = \infty$ and $x_{min} = 0$, the integral results $\frac{3}{2}\pi$ and the final result is

$$Y_a \approx \frac{135}{8\pi^3 (1.66) g_*^S \sqrt{g_*^\rho}} \left(\frac{\Gamma_N M_{Pl}}{m_a^2} \right) \approx 10^{-6} \,, \tag{C.15}$$

   where we have inserted the chosen values for the parameters and computed Γ_N at $T = M_N$.

Therefore, the generated ALP Yield due to the processes 1, 2, 3, 4, is negligible with respect to the Yield coming from the top (and gluon) production, i.e. $Y_a \simeq (10^{-3} \div 10^{-4})$.

List of Figures

2.1 Tree-level, one-loop vertex and one-loop self-energy Feynman diagrams contributing to heavy neutrino decays [9]. 13

2.2 A sketch of the minimal field energy for a given value of the Chern-Simons number N_{CS} [82]. 15

2.3 Evolution of the N_1 (left panel) and $B-L$ (right panel) Yields as function of z, in the thermal leptogenesis with one RH neutrino. Weak washout with $K = 0.1$, realized by e.g. $M_N = 10^{10}$ GeV and $y_\nu = 1.88 \cdot 10^{-4}$. Comparison zero initial abundance vs thermal initial abundance. 23

2.4 Evolution of the N_1 (left panel) and $B-L$ (right panel) Yields as function of z, in the thermal leptogenesis with one RH neutrino. Strong washout with $K = 10$, realized by e.g. $M_N = 10^{10}$ GeV and $y_\nu = 1.88 \cdot 10^{-3}$. Comparison zero initial abundance vs thermal initial abundance. 23

2.5 Left panel: weak washout with $K = 0.1$, the washout processes are always out-of-equilibrium. Right panel: strong washout with $K = 10$, the washout processes are in equilibrium for $1 \lesssim z \lesssim 10$. 25

3.1 The $g\,g \to g\,a$ scattering rate at leading order in the thermal plasma can be obtained either by summing the Feynman diagrams, S,T,U,X, in the upper row, or, equivalently, by summing the imaginary parts of the two-loop thermal diagrams in the lower row. In both cases, the result is infrared divergent, such that proper inclusion of higher order effects is needed [99]. 31

3.2 Thermal diagram 'Decay' is equivalent to diagram D plus the resummation of higher order diagrams with corrections to gluon propagator. Thick lines denote propagator of the thermal gluon g_T [99]. 31

3.3 Cosmological ALP Yield. Blue area: freeze-out with $Y_a = Y_a^{eq} \simeq 2.15 \cdot 10^{-3}$. White area: freeze-in with $Y_a = r Y_a^{eq}$, represented by the dashed lines. Left panel: ALP coupled to both top and gluon. Right panel: ALP coupled to gluon only. 35

3.4 Dashed lines represent different values of decoupling (i.e. freeze-out) temperature T_d in the freeze-out case. Blue area: freeze-out with $Y_a = Y_a^{eq} \simeq 2.15 \cdot 10^{-3}$. White area: freeze-in with $Y_a = rY_a^{eq}$. Left panel: ALP coupled to both top and gluon. Right panel: ALP coupled to gluon only. 36
3.5 Branching ratios of ALP decay channels. Benchmark: $M_N = m_a/3$. . . . 37

4.1 Parameter space for ALP leptogenesis: the area where ALP leptogenesis is possible is the white one. Below the orange line ($T_d^a = v_{EW}$), sphalerons are active. Above the blue line ($T_d^a = M_N/20$), the washout processes are estimated to be out-of-equilibrium when the ALP decay $a \to N\,N$ becomes efficient. The dashed lines represent values of reheating temperature such that $Y_a \simeq 10^{-4}$ in the freeze-in case. 40
4.2 Parameter space without considering the top Yukawa coupling for ALP production: the area where ALP leptogenesis is possible is the white one. The dashed lines represent values of reheating temperature T_{RH} such that $Y_a \simeq 10^{-4}$ in the freeze-in case. Other lines as in Fig. 4.1. 40
4.3 The area between the orange and the green lines denotes where dilution significantly occurs (matter-dominated phase). Other lines as in Fig. 4.1. ALP is mainly produced via the top Yukawa coupling and it is frozen out with $Y_a = 2.15 \cdot 10^{-3}$. 42
4.4 The area between the orange and the green lines denotes where dilution significantly occurs (matter-dominated phase). The dashed lines show the reheating temperature values for which the ALP is frozen-in with $Y_a = 10^{-4}$. The ALP is coupled to both top quarks and gluons. Other lines as in Fig. 4.1. 43
4.5 Parameter space without considering the top Yukawa coupling for ALP production.The area between the orange and the blue lines denotes where dilution significantly occurs (matter-dominated phase). The dashed lines show the reheating temperature values for which the ALP is frozen-in with $Y_a = 10^{-4}$. Other lines as in Fig. 4.1. 43
4.6 ALP Yield as function of z. It is frozen out with initial abundance $Y_a = Y_a^{eq} = 2.15 \cdot 10^{-3}$. 49
4.7 ALP leptogenesis: Majorana neutrino Yield as function of z. Comparison between thermal and ALP leptogenesis with same parameters. 49
4.8 ALP leptogenesis: $B - L$ Yield as function of z. Comparison between thermal and ALP leptogenesis: one sees that ALP leptogenesis avoids the strong washout effects of standard thermal leptogenesis, and thus allows to obtain a baryon asymmetry larger than more than two orders of magnitude for the same values of parameters. 50

4.9 ALP leptogenesis: the rates $\tilde{\Gamma}$ of N's decay (red line), ALP's decay (orange line) and washout processes,i.e. inverse decay of N(green line), are compared to Hubble parameter H. The dashed black line corresponds to $\tilde{\Gamma}/H = 1$. Above that line, processes are in thermal equilibrium with the plasma. Below that line, processes are out-of-equilibrium. The advantage of ALP leptogenesis is that we can avoid washout effects for some regions of parameter space. This is explicated by this plot: washout processes are out-of-equilibrium when the ALP's decay comes into equilibrium. 51
4.10 Resonant ALP leptogenesis with $M_{1,2} \simeq 10^4$ GeV. RHN Yield as function of z, with zero initial abundance for RHNs, $Y_N(10^{-3}) = 0$, as initial condition. . . . 52
4.11 Resonant ALP leptogenesis with $M_{1,2} \simeq 10^4$GeV. $B - L$ Yield as function of z, with zero initial abundance for RHNs, $Y_N(10^{-3}) = 0$, as initial condition. The advantages of ALP resonant leptogenesis are manifest: one sees that this mechanism can avoid the strong washout effects of standard thermal leptogenesis, and thus allows to obtain a baryon asymmetry larger than more than two orders of magnitude for the same values of parameters. Therefore, we expect that a smaller resonant enhancement is needed with respect to thermal leptogenesis with same parameter values. Eventually, the asymptotic value of the $B - L$ asymmetry, for the ALP resonant leptogenesis (blue solid line), reproduces successfully the experimental data of the BAU (1.5). 53
4.12 Bath temperature scaling with respect to scale factor in scenarios of early matter-domination induced by the ALP. The gray line denotes the standard case, in which the ALP only decays directly into radiation, while the dashed red one the case in which it also decays into non-relativistic matter, i.e. RHNs (dominant channel), that is relevant for ALP leptogenesis. The gray line and the dashed red line actually overlap. 56
4.13 Temperature as a function of scale factor a/a_0 in scenarios of early matter-domination induced by the ALP. The cases in which the dominant channel is either $\Gamma_{a\to NN}$ (relevant for ALP leptogenesis) or $\Gamma_{a\to SM}$ are plotted respectively as dashed red and orange lines. 57
4.14 Energy densities of radiation, Majorana neutrinos and ALP as functions of a/a_0 in scenarios of early matter-domination induced by the ALP. Solid and dashed lines refers to cases $\Gamma_{a\to SM} < 0.1\Gamma_{a\to NN}$ (relevant for ALP leptogenesis) and $\Gamma_{a\to SM} = 20\Gamma_{a\to NN}$, respectively. 57
4.15 Energy density of ALP, RHN and radiation for a benchmark choice of parameters where early matter-domination is realised. The ALP dominates the energy content of the Universe for $a/a_0 \in [26, 2\cdot 10^3]$. The temperature slope is affected by matter-dominated phase for $a/a_0 \in [5 \cdot 10^2, 2 \cdot 10^3]$. 59

4.16 Yields of ALP, RHN and radiation for a benchmark choice of parameters where early matter-domination induced by the ALP is realized. Y_a and Y_N get diluted for $a/a_0 \in [5 \cdot 10^2, 2 \cdot 10^3]$ by a factor $\sim 10^2$. The dashed lines represent the constant initial values of the Yields and they are plotted as a reference to enlighten the dilution. The exponential drop of Y_a and Y_N for $a/a_0 \gtrsim 2 \cdot 10^3$ is due to their decay. 59
4.17 Comoving entropy $S = sa^3$ as function of a/a_0 for a benchmark choice of parameters where early matter-domination induced by the ALP is realized. During the radiation-domination its value is constant, while in matter-domination one finds a huge increase, corresponding to a significant entropy injection due to the ALP's decay. 60
4.18 Parameter space of ALP leptogenesis, where the red line corresponds to a dilution factor $D_{SM} = 10^2$. Thus, above the red line, the factor 10^2 in baryon asymmetry, gained by ALP leptogenesis with respect to standard leptogenesis, is diluted away due to the ALP matter-domination. Meanwhile, below the red line, ALP leptogenesis allows to gain some factors with respect to thermal leptogenesis. 61

Bibliography

[1] A. Collaboration, *Observation of a new particle in the search for the Standard Model Higgs boson with the ATLAS detector at the LHC*, *Phys.Lett.B* **716** (2012) 1–29, [1207.7214].

[2] C. Collaboration, *Observation of a new boson at a mass of 125 GeV with the CMS experiment at the LHC*, *Phys.Lett.B* **716** (2012) 30–61, [1207.7235].

[3] P. J. Mohr, D. B. Newell and B. N. Taylor, *CODATA recommended values of the fundamental physics constants: 2014*, *Rev.Mod.Phys.* **88, 035009** (2016) .

[4] Particle Data Group collaboration, R. L. Workman et al., *Review of Particle Physics*, *PTEP* **2022** (2022) 083C01.

[5] S.-K. Collaboration and Y. Fukuda, *Evidence for oscillation of atmospheric neutrinos*, *Phys.Rev.Lett.* **81** (1998) 1562–1567, [hep-ex/9807003].

[6] M. C. Gonzalez-Garcia, M. Maltoni and T. Schwetz, *NuFIT: Three-Flavour Global Analyses of Neutrino Oscillation Experiments*, *Universe 7* **12** (2021) 459, [2111.03086].

[7] e. a. Aghanim, Nabila, *Planck 2018 results.I.Overview and the cosmological legacy of Planck*, *AA* **641** (2020) A1, [1807.06205].

[8] J. M. Cline, *Baryogenesis*, 2006.

[9] D. Bodeker and W. Buchmuller, *Baryogenesis from the weak scale to the grand unification scale*, *Rev.Mod.Phys.* **93, 3, 035004** (2021) 22, [2009.07294].

[10] M. Fukugita and T. Yanagida*Phys.Lett.* **B,174** (1986) 45–47.

[11] S. Davidson, E. Nardi and Y. Nir, *Leptogenesis*, *Phys. Rept.* **466** (2008) 105–177, [0802.2962].

[12] B. Garbrecht, *Why is there more matter than antimatter? Calculational methods for leptogenesis and electroweak baryogenesis*, *Progress in Particle and Nuclear Physics 110 (2020), 103727* (2020) , [1812.02651].

[13] A. Ringwald, *Axions and Axion-Like Particles*, in *49th Rencontres de Moriond on Electroweak Interactions and Unified Theories*, pp. 223–230, 2014. 1407.0546.

[14] C. Antel et al., *Feebly Interacting Particles: FIPs 2022 workshop report*, in *Workshop on Feebly-Interacting Particles*, 5, 2023. 2305.01715.

[15] J. Garayoa, S. Pastor, T. Pinto, N. Rius and O. Vives, *On the full Boltzmann equations for Leptogenesis*, *JCAP 0909:035* (2009) , [0905.4834].

[16] E. Komatsu, S. K.M., J. Dunkley, C. Bennett and B. e. a. Gold, *Seven-Year Wilkinson Microwave Anisotropy Probe (WMAP) Observations: Cosmological Interpretation*, *Astrophys.J.SUppl.* **192:18** (2011) , [1001.4538].

[17] G. Steigman, *Primordial Nucleosynthesis: The Predicted and Observed Abundances and Their Consequences*, 1008.4765.

[18] V. Simha and G. Steigman, *Constraining the Early-Universe Baryon Density and Expansion Rate*, *JCAP* **0806:016** (2008) , [0803.3465].

[19] A. Collaboration, *Search for antihelium in cosmic rays*, *Phys.Lett.B* **461** (1999) 387–396, [hep-ex/0002048].

[20] A. Collaboration, *Antiproton Flux, Antiproton-to-Proton Flux Ratio, and Properties of Elementary Particle Fluxes in Primary Cosmic Rays Measured with the Alpha Magnetic Spectrometer on the International Space Station*, *Phys.Rev.Lett.* **117,091103** (2016) .

[21] E. W. Kolb and M. S. Turner, *The Early Universe*, *Front.Phys.* **69** (1990) 1–547.

[22] U. Feldman, U. Schuhle, K. Widing and J. Laming, *Coronal Composition above the Solar Equator and the North Pole as Determined from Spectra Acquired by the SUMER Instrument on SOHO*, *Astrophys.Journal* **505** (1998) 999.

[23] G. Steigman, *Observational Tests of Antimatter Cosmologies*, *Annual Review of Astronomy and Astrophysics* **14** (1976) 339–372.

[24] O. Adriani, G. Bazilevskaya and G. e. a. Barbarino, *Measurement of the flux of primary cosmic ray antiprotons with energies of 60 MeV to 350 GeV in the PAMELA experiment*, *Jetp Lett.* **96** (2013) 621–627.

[25] L. Canetti, M. Drewes and M. Shaposhnikov, *Matter and Antimatter in the Universe*, *New J. Phys.* **14** (2012) 095012, [1204.4186].

[26] A. Cohen, A. De Rujula and S. Glashow, *A Matter-Antimatter Universe?*, *Astrophy.J.* **495** (1998) 539–549, [astro-ph/9707087].

[27] K. A. Olive, D. N. Schramm, G. Steigman, M. S. Turner and J. Yang, *Big-bang nucleosynthesis as a probe of cosmology and particle physics*, **246** (June, 1981) 557–568.

[28] B. D. Fields, K. A. Olive, T.-H. Yeh and C. Young, *Big-Bang Nucleosynthesis After Planck*, *Journal of Cosmology and Astroparticle Physics* **03** (2020) , [1912.01132].

[29] A. D. Sakharov, *Violation of CP invariance, C asymmetry, and baryon asymmetry of the universe*, *Soviet Physics Uspekhi* **34** (1991) 5.

[30] G. t' Hooft, *Symmetry Breaking thorugh Bell-Jackiw Anomalies*, *Phys.Rev.Lett.* **37** (1976) 8.

[31] M. D. Schwartz, *Quantum Field Theory and the Standard Model*, *Cambridge University Press* (2014) .

[32] M. E. Peskin and D. V. Schroeder, *An Introduction To Quantum Field Theory and the Standard Model*, *CRC Press* (1995) .

[33] F. Klinkhamer and N. Manton, *A saddle-point solution in the Weinberg-Salam theory*, *Phys.Rev.D* **30** (1984) 2212.

[34] P. Arnold and L. McLerran, *Sphalerons, small fluctuations, and baryon-number violation in electroweak theory*, *Phys.Rev.D* **36** (1987) 581.

[35] P. Arnold and L. McLerran, *The sphaleron strikes back: A response to objections to the sphaleron approximation*, *Phys.Rev.D* **37** (1988) 1020.

[36] V. Rubakov and M. Shaposhnikov, *Electroweak Baryon Number Non-Conservation in the Early Universe and in High Energy Collisions*, *Usp.Fiz.Nauk.* **166** (1996) 493–537, [hep-ph/9603208].

[37] M. Kobayashi and T. Maskawa, *CP-Violation in the Renormalizable Theory of Weak Interaction*, *Progress of Theoretical Physics* **49, 2** (1973) 652–657.

[38] M. Gavela, P. Hernandez and O. Orloff, J. snd Pene, *Standard Model CP-violation and Baryon asymmetry*, *Mod.Phys.Lett.* **A9** (1994) 795–810, [hep-ph/9312215].

[39] P. Huet and E. Sather, *Electroweak Baryogenesis and Standard Model CP violation*, *Phys.Rev.D* **51** (1995) 379–394, [hep-ph/9404302].

[40] M. Trodden, *Electroweak Baryogenesis*, *Rev.Mod.Phys.* **71** (1999) 1463–1500, [hep-ph/9803479].

[41] K. Kajantie, M. Laine, K. Rummukaine and M. Shaposhnikov, *The Electroweak Phase Transition: A Non-Perturbative Analysis*, *Nucl.Phys.B* **466** (1996) 189–258, [hep-lat/9510020].

[42] K. Kajantie, M. Laine, K. Rummukainen and M. Shaposhnikov, *Is there a hot electroweak phase transition atmml:math xmlns:mml="http://www.w3.org/1998/math/MathML"*, *Physical Review Letters* **77** (sep, 1996) 2887–2890.

[43] S. Dimopoulos and L. Susskind, *Baryon number of the universe*, *Physical Review D* **18** (1978) 4500.

[44] M. Yoshimura, *Unified Gauge Theories and the Baryon Number of the Universe*, *Physical Review Letters* **41** (1978) 281.

[45] V. Kuzmin, V. Rubakov and M. Shaposhnikov, *On anomalous electroweak baryon-number non-conservation in the early universe*, *Physics Letters B* **155** (1985) 36–42.

[46] F. Hahn-Woernle, M. Plumacher and Y. Y. Y. Wong, *Full Boltzmann equations for leptogenesis including scattering*, *JCAP* **08** (2009) 028, [0907.0205].

[47] T. Yanagida, *Horizontal Symmetry and Masses of Neutrinos*, *Progress of Theoretical Physics* **64** (1980) 1103–1105.

[48] R. N. Mohapatra and G. Senjanovic, *Neutrino Masses and Mixings in Gauge Models with Spontaneous Parity Violation*, *Phys.Rev.D* **23** (1981) 165.

[49] S. Khlebnikov and M. Shaposhnikov, *The Statistical Theory of Anomalous Fermion Number Nonconservation*, *Nucl.Phys.B* **308** (1988) 885–912.

[50] D. J. E. Marsh, *Axion Cosmology*, *Phys. Rept.* **643** (2016) 1–79, [1510.07633].

[51] J. E. Kim and G. Carosi, *Axions and the Strong CP Problem*, *Rev. Mod. Phys.* **82** (2010) 557–602, [0807.3125].

[52] R. Peccei and H. Quinn, *CP conservation in the presence of pseudoparticles*, *Phys.Rev.Lett* **38** (1977) 1440.

[53] R. D. Peccei and H. R. Quinn, *Constraints imposed by* CP *conservation in the presence of pseudoparticles*, *Phys. Rev. D* **16** (Sep, 1977) 1791–1797.

[54] S. Weinberg, *A new light boson?*, *Phys. Rev. Lett.* **40** (Jan, 1978) 223–226.

[55] M. Bauer, M. Heiles, M. Neubert and A. Thamm, *Axion-Like Particles at Future Colliders*, *Eur. Phys. J. C* **79** (2019) 74, [1808.10323].

[56] H. Georgi, D. B. Kaplan and L. Randall, *Manifesting the invisible axion at low energies*, *Physics Letters B* **169** (1986) 73–78.

[57] C. A. Baker et al., *An Improved experimental limit on the electric dipole moment of the neutron*, *Phys. Rev. Lett.* **97** (2006) 131801, [hep-ex/0602020].

[58] G. G. di Cortona, E. Hardy, J. P. Vega and G. Villadoro, *The QCD axion, precisely*, *Journal of High Energy Physics* **2016** (jan, 2016) .

[59] P. Agrawal et al., *Feebly-interacting particles: FIPs 2020 workshop report*, *Eur. Phys. J. C* **81** (2021) 1015, [2102.12143].

[60] I. Affleck and M. Dine, *A New Mechanism for Baryogenesis*, *Nucl. Phys. B* **249** (1985) 361–380.

[61] A. E. Nelson and N. Seiberg, *R symmetry breaking versus supersymmetry breaking*, *Nucl. Phys. B* **416** (1994) 46–62, [hep-ph/9309299].

[62] J. Bagger, E. Poppitz and L. Randall, *The R axion from dynamical supersymmetry breaking*, *Nucl. Phys. B* **426** (1994) 3–18, [hep-ph/9405345].

[63] H. P. Nilles, *Supersymmetry, Supergravity and Particle Physics*, *Phys. Rept.* **110** (1984) 1–162.

[64] LHC/LC Study Group collaboration, G. Weiglein et al., *Physics interplay of the LHC and the ILC*, *Phys. Rept.* **426** (2006) 47–358, [hep-ph/0410364].

[65] S. P. Martin, *A Supersymmetry primer*, *Adv. Ser. Direct. High Energy Phys.* **18** (1998) 1–98, [hep-ph/9709356].

[66] J. Wess and J. Bagger, *Supersymmetry and supergravity*, .

[67] D. Bailin and A. Love, *Supersymmetric Gauge Field Theory and String Theory*, .

[68] Particle Data Group collaboration, M. Tanabashi, K. Hagiwara, K. Hikasa, K. Nakamura, Y. Sumino, F. Takahashi et al., *Review of particle physics*, *Phys. Rev. D* **98** (Aug, 2018) 030001.

[69] I. Affleck, M. Dine and N. Seiberg, *Calculable nonperturbative supersymmetry breaking*, *Phys. Rev. Lett.* **52** (May, 1984) 1677–1680.

[70] Z. Li and Z. Sun, *The Nelson-Seiberg theorem generalized with nonpolynomial superpotentials*, *Adv. High Energy Phys.* **2020** (2020) 3701943, [2006.00538].

[71] Y. Hamada, K. Kamada, T. Kobayashi and Y. Ookouchi, *Cosmological constraints on spontaneous R-symmetry breaking models*, *JCAP* **04** (2013) 043, [1211.5662].

[72] B. Bellazzini, A. Mariotti, D. Redigolo, F. Sala and J. Serra, *R-axion at colliders*, *Phys. Rev. Lett.* **119** (2017) 141804, [1702.02152].

[73] J. Preskill, M. B. Wise and F. Wilczek, *Cosmology of the invisible axion*, *Physics Letters B* **120** (1983) 127–132.

[74] R. Barbieri, P. Creminelli, A. Strumia and N. Tetradis, *Baryogenesis through leptogenesis*, *Nuclear Physics B* **575** (may, 2000) 61–77.

[75] E. Ma, *Pathways to naturally small neutrino masses*, *Phys. Rev. Lett.* **81** (Aug, 1998) 1171–1174.

[76] S. Weinberg, *Baryon- and lepton-nonconserving processes*, *Phys. Rev. Lett.* **43** (Nov, 1979) 1566–1570.

[77] P. D. G. Collaboration and C. e. a. Patrignani, *Review of Particle Physics*, *Chinese Phys. C* **40, 100001** (2016) .

[78] J. Liu and G. Segre, *Reexamination of generation of baryon and lepton number asymmetries by heavy particle decay*, *Phys. Rev. D* **48** (1993) 4609–4612, [hep-ph/9304241].

[79] L. Covi, E. Roulet and F. Vissani, *CP violating decays in leptogenesis scenarios*, *Phys. Lett. B* **384** (1996) 169–174, [hep-ph/9605319].

[80] E. Nardi, Y. Nir, E. Roulet and J. Racker, *The importance of flavor in leptogenesis*, *Journal of High Energy Physics* **2006** (jan, 2006) 164–164.

[81] M.-C. Chen, *Tasi 2006 lectures on leptogenesis*, 2007.

[82] T. Akiba, H. Kikuchi and T. Yanagida, *Static minimum-energy path from a vacuum to a sphaleron in the weinberg-salam model*, *Phys. Rev. D* **38** (Sep, 1988) 1937–1941.

[83] A. Polyakov, *Gauge Fields and Strings (1st ed.).*, *Routledge.* (1987) .

[84] S. R. Coleman, *The Uses of Instantons*, *Subnucl. Ser.* **15** (1979) 805.

[85] A. Belavin, A. Polyakov, A. Schwartz and Y. Tyupkin, *Pseudoparticle solutions of the yang-mills equations*, *Physics Letters B* **59** (1975) 85–87.

[86] Y. Burnier, M. Laine and M. Shaposhnikov, *Baryon and lepton number violation rates across the electroweak crossover*, *Journal of Cosmology and Astroparticle Physics* **2006** (feb, 2006) 007–007.

[87] L. s Bento, *Sphaleron relaxation temperatures*, *Journal of Cosmology and Astroparticle Physics* **2003** (nov, 2003) 002–002.

[88] W. Buchmuller, P. Di Bari and M. Plumacher, *Leptogenesis for pedestrians*, *Annals Phys.* **315** (2005) 305–351, [hep-ph/0401240].

[89] M. Plümacher, *Baryogenesis and lepton number violation*, *Zeitschrift fur Physik C-Particles and Fields* **74** (1997) 549 – 559.

[90] V. Brdar, A. J. Helmboldt, S. Iwamoto and K. Schmitz, *Type i seesaw mechanism as the common origin of neutrino mass, baryon asymmetry, and the electroweak scale*, *Physical Review D* **100** (oct, 2019) .

[91] B. Shuve and C. Tamarit, *Phase Transitions and Baryogenesis From Decays*, *JHEP* **10** (2017) 122, [1704.01979].

[92] M. A. Luty, *Baryogenesis via leptogenesis*, *Phys. Rev. D* **45** (Jan, 1992) 455–465.

[93] G. Giudice, A. Notari, M. Raidal, A. Riotto and A. Strumia, *Towards a complete theory of thermal leptogenesis in the SM and MSSM*, *Nuclear Physics B* **685** (may, 2004) 89–149.

[94] A. Pilaftsis and T. Underwood, *Resonant lepogenesis*, *Nucl.Phys.* **B692** (2004) 303–345, [hep-ph/0309342].

[95] E. W. Kolb and S. Wolfram, *Baryon number generation in the early universe*, *Nuclear Physics, Section B* **172** (1980) 224 – 284.

[96] A. Riotto, *Baryogenesis and leptogenesis*, *J. Phys. Conf. Ser.* **335** (2011) 012008.

[97] M. Garny, A. Kartavtsev and A. Hohenegger, *Leptogenesis from first principles in the resonant regime*, 1112.6428.

[98] A. Pilaftsis, CP *violation and baryogenesis due to heavy majorana neutrinos*, *Phys. Rev. D* **56** (Nov, 1997) 5431–5451.

[99] A. Salvio, A. Strumia and W. Xue, *Thermal axion production*, *JCAP* **01** (2014) 011, [1310.6982].

[100] Y. Hamada, K. Kamada, T. Kobayashi and Y. Ookouchi, *More on cosmological constraints on spontaneous R-symmetry breaking models*, *JCAP* **01** (2014) 024, [1310.0118].

[101] T. Hiramatsu, M. Kawasaki, K. Saikawa and T. Sekiguchi, *Axion cosmology with long-lived domain walls*, *Journal of Cosmology and Astroparticle Physics* **2013** (jan, 2013) 001–001.

[102] M. Gorghetto, E. Hardy and G. Villadoro, *Axions from Strings: the Attractive Solution*, *JHEP* **07** (2018) 151, [1806.04677].

[103] R. Davis, *Cosmic axions from cosmic strings*, *Physics Letters B* **180** (1986) 225–230.

[104] M. Yamaguchi, M. Kawasaki and J. Yokoyama, *Evolution of axionic strings and spectrum of axions radiated from them*, *Phys. Rev. Lett.* **82** (Jun, 1999) 4578–4581.

[105] P. Sikivie, *Axions, domain walls, and the early universe*, *Phys. Rev. Lett.* **48** (Apr, 1982) 1156–1159.

[106] T. Hiramatsu, M. Kawasaki, K. Saikawa and T. Sekiguchi, *Production of dark matter axions from collapse of string-wall systems*, *Phys. Rev. D* **85** (May, 2012) 105020.

[107] E. Massó, F. Rota and G. Zsembinszki, *Axion thermalization in the early universe*, *Phys. Rev. D* **66** (Jul, 2002) 023004.

[108] E. Braaten and R. D. Pisarski, *Soft amplitudes in hot gauge theories: A general analysis*, *Nuclear Physics B* **337** (1990) 569–634.

[109] E. Braaten and T. C. Yuan, *Calculation of screening in a hot plasma*, *Phys. Rev. Lett.* **66** (Apr, 1991) 2183–2186.

[110] P. Graf and F. D. Steffen, *Thermal axion production in the primordial quark-gluon plasma*, *Phys. Rev. D* **83** (2011) 075011, [1008.4528].

[111] M. Le Bellac, *Thermal field theory*, .

[112] R. Contino, A. Mitridate, A. Podo and M. Redi, *Gluequark Dark Matter*, *JHEP* **02** (2019) 187, [1811.06975].

[113] M. Cirelli, Y. Gouttenoire, K. Petraki and F. Sala, *Homeopathic Dark Matter, or how diluted heavy substances produce high energy cosmic rays*, *JCAP* **02** (2019) 014, [1811.03608].

[114] P. S. B. Dev, P. Millington, A. Pilaftsis and D. Teresi, *Flavour effects in resonant leptogenesis from semi-classical and kadanoff-baym approaches*, *Journal of Physics: Conference Series* **631** (jul, 2015) 012087.

[115] I. Brivio, K. Moffat, S. Pascoli, S. Petcov and J. Turner, *Leptogenesis in the neutrino option*, *Journal of High Energy Physics* **2019** (oct, 2019) .

[116] S. Davidson and A. Ibarra, *A lower bound on the right-handed neutrino mass from leptogenesis*, *Physics Letters B* **535** (may, 2002) 25–32.

[117] M. Blennow, E. Fernández-Martínez, J. Hernández-García, J. López-Pavón, X. Marcano and D. Naredo-Tuero, *Bounds on lepton non-unitarity and heavy neutrino mixing*, 2023.

[118] I. Chakraborty, H. Roy and T. Srivastava, *Searches for heavy neutrinos at multi-TeV muon collider: a resonant leptogenesis perspective*, *The European Physical Journal C* **83** (apr, 2023) .

[119] T. H. Kwok, L. Li, T. Liu and A. Rock, *Searching for heavy neutral leptons at a future muon collider*, 2023.

[120] P. Li, Z. Liu and K.-F. Lyu, *Heavy neutral leptons at muon colliders*, *Journal of High Energy Physics* **2023** (mar, 2023) .

[121] L. J. Hall, K. Jedamzik, J. March-Russell and S. M. West, *Freeze-in production of FIMP dark matter*, *Journal of High Energy Physics* **2010** (mar, 2010) .

[122] J. A. Harvey, E. W. Kolb, D. B. Reiss and S. Wolfram, *Calculation of cosmological baryon asymmetry in grand unified gauge models*, *Nuclear Physics, Section B* **201** (1982) 16 – 100.